NASA CR-121177
PWA™-4683

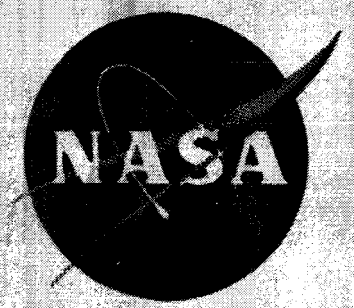

FINAL REPORT

DEVELOPMENT OF MAINSHAFT SEALS FOR ADVANCED AIR BREATHING PROPULSION SYSTEMS

by
L. J. Dobek

PRATT & WHITNEY AIRCRAFT
DIVISION OF UNITED AIRCRAFT CORPORATION

Prepared for
NATIONAL AERONAUTICS AND SPACE ADMINISTRATION

NASA LEWIS RESEARCH CENTER
CONTRACT NAS3-15346
L. P. LUDWIG, PROJECT MANAGER

1. Report No.	2. Government Accession No.	3. Recipient's Catalog No.
NASA CR-121177		

4. Title and Subtitle	5. Report Date
DEVELOPMENT OF MAINSHAFT SEALS FOR ADVANCED AIR BREATHING PROPULSION SYSTEMS	March 1973
	6. Performing Organization Code
7. Author(s)	8. Performing Organization Report No.
L. J. Dobek	PWA^{TM}-4683
	10. Work Unit No.
9. Performing Organization Name and Address	
Pratt & Whitney Aircraft Division of United Aircraft Corporation East Hartford, Connecticut 06108	11. Contract or Grant No. NAS3-15346
	13. Type of Report and Period Covered
12. Sponsoring Agency Name and Address	Contractor Report
National Aeronautics and Space Administration Washington, D. C. 20456	14. Sponsoring Agency Code

15. Supplementary Notes

Project Manager, Lawrence P. Ludwig, Fluid Systems Components Division, NASA Lewis Research Center, Cleveland, Ohio

16. Abstract

A gas-film face seal design incorporating shrouded Rayleigh step lift pads at the primary sealing face was analyzed for performance over a wide range of gas turbine engine conditions. Acceptable leakage rates and operation without rubbing contact was predicted for engine conditions that included sealed pressures to 345 N/cm^2 (500 psi), sliding speeds to 183 m/sec (600 ft/sec) and sealed gas temperatures to 922°K (1200°F).

In the experimental evaluation, measured gas leakage rates were, in general, close to that predicted and sometimes lower.

Satisfactory performance of the gas-film seal was demonstrated at the maximum seal seat axial runout expected in present positive contact face seal applications. Stable operation was shown when testing was performed with air-entrained dirt.

Successful operation of the seal was demonstrated to a maximum pressure differential of 345 N/cm^2 (500 psi), to a maximum seal sliding speed of 183 m/sec (600 ft/sec), and to a maximum sealed gas temperature of 922°K (1200°F). One (1) hour of continuous operation at a pressure/speed combination of 345 N/cm^2 (500 psi) and 152.4 m/sec (500 ft/sec) was included. Although endurance testing was successful at 811°K (1000°F), it was indicated that improved piston ring secondary sealing and additional seal carrier cooling were needed to permit endurance evaluation at 922°K (1200°F) and above.

17. Key Words (Suggested by Author(s))	18. Distribution Statement
Gas-Film Seals Mainshaft Seals Rayleigh Step Pads Self-Acting Seals	Unclassified - Unlimited

19. Security Classif. (of this report)	20. Security Classif. (of this page)	21. No. of Pages	22. Price*
Unclassified	Unclassified	122	$3.00

* For sale by the National Technical Information Service, Springfield, Virginia 22151

FOREWORD

This report describes the work accomplished on Contract NAS3-15346 by the Pratt & Whitney Aircraft Division of United Aircraft Corporation for the Lewis Research Center of the National Aeronautics and Space Administration. This work was initiated 7 July 1971 and completed 6 February 1973.

Lawrence P. Ludwig of the National Aeronautics and Space Administration Fluid Systems Components Division was the Project Manager and Leonard W. Schopen, NASA Research Center was the Contracting Officer.

Valentine P. Povinelli was Program Manager for Pratt & Whitney Aircraft from the inception of this Contract until 31 August 1972. From 1 September 1972 until Contract completion Louis J. Dobek was the Program Manager.

Appreciation is extended for assistance in the preparation of material for this report to Edward J. Tobiasz and Wellington J. Walker.

TABLE OF CONTENTS

LIST OF ILLUSTRATIONS

LIST OF ILLUSTRATIONS (Cont'd)

LIST OF ILLUSTRATIONS (Cont'd)

LIST OF ILLUSTRATIONS (Cont'd)

LIST OF ILLUSTRATIONS (Cont'd)

LIST OF ILLUSTRATIONS (Cont'd)

LIST OF ILLUSTRATIONS (Cont'd)

LIST OF TABLES

LIST OF TABLES (Cont'd)

SUMMARY

The work performed for this Contract was done on a gas-film seal of NASA design which employed Rayleigh step shrouded pads for generating self-acting lift force at the primary sealing face. A performance analysis was completed on the seal design prior to testing. This analysis, which was done to establish an analytical base for evaluation of the seal performance, predicted operation without rubbing contact and acceptable leakage rates for a wide range of gas turbine operating conditions that included sealed pressures to 345 N/cm^2 (500 psi), seal sliding speeds to 183 m/sec (600 ft/sec) and sealed gas temperatures to 922°K (1200°F).

Also a structural analysis of the seal was completed, and recommendations were made and incorporated into the design of the test hardware to permit evaluation to 345 N/cm^2 (500 psi) differential pressure across the seal, 183 m/sec (600 ft/sec) seal sliding speed, and 922°K (1200°F) sealed gas temperature.

The gas leakage rates measured in the experimental evaluation were, in general, close to that predicted and lower than that predicted for endurance running.

Experimental evaluation was conducted on two (2) seals supplied by NASA with instrumented nosepieces to measure gas-film seal thickness under dynamic conditions. Due to instrumentation failures, testing was terminated before reliable thickness measurements could be determined.

The gas-film seal was tested for 31.5 hours with an axial seal seat runout of 57.15 microns (2.25 mils) which is at or above the maximum level expected in mainshaft carbon face seal applications. Testing included operation to a maximum pressure differential across the seal of 345 N/cm^2 (500 psi) and to a maximum seal sliding speed of 152.4 m/sec (500 ft/sec). In general, measured leakages were found to be below predicted values and performance was satisfactory.

Satisfactory operation of the gas-film seal was demonstrated when tested with Arizona Road Dust (crushed-quartz) metered into the sealing air supply at a rate of 3.5 gm/hr (0.125 oz/hr). Testing included operation to a maximum pressure differential across the seal of 206.8 N/cm^2 (300 psi), to a maximum seal sliding speed of 137 m/sec (450 ft/sec), and to a maximum sealed gas temperature of 643°K (699°F). Wear was observed with increased leakage as testing progressed, but seal operation was stable throughout this work. Included in the testing was the evaluation of a NASA supplied contaminate particle rejector which was shown to be ineffective in removing the particles entrained in the sealing air.

The seal design was also tested at elevated sealed gas temperatures of 366°K (200°F) to 922°K (1200°F). A total of 222.25 hours of testing was completed. Seal performance was generally good with measured leakages close to the predicted values. Successful operation without rubbing contact was demonstrated to a maximum pressure differential of 345 N/cm^2 (500 psi), to a maximum sliding speed of 183 m/sec (600 ft/sec) and to a maximum sealed gas temperature of 811°K (1000°F). One (1) hour of continuous operation at a pressure-speed combination of 345 N/cm^2 (500 psi) and 152.4 m/sec (500 ft/sec) was included. Although endurance testing was successful to 811°K (1000°F), the results indicated that improved piston ring secondary sealing and additional seal carrier cooling was needed to permit endurance evaluation at 922°K (1200°F).

II. INTRODUCTION

Advanced air-breathing engines require the development of mainshaft seals capable of accomodating increasingly severe environments. Contract NAS 3-15346 was directed at continuing the prior work done under Contract NAS3-7609 (Reference 1) to develop mainshaft seals capable of operating at higher pressures, temperatures, and surface speeds than are employed in current production engines. The maximum levels of these parameters investigated in this Contract were a pressure differential of 345 N/cm^2 (500 psi), a sealed gas temperature of 922°K (1200°F), and a seal sliding speed of 183 m/sec (600 ft/sec).

Positive-contact mainshaft seals are commonly used in current engines. A typical seal of this type is shown in Figure 1. Despite significant advances in nosepiece materials, seal seat hardface coatings and materials, lubrication technology, heat-transfer technology, and surface finishing, all attempts to significantly extend the operating range of the present positive contact carbon face seal have demonstrated a limited growth potential. Current practice is to use these seals at conditions not exceeding a pressure differential of 103.5 N/cm^2 (150 psi), a gas temperature of 866°K (1100°F), and a sliding speed of 114 m/sec (375 ft/sec). It is expected that advanced engines will operate at pressure differentials of 173 N/cm^2 (250 psi), gas temperatures of 922°K (1200°F), and sliding speeds of 137.2 m/sec (450 ft/sec). Conventional positive-contact seals are entirely inadequate for these advanced conditions.

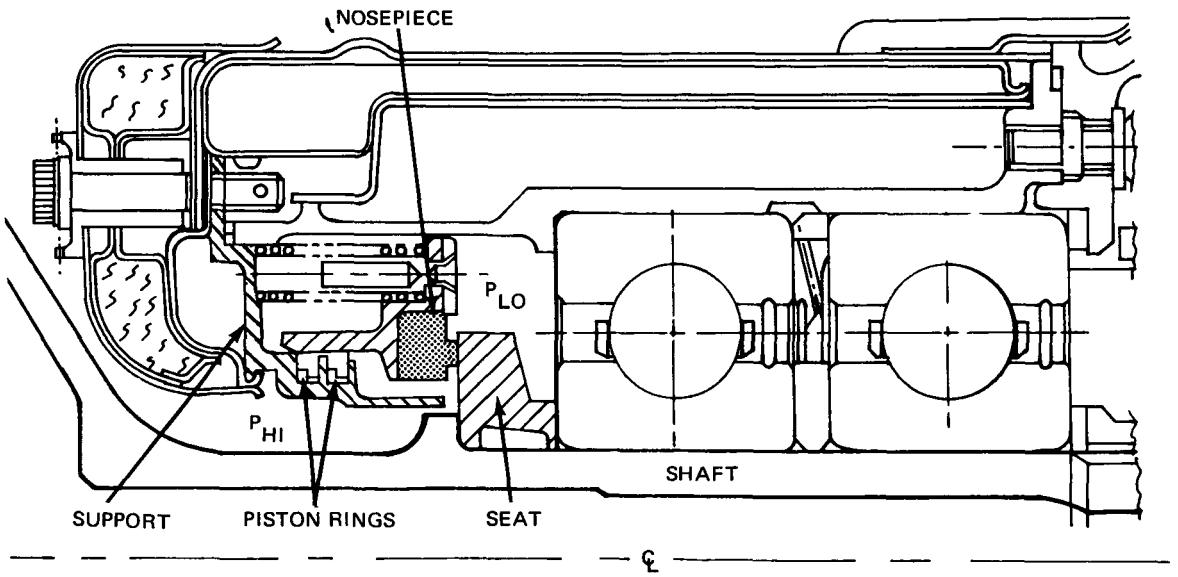

Figure 1 Typical Positive-Contact Face Seal

The most common alternative to the positive-contact seal is the labyrinth seal; however, once certain limitations of temperature and pressure differentials are reached, the simple, lightweight labyrinth seals must give way to complicated multi-labyrinth designs similar to the one shown in Figure 2. These designs utilize high pressure air bleed-off and cold air pressurization schemes. The seal becomes heavy and bulky, and its high air leakages penalizes engine performance.

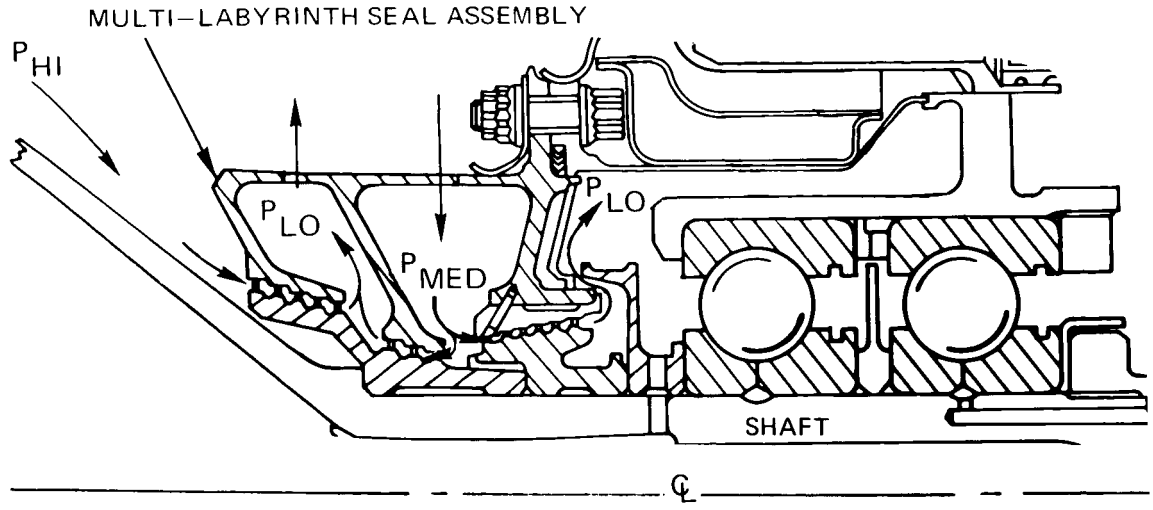

Figure 2 Typical Multi-Labyrinth Seal

A seal design which operates with low leakage and has high speed and high pressure capability is the self-acting gas-film seal. Work on development of this gas-film seal was initiated under Contract NAS3-7609 and continued under this Contract.

A seal design similar to the "wide pad" concept successfully evaluated in Phase III of Contract NAS3-7609 was analyzed, modified to permit operation at higher pressures, speeds, and temperatures, and experimentally evaluated (Figure 3).

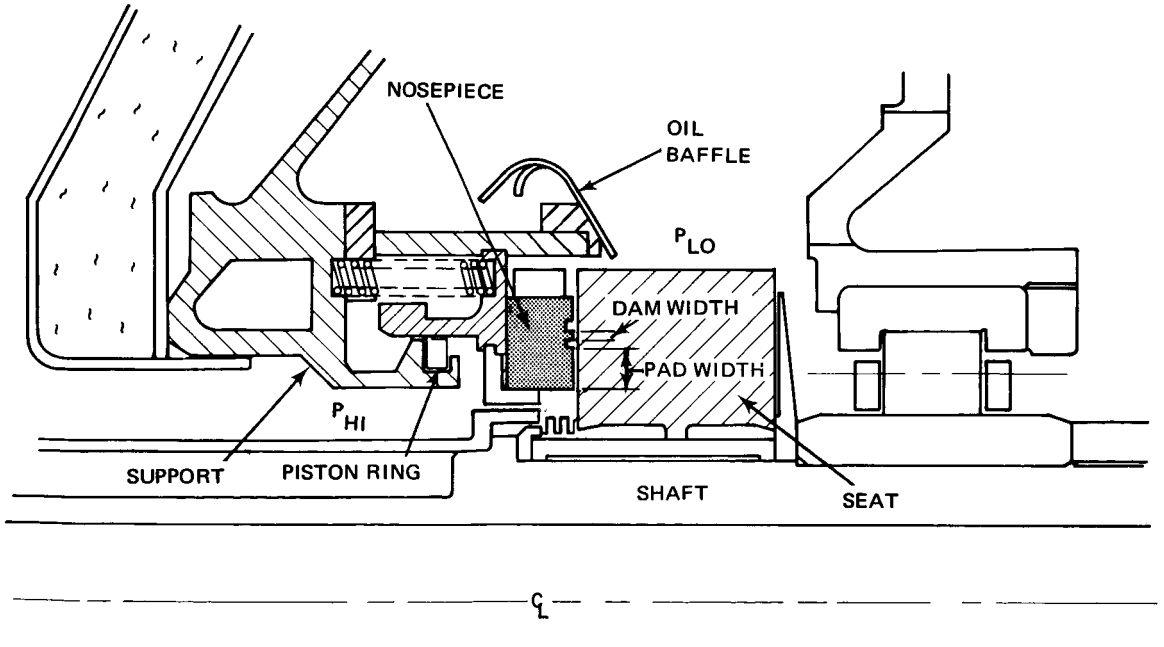

Figure 3 Typical Gas-Film Seal With Self-Acting Rayleigh Step Pads

The general objective of this work was to demonstrate the feasibility of operating the self-acting gas-film seal at advanced engine conditions. Specifically, the objectives were to: (a) determine if the self-acting seal can operate without rubbing contact at pressures to 345 N/cm^2 (500 psi), at speeds to 152.4 m/sec (500 ft/sec) and at temperatures to 922°K (1200°F), (b) measure seal leakage rates, (c) measure operating gas-film thicknesses, (d) determine if the seal can operate at extreme seat runout conditions, and (e) evaluate the effect of air-entrained dirt on seal performance and wear.

The technical program effort under this Contract consisted of seven (7) separate tasks. Task I required the Contractor to conduct a performance analysis on the seal design furnished by NASA establishing a base from which to evaluate experimental leakage results. In the course of the analysis, it was also required to determine whether the design was structurally suitable for testing at the maximum Contract conditions. Under Task II, it was required that the rig used previously under Contract NAS3-7609 be redesigned and modified to allow safe operation at maximum Contract conditions. Task III required the measurement of gas-film thickness under dynamic conditions on the two (2) instrumented seals supplied by NASA.

Elevated temperature tests of the seal analyzed in Task I were required in Task IV. Operating conditions were sliding speeds of 106.7 to 152.4 m/sec (350 to 500 ft/sec), seal differential pressures of 34.5 to 345 N/cm^2 (50 to 500 psi), and sealed gas temperatures from 366 to 922°K (200 to 1200°F). Task V presented reporting requirements. The requirements for Task VI were to conduct experimental evaluation tests on the Task I seal to determine the effects of an axial seat runout between 50.8 and 76.2 microns (2 to 3 mils) on seal performance. This is greater than the normal assembly requirement for conventional seals. In Task VII, the Contractor was required to modify the seal test rig for dirt contamination tests and conduct testing on the Task I seal with contaminate particles of Arizona Road Dust introduced into the seal pressurizing air in sufficient quantity to provide a reasonable test of seal tolerance to contaminates. Elevated temperature endurance testing of the Task I seal was required in Task VIII; the test conditions were seal sliding speeds from 122 to 183 m/sec (400 to 600 ft/sec), seal pressure differentials from 206.8 to 345 N/cm^2 (300 to 500 psi), and sealed gas temperatures from 700 to 922°K (800 to 1200°F).

III. CONCLUSIONS AND RECOMMENDATIONS

Experimental evaluation of the self-acting gas-film seal analyzed under Task I of this Contract revealed the following:

- In general, seal air leakages measured during experimental evaluation were at or slightly below predicted values throughout the operational ranges investigated.
- Successful operation without rubbing contact was demonstrated over the range of conditions investigated, including a maximum pressure differential of 345 N/cm^2 (500 psi), a maximum speed of 152.4 m/sec (500 ft/sec) and a maximum temperature of 922°K (1200°F).
- Successful operation was demonstrated for one (1) hour at 345 N/cm^2 (500 psi) pressure differential across the seal, 152.4 m/sec (500 ft/sec) seal sliding speed, and temperatures of 622 to 811°K (660 to 1000°F)
- Extended endurance capability was demonstrated at elevated temperature levels of 700 to 811°K (800 to 1000°F).
- Endurance capability at a temperature of 922°K (1200°F) was limited by secondary seal piston ring operation and high operating temperatures of the seal carrier.
- Successful operation at the maximum axial seal seat runout of 57.15 microns (2.25 mils) expected in positive-contact face seal applications was demonstrated.
- Stable sealing was obtained at low pressure/high speed combinations with maximum seat runout by increasing the total spring force from 81.4N (18.25 lb) to 138.3 N (31.0 lb).
- Satisfactory seal operation was demonstrated during testing with air-entrained dirt.
- The "thin section" seal seat distorted unacceptably when installed on the test rig hub, apparently due to torque loads induced by the locking nut at assembly.

A. CONCLUSIONS

In consideration of the above observations the following conclusions can be made:

- The design system for predicting seal air leakage is acceptable since measured values were in general slightly lower than predicted.
- The seal should operate satisfactorily under the conditions of axial seat runout and dirt ingestion anticipated in normal engine operation.
- Piston ring design and effective seal carrier cooling must be developed to extend the seal's elevated temperature endurance capability.

- Further investigation is necessary to determine the cause of distortion on the "thin section" seal seat.

- Further effort is necessary to determine optimum seal spring loading which will allow stable seal operation at maximum seat runout over the entire range of pressure/speed combinations investigated.

B. RECOMMENDATIONS

Based on the above conclusions, the Contractor recommends the following:

Alternate piston ring designs should be analyzed and experimentally evaluated as part of the development of gas-film seals for elevated temperature locations in gas turbine engines. In addition, schemes to reduce seal carrier operating temperature should be analyzed and evaluated.

IV. SEAL DESIGN ANALYSIS (TASK I)

Task I specified that a design analysis be performed on the seal concept shown on NASA drawing CF 849668. A cross section view of that seal is presented in Figure 4. The features of the primary seal face, including the Rayleigh pads, are unchanged from those of the "wide pad seal" previously studied under Contract NAS3-7609 and described in NASA Report CR-72987 (Reference 1). Modifications to the overall seal design were required, however, to permit the seal to be evaluated at more extreme test conditions. The seal design analysis was done in three steps:

1) Performance Analysis Without Consideration of Distortion Effects – The analysis resulted in generation of film load capacity curves over the full range of operational conditions anticipated under experimental portions of this program.

2) Mechanical Design Analysis – The structural behavior of the seal due to thermal, mechanical, and pressure loads was analyzed using heat generation and temperature data developed under Contract NAS3-7609.

3) Performance Analysis Corrected For Distortion Effects – Primary seal face performance was predicted considering the effects of nosepiece, carrier, and seal seat distortion on film thickness.

As a result of this design analysis the following five (5) modifications to this seal design were recommended to NASA for incorporation into the test seal hardware to be supplied for Tasks IV and VI through VIII.

1) Increase spring force to 111 N (25 lb) to provide sufficient gas film stiffness at maximum speed.

2) Chamfer the inner edge of the carrier or relieve the rear side of the carbon so that the clockwise tilt of the carrier will not cause separation between the nosepiece and carrier. This rotation would be caused by operation at maximum temperature and pressure.

3) Specify a radius greater than 0.038 cm (0.015 in) at the corners of the two key slots in the seal seat to reduce the stress concentration.

4) Design piston ring to minimize the effect of thermal coning of the support.

5) Specify material having a low coefficient of thermal expansion for the carrier to reduce the relative thermal growth between the carrier and the nosepiece.

The specific details of the mechanical design and seal performance analysis are presented in the following sections.

A. PERFORMANCE ANALYSIS WITHOUT DISTORTION EFFECTS

The steady-state axial forces in the seal nosepiece and carrier are shown in Figure 5. The mean film thickness was found by equating the opening forces with the closing forces:

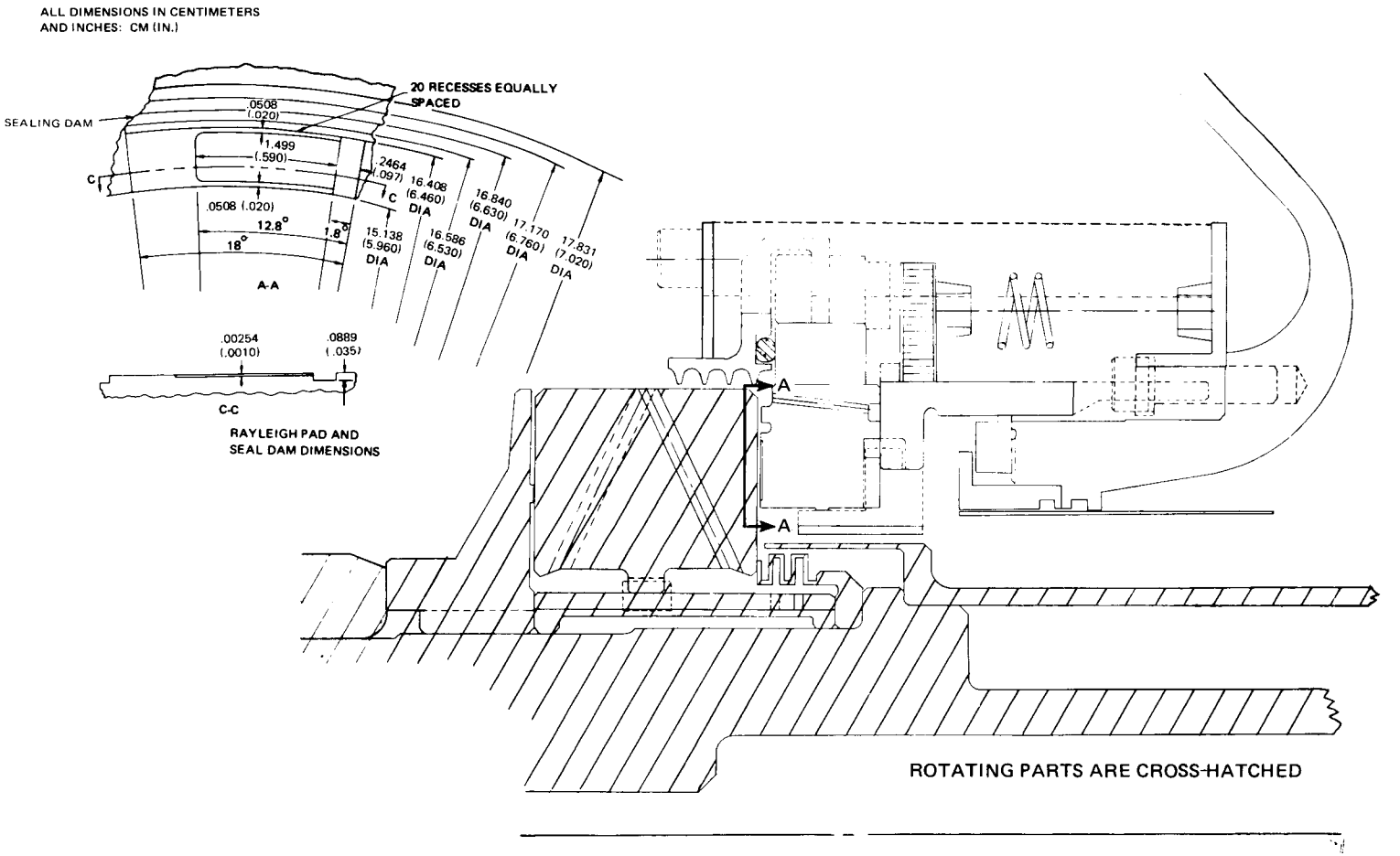

Figure 4 Gas-Film Seal Design Shown on NASA Drawing CF-849668

$$F_P + F_D = F_B + F_S \qquad \text{(Equation 1)}$$

where: F_P = Rayleigh pad load capacity
F_D = Seal dam load capacity
F_B = Hydraulic balance force
F_S = Spring force

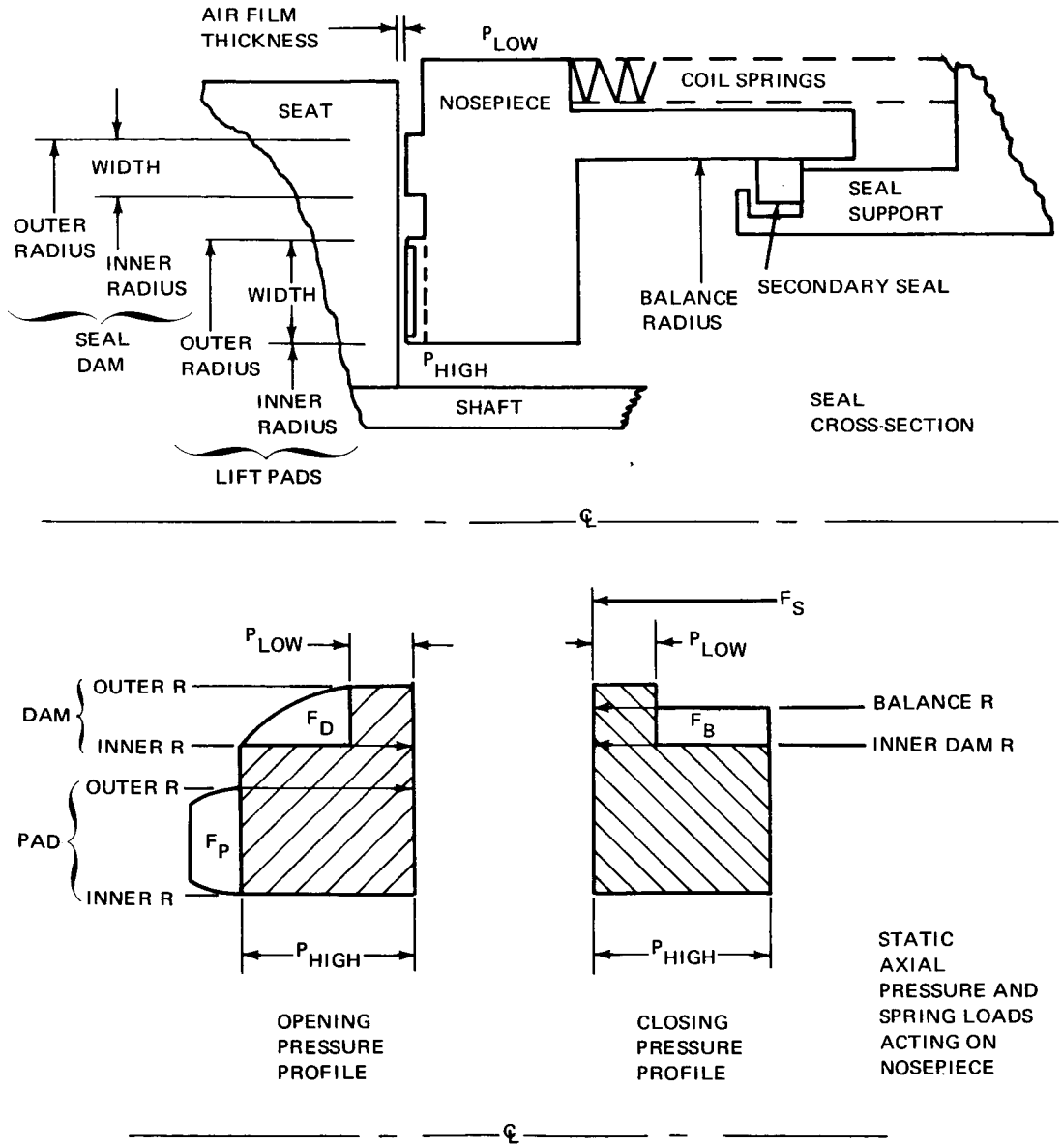

Figure 5 Schematic Diagram of the Steady-State Forces Acting on the Nosepiece and Seal Seat. Forces Represented by the Cross-Hatched Regions of the Axial Pressure Profiles are Equal and Opposite, and Therefore Omitted from the Equation

The operating characteristics of the twenty (20) Rayleigh pads machined into the nosepiece surface were determined with the aid of the computer program described in Appendix B of Reference 2.

The Rayleigh pad load capacity (F_p of Equation 1) is shown in Figures 6 and 7 as a function of film thickness and surface speed at film temperatures of 366°K (200°F) and 700°K (800°F), respectively. Nominal surface speeds from 107 m/sec (350 ft/sec) to 183 m/sec (600 ft/sec) were considered using the seal balance diameter to calculate the nominal surface speed. Table 1 shows the nominal surface speeds, corresponding surface speeds at the Rayleigh pad mean diameter, and the shaft speeds considered in the analysis.

TABLE I

ANALYSIS CONSIDERATIONS

Nominal Surface Speed @ Balance Diameter		Surface Speed @ Rayleigh Pad Mean Diameter		Shaft Speed	
m/sec	(ft/sec)	m/sec	(ft/sec)	rad/sec	(rpm)
107	(350)	100	(329)	1,272	(12,150)
122	(400)	115	(376)	1,454	(13,890)
137	(450)	129	(423)	1,636	(15,630)
152	(500)	143	(470)	1,818	(17,365)
183	(600)	172	(565)	2,181	(20,835)

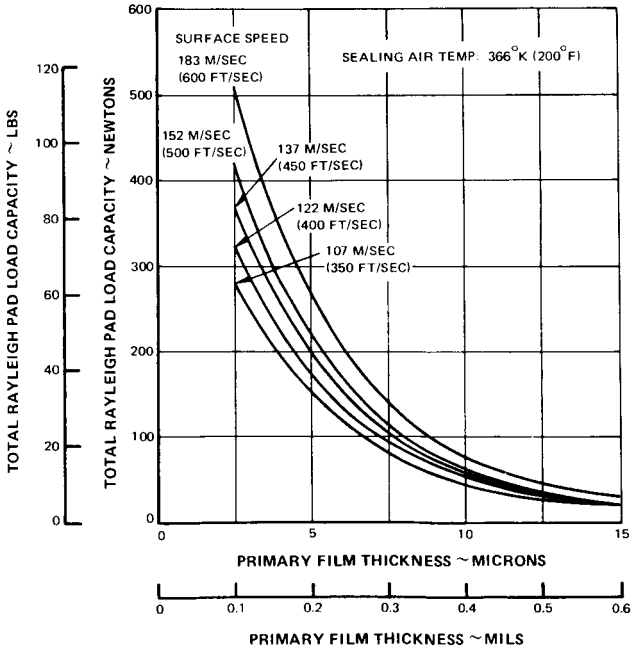

Figure 6 Rayleigh Pad Load Capacity Versus Primary Film Thickness

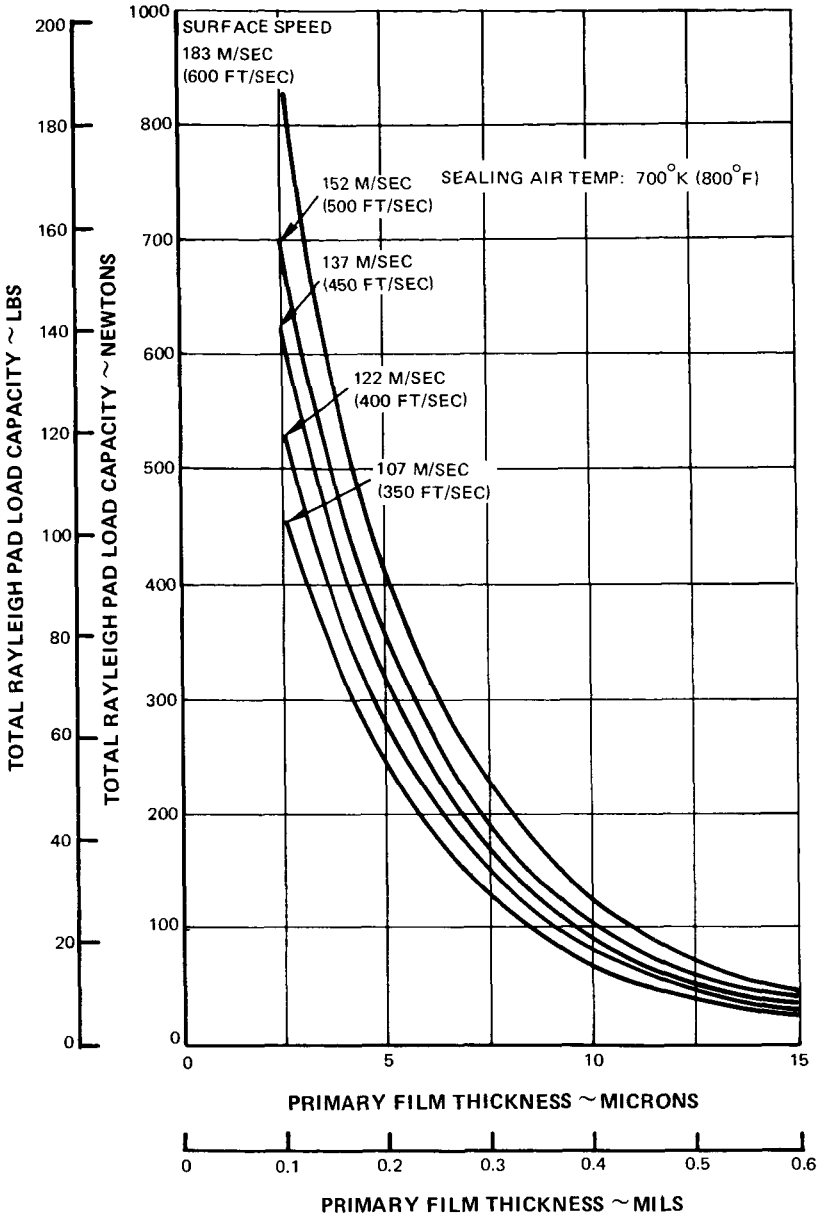

Figure 7 Rayleigh Pad Load Capacity Versus Primary Film Thickness

Air temperatures of 366°K (200°F) and 700°K (800°F) were used because they represent the temperature in the gas-film at room temperature and 922°K (1200°F) operating conditions, respectively.

The computer program described in Reference 3 was used to determine seal dam load capacity (F_D of Equation 1). Curves of load capacity versus film thickness were calculated for seal differential pressures from 34.5 N/cm^2 (50 psi) to 345 N/cm^2 (500 psi) and are shown in Figure 8. The slight increase in load capacity with the increasing film thickness, more evident at the high pressures, is indicative of the transition in flow regimes from laminar to turbulent.

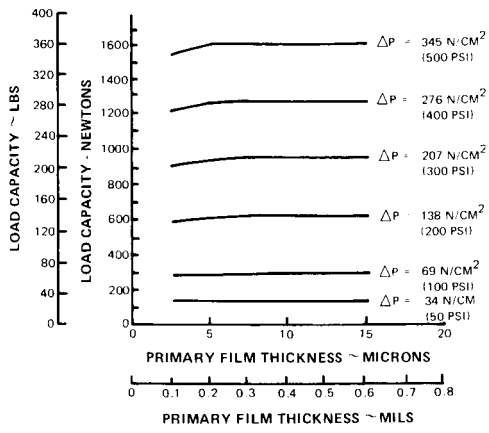

Figure 8 Seal Dam Load Capacity Versus Primary Film Thickness

The hydraulic balance load (F_B of Equation 1) is the force resulting from the pressure differential across the seal, and was calculated by multiplying the seal pressure drop by the annular area between the inner edge of the seal dam and the balance diameter of the secondary seal. Table II defines the hydraulic balance force and the total closing force for two separate values of spring force.

TABLE II

HYDRAULIC BALANCE FORCE AND TOTAL CLOSING FORCE

Pressure Differential		Hydraulic Balance Force (F_B)		Total Closing Force ($F_B + F_S$) with 111 N (25 lb) Spring Force (F_S)		Total Closing Force ($F_B + F_S$) With 75 N (17 lb) Spring Force (F_S)	
N/cm^2	(psi)	N	(lb)	N	(lb)	N	(lb)
345	(500)	1,618	(360.9)	1,729	(385.9)	1,694	(377.9)
276	(400)	1,294	(288.7)	1,405	(313.7)	1,370	(305.7)
207	(300)	970	(216.5)	1,081	(241.5)	1,046	(233.5)
138	(200)	647	(144.4)	758	(169.4)	743	(161.4)
69	(100)	323	(72.2)	434	(97.2)	399	(89.2)
34	(50)	162	(36.1)	273	(61.0)	238	(53.1)

To determine the operating film thickness, the total closing force ($F_B + F_S$) can be cross-plotted against the total seal opening force ($F_P + F_D$) for a given set of conditions. Figure 9 is a typical example for a specific set of conditions.

Primary seal air leakage was found as a function of film thickness by the same compressible fluid flow program used to determine the seal dam load capacity. Figures 10 through 13 are plots of air leakage as a function of film thickness. Cross-plotted over the leakage curves are the operating film thicknesses, for constant operating speeds, as determined from the seal force balance calculations for two values of spring force. The larger spring force decreases the primary film thickness resulting in an increase in the primary film stiffness.

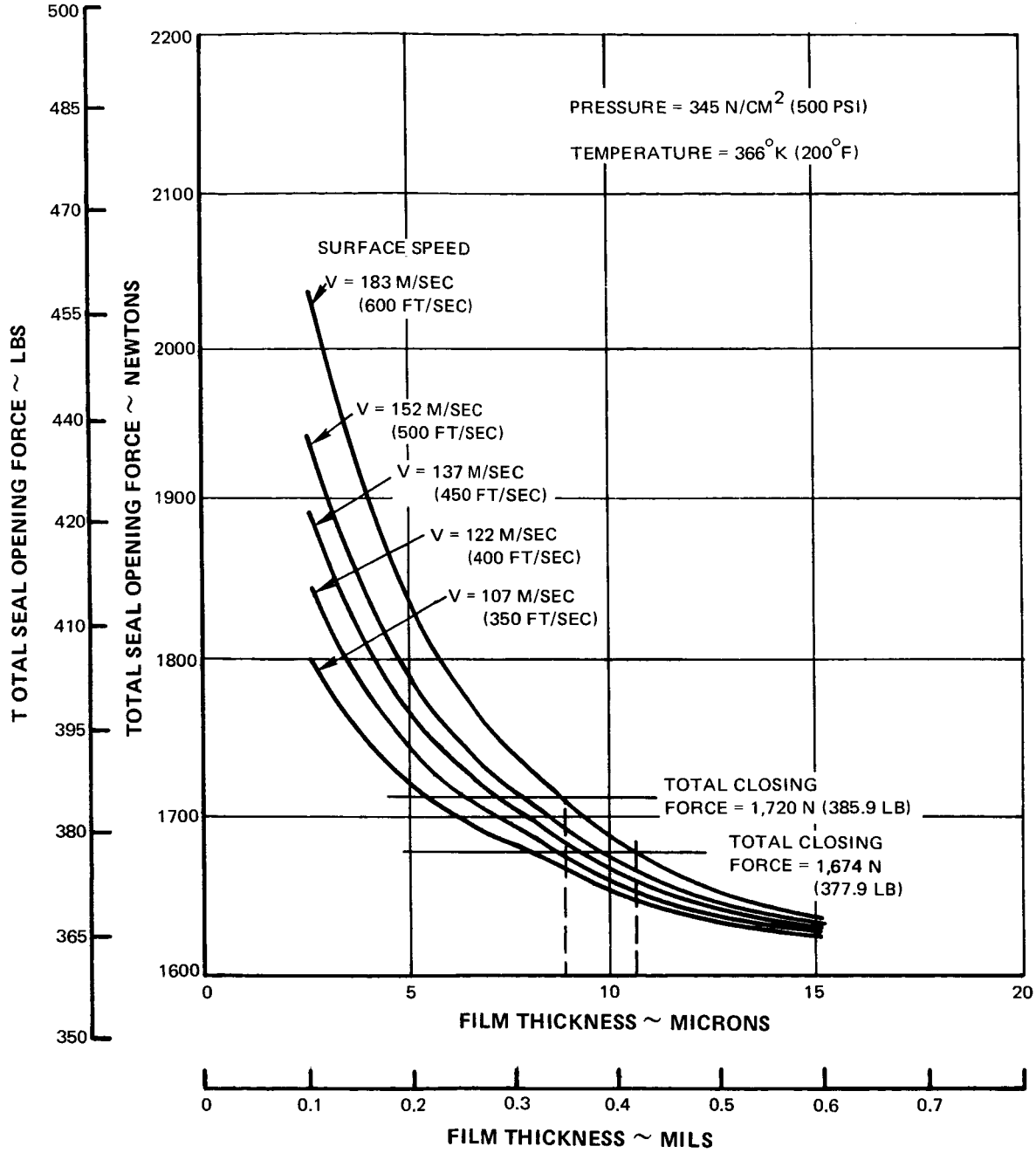

Figure 9 Typical Seal Force Balance Diagram

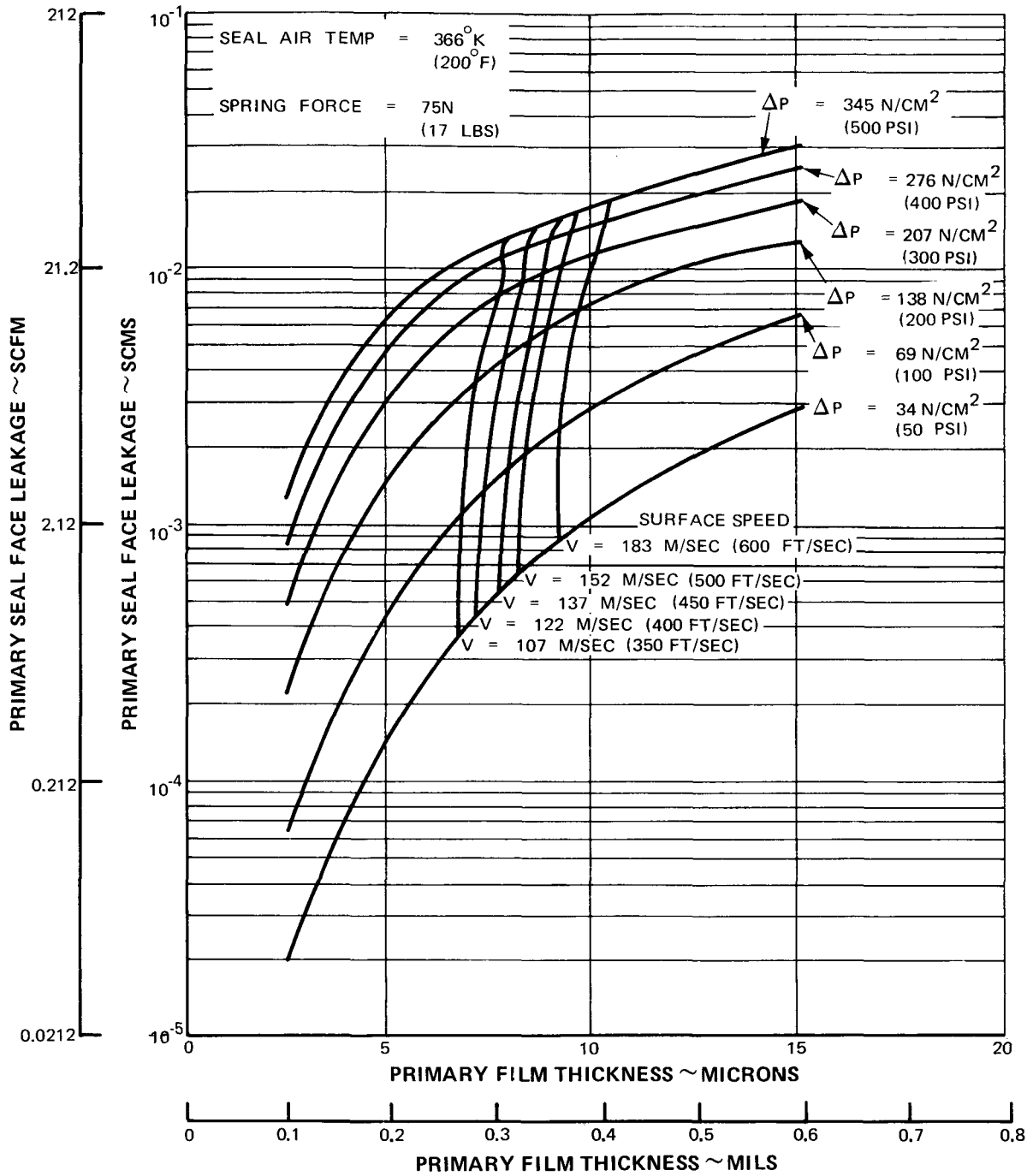

Figure 10 Primary Seal Face Leakage Versus Primary Film Thickness

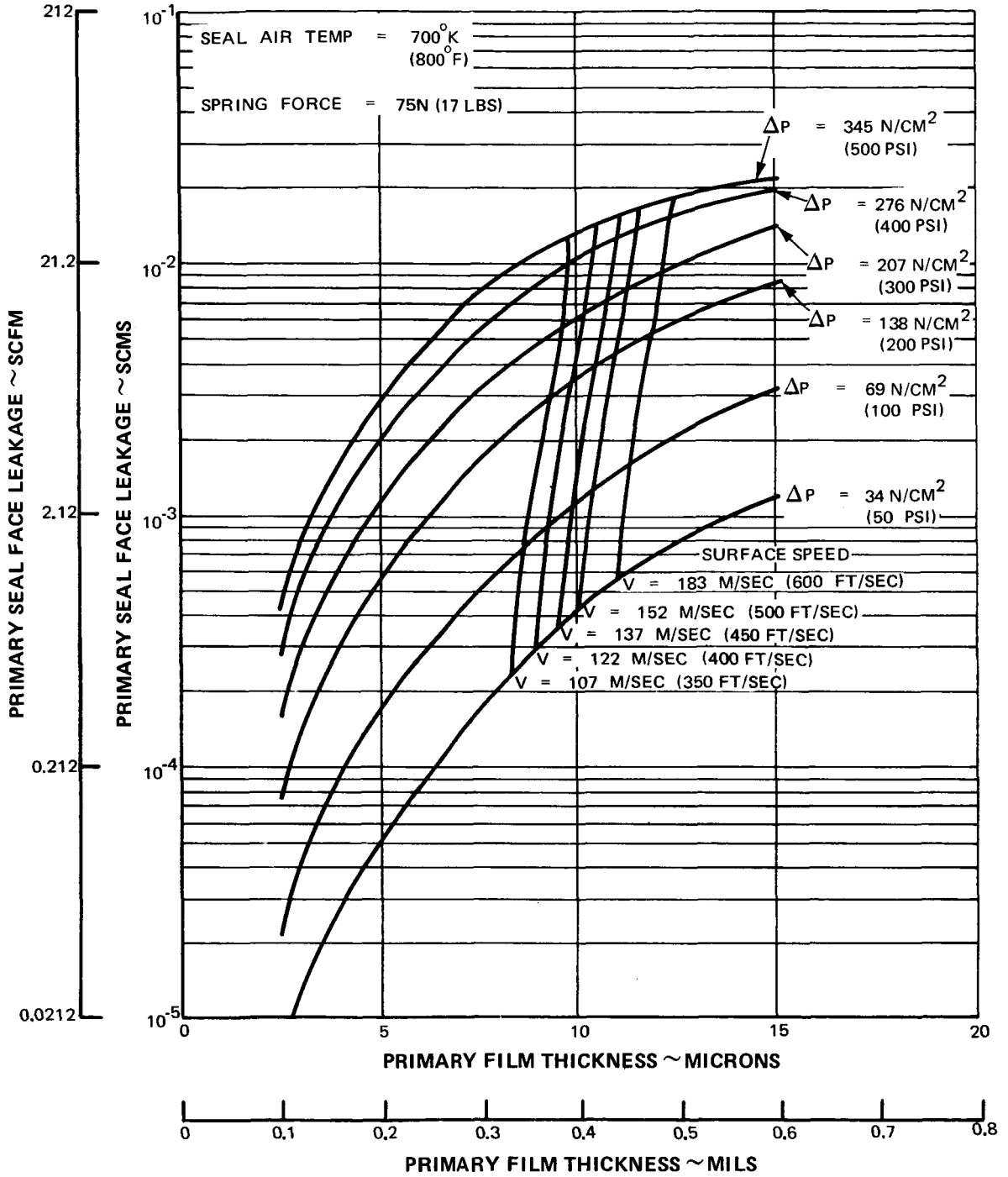

Figure 11 Primary Seal Face Leakage Versus Primary Film Thickness

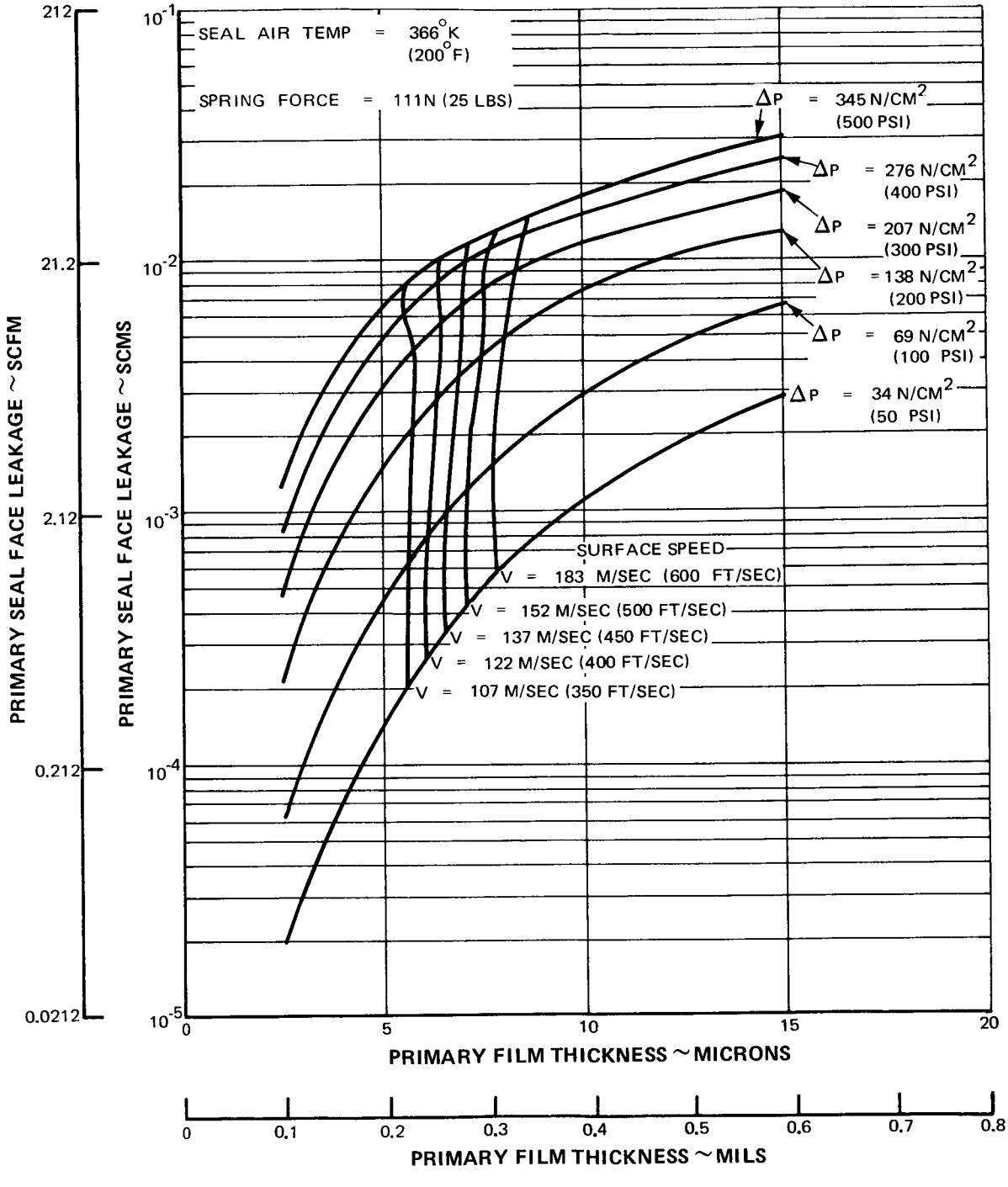

Figure 12 Primary Seal Face Leakage Versus Primary Film Thickness

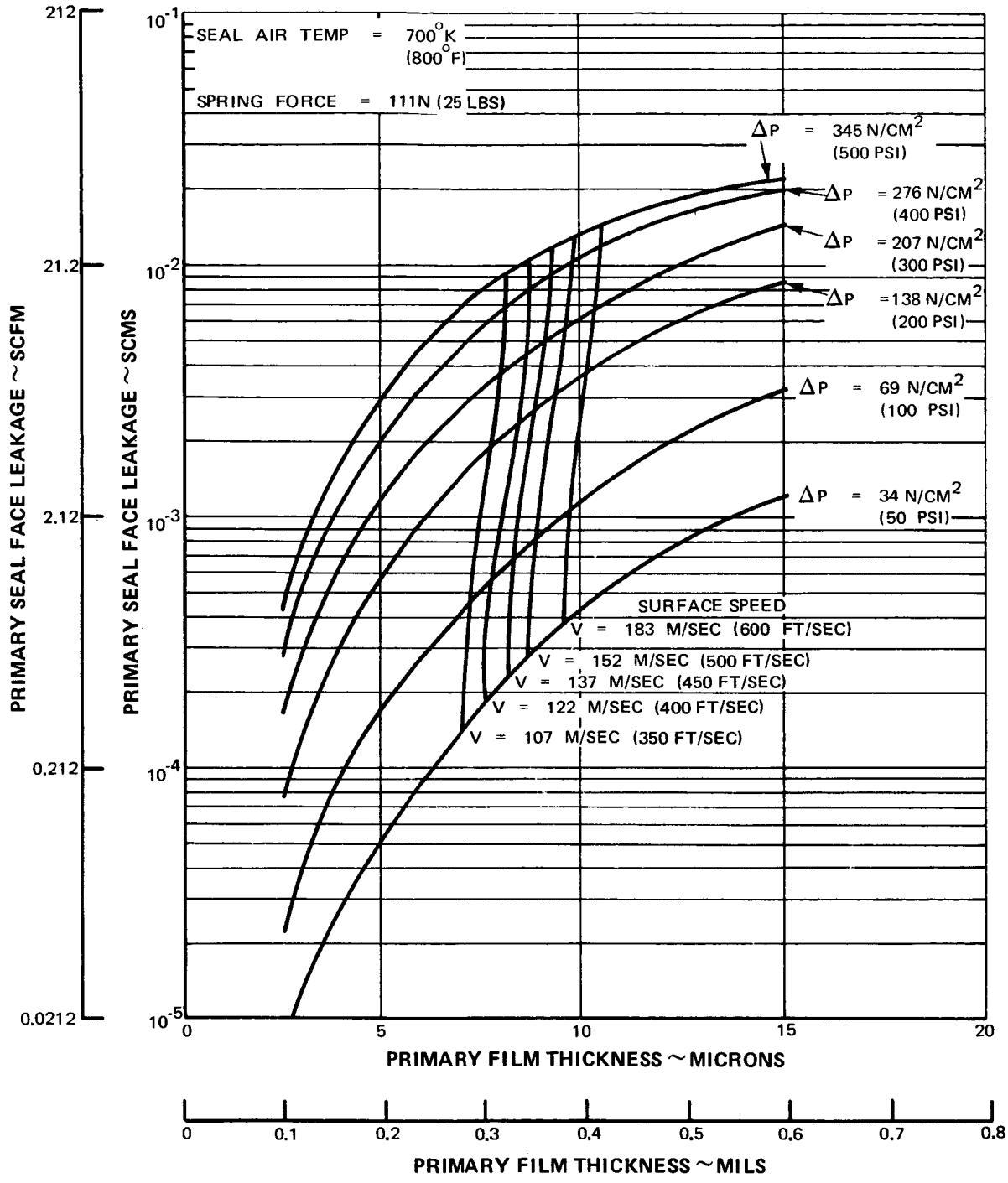

Figure 13 Primary Seal Face Leakage Versus Primary Film Thickness

This stiffness controls responses of the nosepiece to dynamic runout of the seal seat. With a stiffer film, smaller dynamic changes in film thickness will occur. Dynamic analysis of the nosepiece has shown that with a 25.4 micron (1 mil) axial seal seat runout, a gas-film stiffness of less than 175,000 N/cm (100,000 lb/in) can result in a dynamic change in film thickness exceeding the nominal operating film thickness, resulting in seal contact. For the NASA seal design at 345 N/cm^2 (500 psi), 183 m/sec (600 ft/sec), and 75 N (17 lb) spring force, the film stiffness was 140,000 N/cm (80,000 lb/in); this allows a 12.7 micron (0.5 mil) dynamic change in film thickness. For the undamped dynamic model, contact occurs since the nominal operating film thickness is 12.57 microns (0.495 mils), therefore, the 111 N (25 lb) spring force was recommended which results in a smaller operating film thickness, but a higher than adequate film stiffness and operation without rubbing contact is predicted over the full range of conditions shown in Figures 12 and 13.

B. SEAL MECHANICAL DESIGN ANALYSIS

Analysis of nosepiece and carrier distortion was done with the aid of a 3 dimensional finite element stress analysis computer program named "ASKA", described in Appendix A. The program has the option of connecting one part to another part in a selected direction while leaving the parts free to move, relative to each other, in the other two coordinate directions.

Figure 14 shows the analytical model of the nosepiece and carrier assembly. The nosepiece is subsystem one and the carrier is subsystem two. The subsystems are connected by specifying that node 50 in subsystem one and node 1 in subsystem two are rigidly attached in the axial direction only. This type of connection ensures that the radial deflection of each subsystem will be independent of the other. Also, the subsystems are free to tilt independently, but the carrier must have a clockwise tilt relative to the nosepiece if the connection is to represent the truepoint of contact.

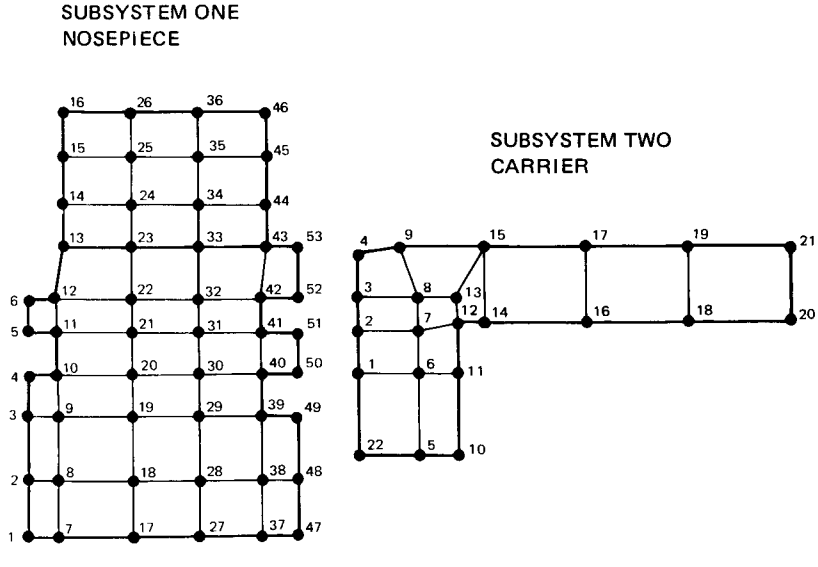

Figure 14 Analytical Model of Nosepiece and Carrier Assembly

The separate and combined effects of pressure and temperature on nosepiece and carrier displacements were examined. The axial forces applied were the forces identified in the force balance analysis (pad load, seal dam load, spring force, and balance load) at the maximum speed and pressure conditions. Radial pressure loading was applied to the inner diameter of the nosepiece and carrier except for the interval between node 18 and node 20 on the carrier. Node 18 is the point at which the secondary seal contacts the carrier and produces a sharply defined boundary on the pressure load.

Figure 15 shows the resulting tilt of the nosepiece and carrier, due only to pressure loads. For the room temperature and high pressure condition, the initial assumption of clockwise carrier tilt relative to the nosepiece was not borne out by the calculations, indicating that the carrier nosepiece contact point is at a larger radius. The exact contact point, for this case, was not determined since it is an iterative and lengthy procedure, but analysis showed the effect of a larger contact radius is to reduce the unbalance moments on the nosepiece and to reduce the nosepiece tilt angle to equal the carrier tilt angle.

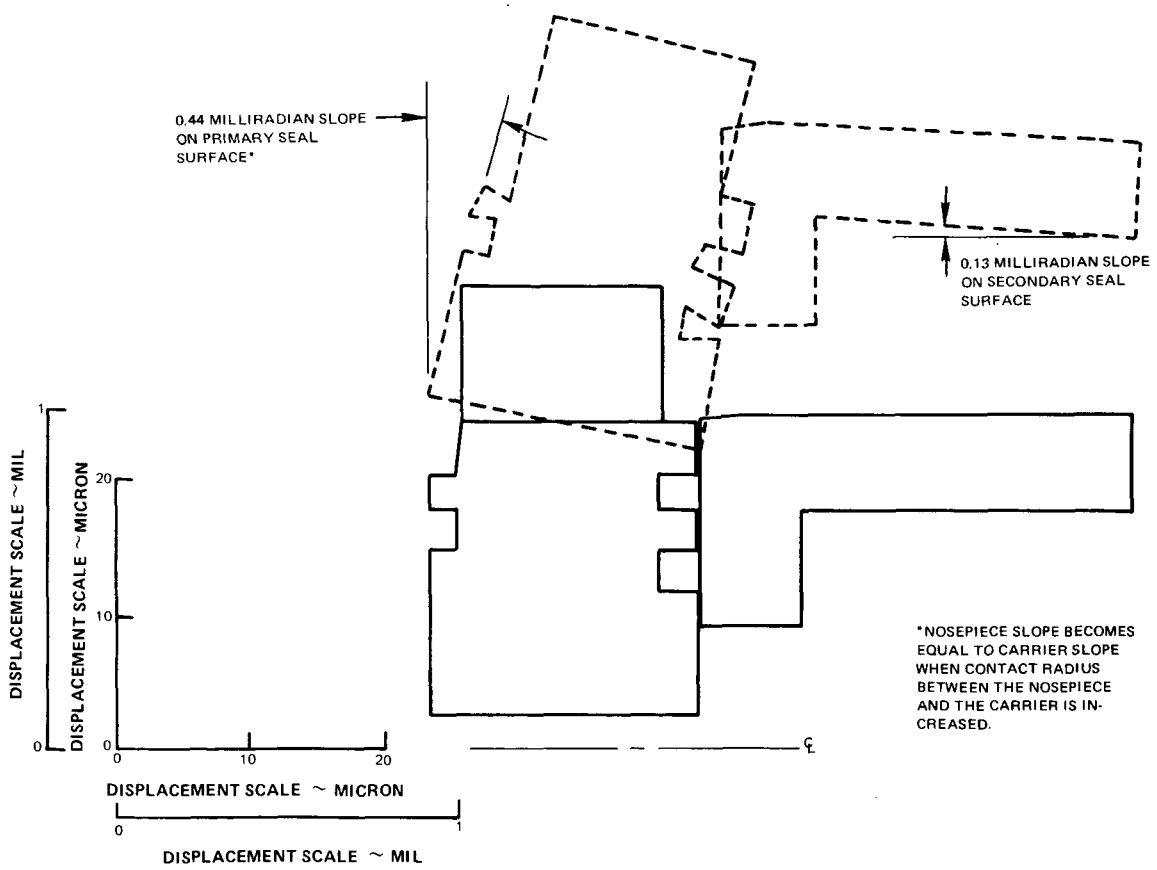

Figure 15 Nosepiece and Carrier Displacements Due to Pressure Loading [Seal Differential Pressure of 345N/cm^2 (500 psi)]

Figure 16 shows the effect of high temperature operation on nosepiece and carrier distortion. Temperature distribution was based upon the information published in the Phase II Final Report for Contract NAS3-7609 (NASA CR-72737). The displacement diagram predicts a large radial growth and a large clockwise slope of the carrier relative to the nosepiece. Carrier thermal displacements are significantly larger than nosepiece displacements because the carrier material has a relatively high expansion rate and the carrier temperatures (particularly in the flange adjacent to the nosepiece) are higher than nosepiece retaining ring temperatures.

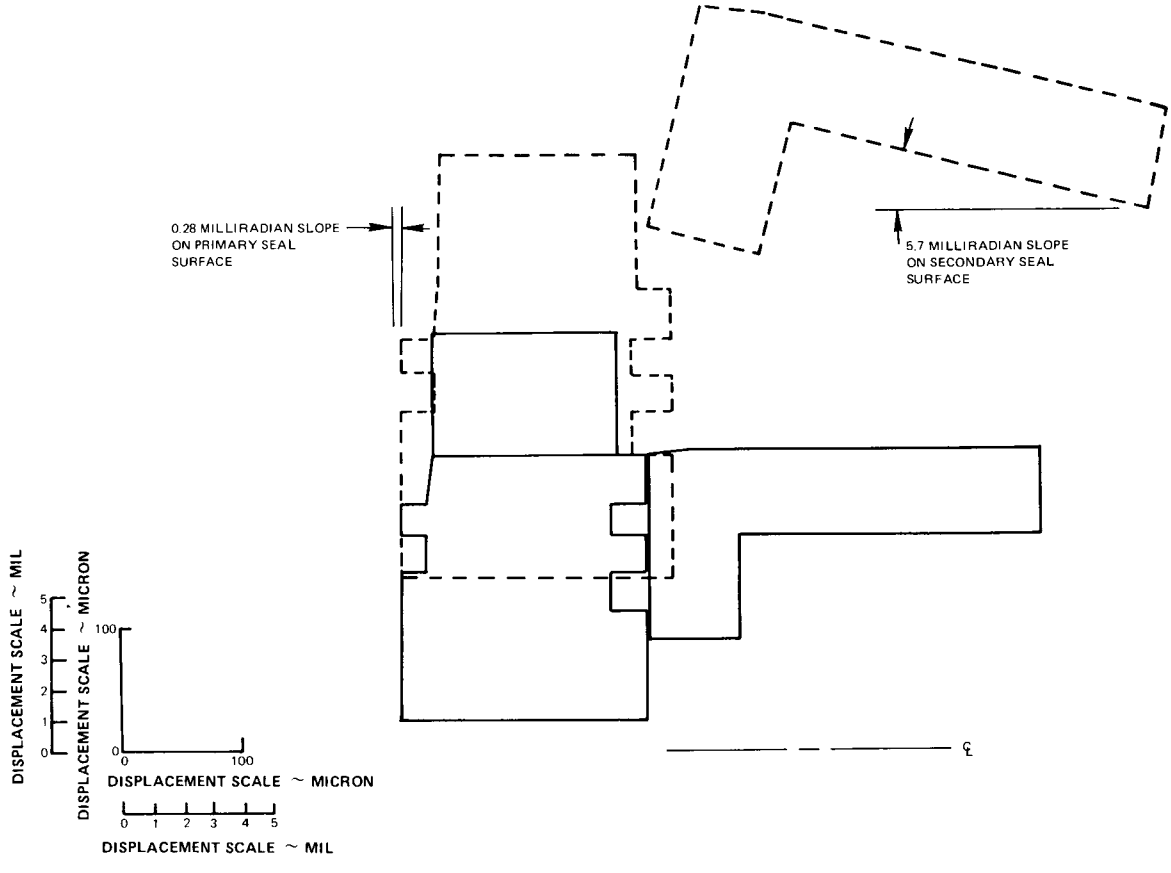

Figure 16 Nosepiece and Carrier Displacements Due to Temperature Loading [Gas temperature of 922°K (1200°F)]

The displacement diagram shown in Figure 17 predicts the effects of simultaneous high pressure and high temperature operation on nosepiece and carrier displacements. The results of this analysis indicate that the 0.44 milliradian clockwise tilt of the nosepiece due to pressure loading is added to the 0.28 milliradian tilt due to thermal effects to produce a total slope of 0.72 milliradian on the nosepiece sealing surface. Thermal displacements of the carrier limit contact between the carrier and the nosepiece to the node 1 - node 50 location. The nosepiece tilt due to pressure is not restrained by the carrier as it was in Figure 15.

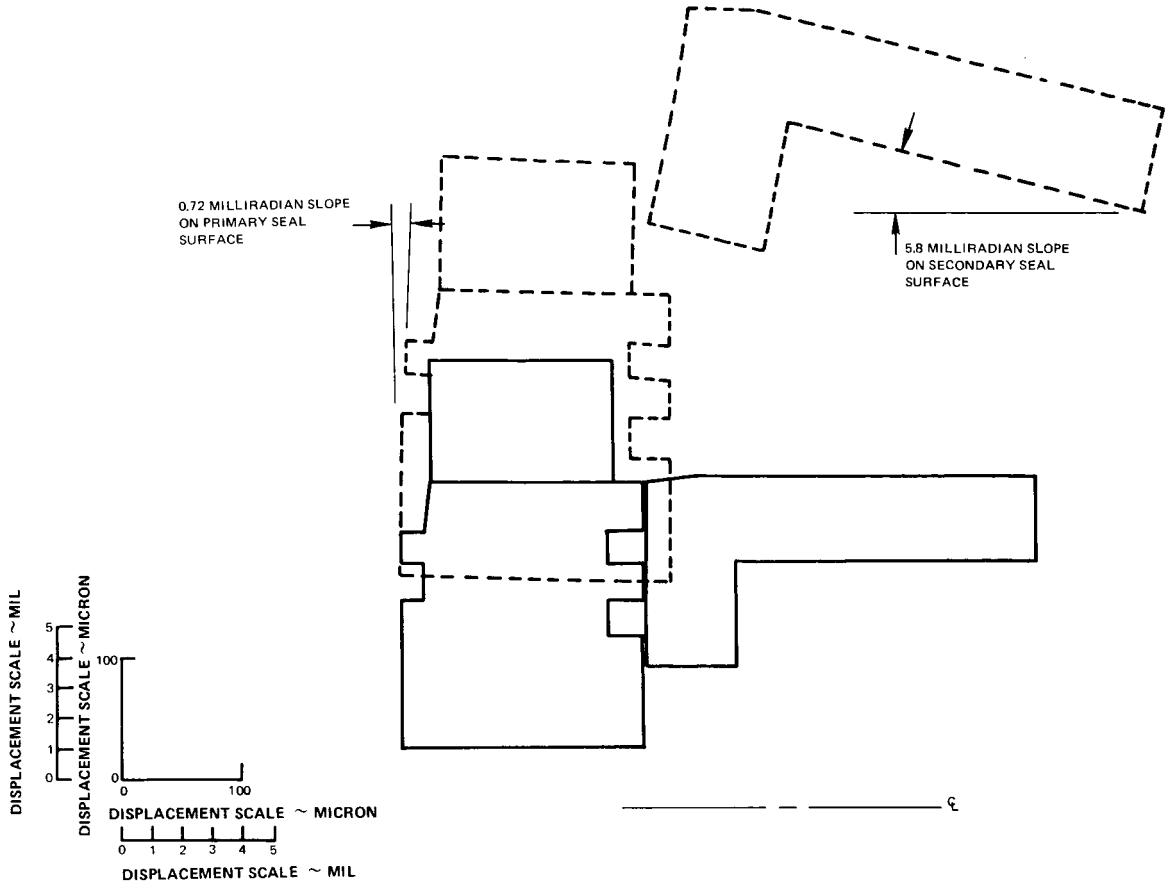

Figure 17 Nosepiece and Carrier Displacements Due to Pressure and Temperature Loading [Seal Differential Pressure of 345N/cm^2 (500 psi), Gas Temperature of 922°K (1200°F)]

The inner edge of the carrier (identified as node 22 in subsystem 2) needed to be chamfered as shown in Figure 18. This modification was recommended so that clockwise tilt of the carrier would not cause separation between the carrier and the nosepiece at the node 1 - node 50 connection which is the inner edge of the sealing surface between the two parts. As an alternate method of modification, the rear side of the carbon could be relieved.

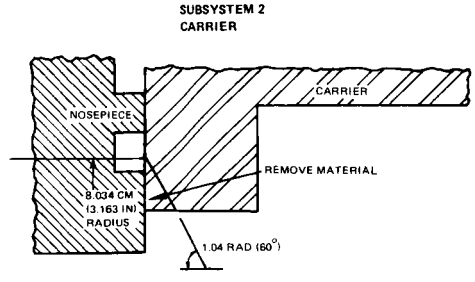

Figure 18 Carrier Modification

The individual and combined effects of axial clamping, centrifugal and pressure loading, and high temperature operation on seal seat dimensional changes were calculated and the results are shown in Figure 19, 20 and 21.

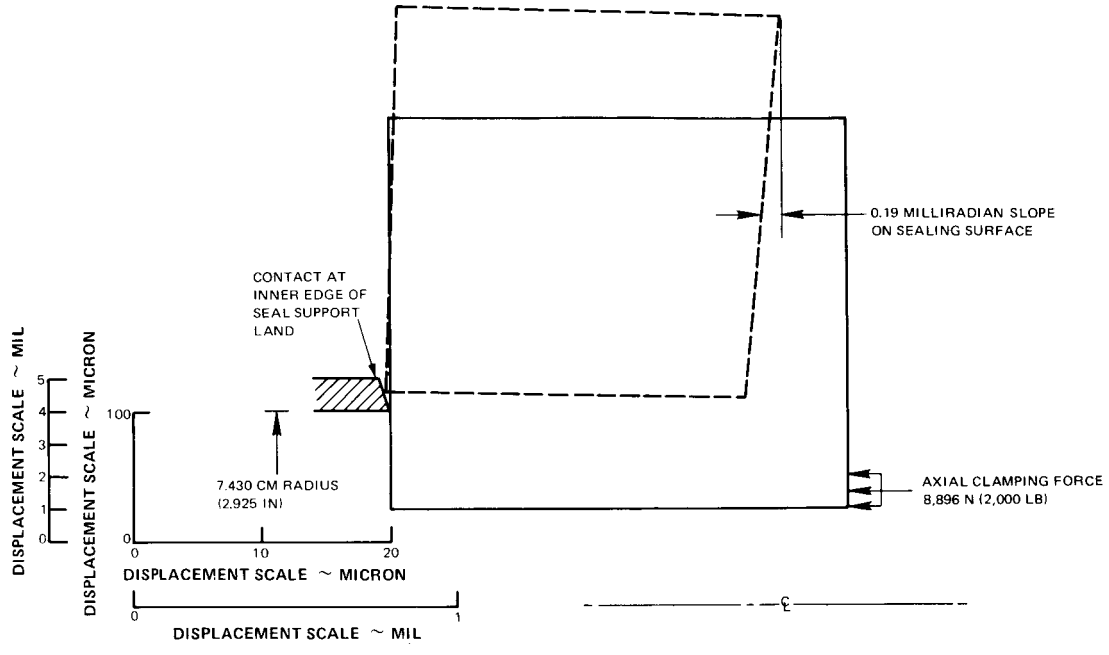

Figure 19 Seal Seat Displacement Due to Clamping Force and Centrifugal Loading [Axial Clamping Force of 8,896 N (2,000 lb), Seal Surface Speed of 183 m/sec (600 ft/sec)]

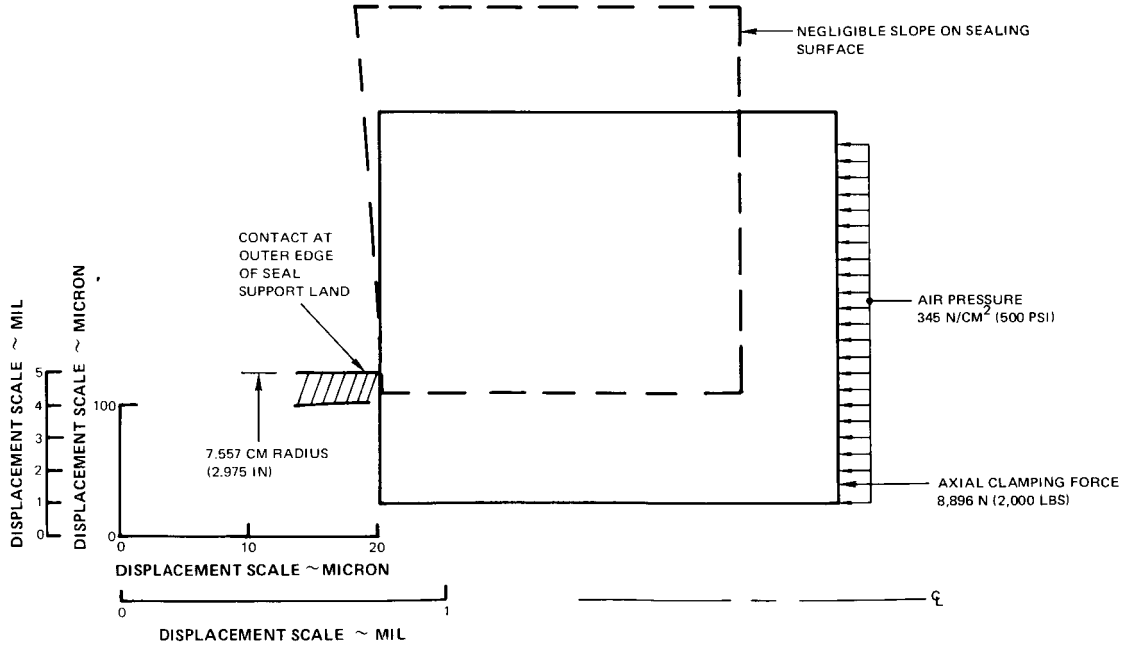

Figure 20 Seal Seat Displacement Due to the Clamping Force, Centrifugal Loading, and Pressure Loading [Ambient Temperature Gas, Seal Surface Speed of 183 m/sec (600 ft/sec)]

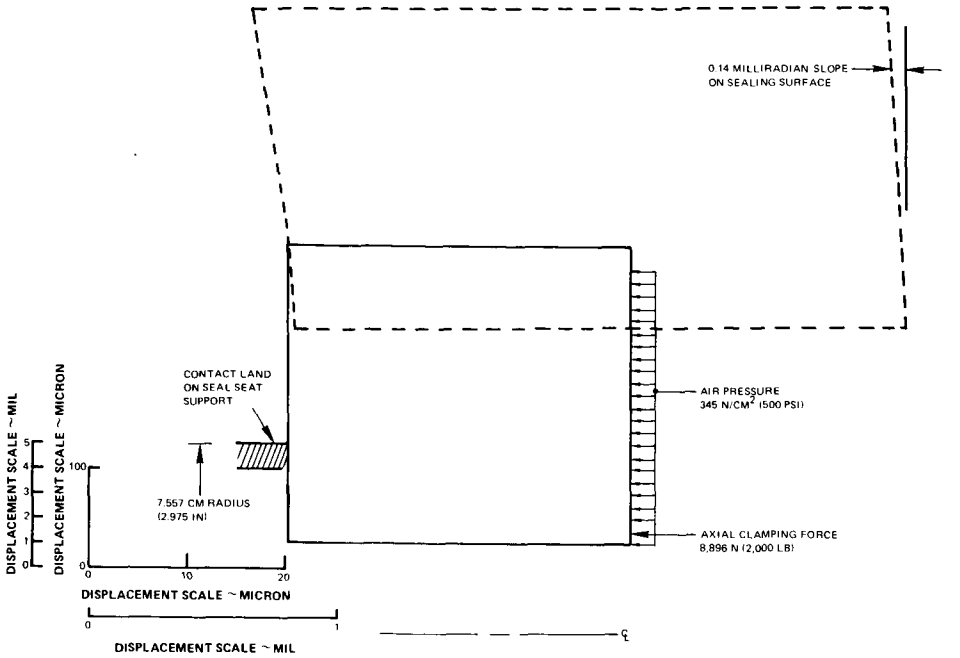

Figure 21 Seal Seat Displacement Due to the Clamping Force, Centrifugal Load, Pressure Load, and Temperature Loading [Thermal Growth Effects are Included, Seal Surface Speed of 183 m/sec (600 ft/sec)]

The seal seat is positioned in the axial direction by a support ring with a contact land which is 0.127 cm (0.050 in) wide [inside and outside diameters are 14.86 cm (5.85 in) and 15.11 cm (5.95 in), respectively]. The true contact radius, however, varies with the direction of tilt of the seal seat relative to the support land. For example, clockwise tilt of the seal seat would cause seal seat contact at the inner edge of the support land. Changes in contact position on the support land alter the moment loads on the seal seat.

Figure 19 shows that the clamping force and centrifugal load cause a clockwise tilt of the seal seat with an angular displacement of the sealing face of 0.19 milliradian. This condition is produced by high speed, low pressure, and low temperature operation of the seal.

When the pressure differential across the seal is raised to 345 N/cm^2 (500 psi) a change in angular displacement of 0.19 milliradians (counter clockwise) occurs, resulting in a negligible tilt of the sealing surface and a small counter clockwise tilt at the support land. Figure 20 illustrates the resulting seal seat displacements under high speed, high pressure, and low temperature conditions.

Figure 21 represents the combined effects of high speed, high pressure, and high temperature when the seal seat operating temperature distribution is as shown in the Phase II final report for Contract NAS3-7609 (NASA CR-72737). Thermal gradients in the nosepiece cause the seal seat to tilt 0.14 milliradians in the counter clockwise direction.

The seal seat displacements shown in Figures 20 and 21 occur when the support land angular displacement is negligible so that the seal seat is loaded against the outer edge of the land. If

axial loads on the support cause a counter clockwise tilt of the land surface large enough to limit contact to the inner edge of the land, then a 0.28 milliradian counter clockwise tilt angle must be added to the results shown in Figures 20 and 21.

For the combined loading case, a tangential or hoop stress of 35,800 N/cm^2 (52,000 psi) is found at the inner surface of the seal seat. The primary cause of this stress is the centrifugal load. This stress would be allowable on a smooth surface since the yield strength of the seal seat material, TZM, at 589°K (600°F) is 68,900 N/cm^2 (100,000 psi). However, a stress concentration is created by the sharp corners at each of the two key slots. An acceptable safe limit for the stress concentration factor is 1.5, which would then give a maximum stress of 53,700 N/cm^2 (78,000 psi). A generalized formula for tensile loading is applied to find the minimum allowable fillet radius for a maximum stress concentration factor of 1.5.

$$k = \sqrt{.5\,\frac{d}{r} + .85 + .08} \qquad \text{(Equation 2)}$$

where k = Stress Concentration Factor
d = Width of Minimum Section
r = Fillet Radius

Since k = 1.5, d = 0.0825 cm (0.032 in)
r $\geqslant$ 0.0353 cm (0.0139 in)

It was recommended that the key slot minimum corner radius be increased from 0.013 cm (0.005 in) to 0.038 cm (0.015 in).

C. PERFORMANCE ANALYSIS CORRECTED FOR DISTORTION EFFECTS

The extreme operating conditions projected for Contract testing cause seal component distortions which have significant effects on seal performance. The sealing surface tilt angles shown in Figures 17 and 21 cause the seal dam film thickness to be 4.57 microns (0.18 mil) greater than the Rayleigh pad mean film thickness at 345 N/cm^2 (500 psi). Radial growth of the carrier balance diameter relative to the nosepiece seal dam raises closing forces and decreases the mean film thickness at the Rayleigh pad.

Table III shows the corrected total closing forces with a 111 N (25 lb) spring force.

TABLE III

CORRECTED TOTAL CLOSING FORCES WITH A 111 N (25 LB) SPRING FORCE

Pressure Differential		Initial Hydraulic Balance Force (F_B)		Corrected Hydraulic Balance Force (F_B)		Corrected Total Closing Force	
N/cm^2	(psi)	N	(lbs)	N	(lbs)	N	(lbs)
345	(500)	1,618	(360.9)	1,909	(425.95)	2,021	(450.95)
276	(400)	1,294	(288.7)	1,527	(340.76)	1,638	(365.76)
207	(300)	970	(216.5)	1,146	(255.57)	1,257	(280.57)
138	(200)	647	(144.4)	764	(170.38)	875	(195.38)
69	(100)	323	(72.2)	382	(85.19)	493	(110.19)
35	(50)	162	(36.1)	191	(42.59)	302	(67.59)

Seal dam load capacity was assumed to be unaltered by changes in film thickness or tilt angle (i.e., the flat portions of the curves in Figure 8 were used in the force balance equation). The force balance equation was solved for Rayleigh pad loading and the mean Rayleigh pad film thickness was found in Figure 7. With the seal in the tilted portion, the film thickness at the Rayleigh pad is different from that at the seal dam. To determine primary seal leakage, which is related to seal dam film thickness, a relation between Rayleigh pad film thickness and seal dam film thickness must be established. From the nosepiece distortion study, it was determined that the film thickness increment is 4.57 microns (0.18 mils) at 345N/cm^2 (500 psi). This film thickness increment varies linearly with pressure such that at zero pressure differential there would be no seal tilt and therefore no film thickness increment. The seal dam film thickness is determined by adding the specific film thickness increment to the previously determined Rayleigh pad film thickness. These seal dam thicknesses are cross-plotted on the seal leakage curves resulting in the seal performance map shown in Figure 22.

Film thickness at the inner edge of the Rayleigh pads is 7.10 microns (0.28 mils) less than the seal dam film thickness. Minimum operating film thickness was found by subtracting 7.10 microns (0.28 mils) from the values shown in Figure 22. The curves indicate that at maximum pressure and temperature conditions the operating film thickness at the inner edge of the seal approaches zero as the surface speed is reduced to 107 m/sec (350 ft/sec). A minimum film thickness margin of at least 2.54 microns (0.1 mils) was recommended in order to allow for film thickness variations due to surface waviness and the dynamic effects of seal seat runout.

It was recommended that the material specified for the carrier be changed to reduce thermal growth of the carrier. A more precise match between the carrier balance diameter and the nosepiece seal dam over the full temperature range is needed to avoid excessive loss in film thickness at the high pressure, high temperature operating conditions.

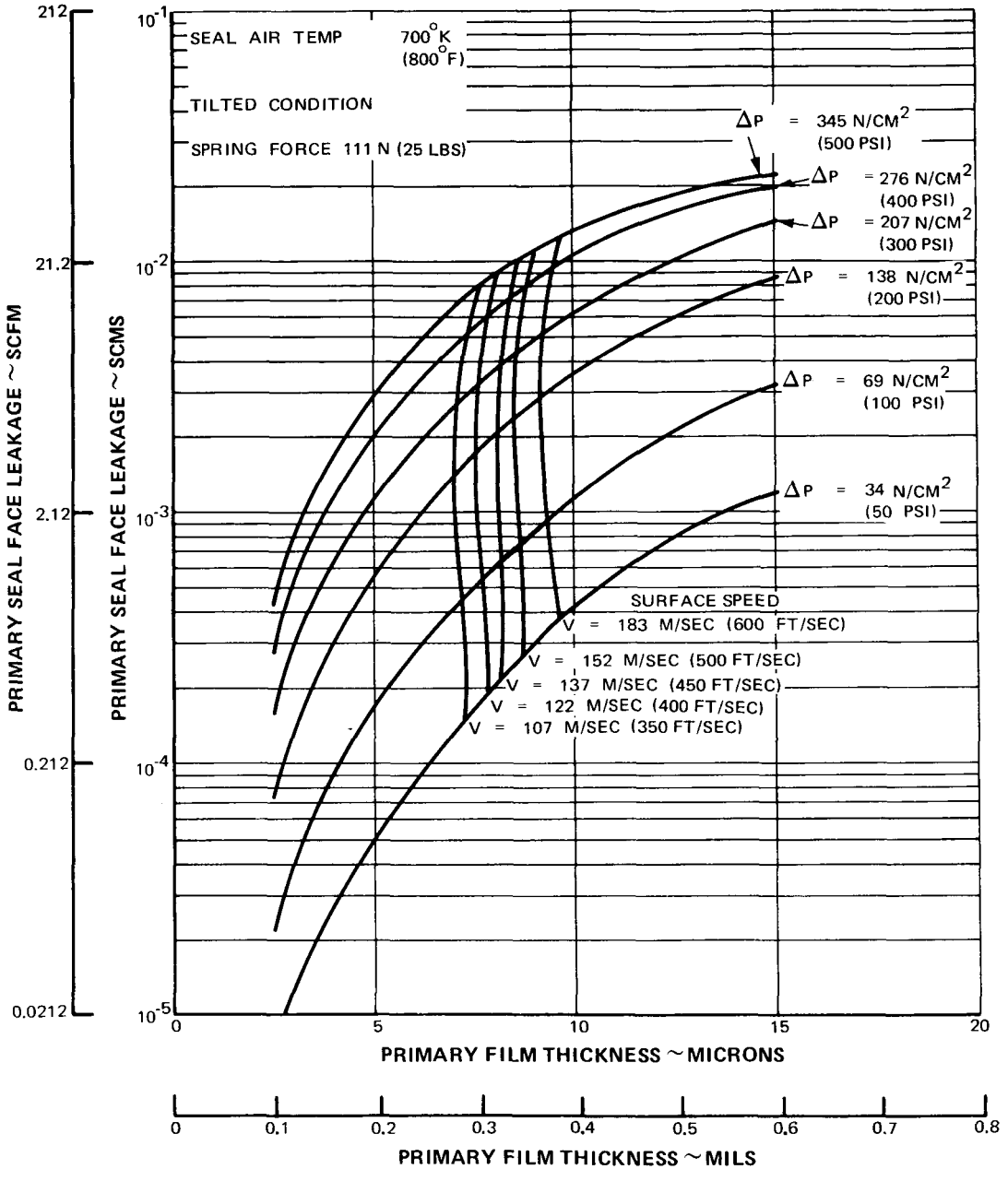

Figure 22 Primary Seal Face Leakage Versus Primary Film Thickness

V. TEST RIG REVISIONS AND PROCUREMENT OF NEEDED PARTS (TASK II)

The test program of the Contract was based on continued use of the NASA owned test rig which was designed and built under Contract NAS3-7609. The rig was originally designed for operation at maximum conditions of 207 N/cm^2 (300 psi) pressures differential across the test seal, 152 m/sec (500 ft/sec) sliding speed at a sealing dam diameter of 16.76 cm (6.6 in), and 922°K (1200°F) gas temperature in the high pressure compartment. To meet program conditions, Task II of the Contract required modification of the rig. These modifications included a redesigned light-weight rig shaft, a heat shield added to the rig dome, incorporation of higher strength flange bolts on the rig dome, and a redesigned one-piece duplex ball bearing support. Following review and approval of the design modifications by NASA, the necessary parts rework and procurement was undertaken. The specific rig design analysis and design modification are presented below.

A. TEST RIG ANALYSIS

A rig layout, Figure 23, indicating the modifications required to increase the test rig's capability, was submitted to NASA. The modifications were made for both structural and critical speed considerations which included a redesigned light-weight rig shaft, a heat shield added to the rig dome, higher strength flange bolts on the rig dome, and a one-piece duplex ball bearing support. The summary analysis completed resulting in these modifications is as follows:

1. Critical Speed Analysis

The critical speed analysis of the test rig was performed with a computer program which was based on the rig model shown in Figure 24. In this diagram, the "Original Rig" refers to the rig used in Contract NAS3-7609, while the "Redesigned Rig" refers to the rig as shown in Figure 23.

The analysis revealed that the redesigned rig as shown in Figure 23, with a lighter shaft at the seal end had a first critical speed of 179.4 m/sec (588.5 ft/sec) and a second critical speed of 197.0 m/sec (646.3 ft/sec). These critical speeds were well above the seal sliding speed required for initial Contract testing, but the first critical was below the maximum level of this program.

Since the calculated critical speeds were close to the designed operating range, some further action was required to insure safe rig operation. It was felt that the calculated stiffness of the No. 4 bearing was low and probably ultra-conservative, but this could only be verified experimentally. Also, the stiffness of the No. 1 and 2 bearings could be enhanced by using preloaded bearings but the resulting increase in critical speed would be marginal. Further analysis indicated that the critical speed could be raised by lightening the rig end of the shaft. A reduction in weight here would increase the first critical speed allowing the rig to operate at a slight margin at maximum program conditions even if the No. 4 bearing stiffness were as low as the originally calculated value.

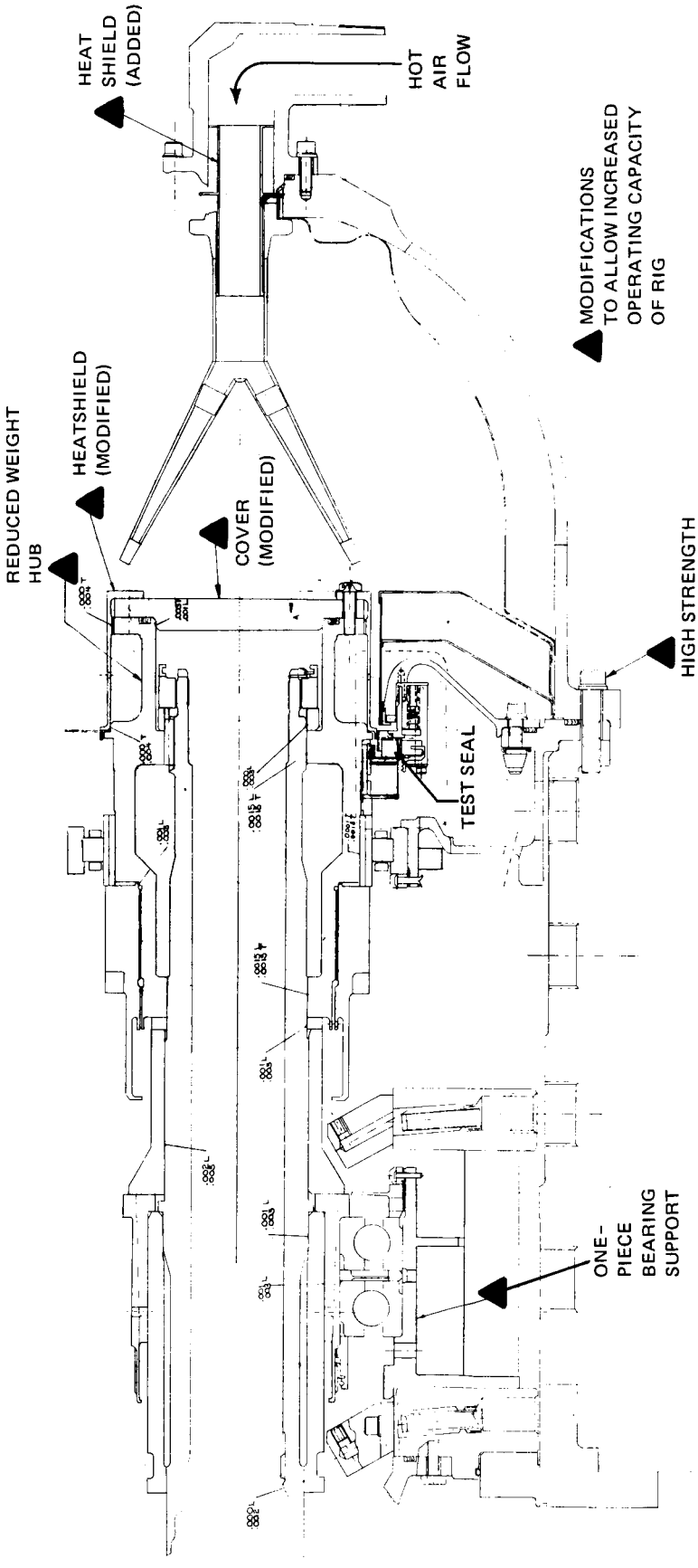

Figure 23 Mainshaft Seal Rig Modifications

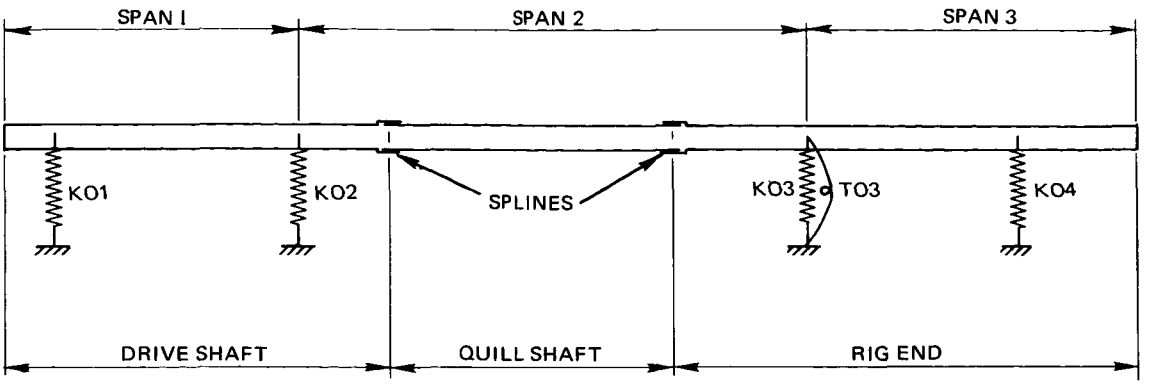

SPAN NO.	SPAN WEIGHT "ORIGINAL RIG" N	(LBS)	"REDESIGNED RIG" N	(LBS)	SPRING NO.	SPRING RATE "ORIGINAL RIG" N/CM	(LB/IN)	"REDESIGNED RIG" N/CM	(LB/IN)
1	38.12	(8.57)	38.12	(8.57)	KO1	8.75×10^5	(0.5×10^6)	8.75×10^5	(0.5×10^6)
					KO2	3.80×10^5	(0.217×10^6)	8.75×10^5	(0.5×10^6)
2	125.97	(28.32)	125.97	(28.32)	KO3	31.5×10^5	(1.8×10^6)	31.5×10^5	(1.8×10^6)
					TO3	82.3×10^5	(4.7×10^6)	82.3×10^5	(4.7×10^6)
3	326.62	(73.43)	270.08	(60.72)	KO4	$.0123 \times 10^5$	(0.7×10^6)	$.0123 \times 10^5$	(0.7×10^6)

Figure 24 Critical Speed Model for Mainshaft Seal Rig

2. Dome Analysis

Analysis of the existing test rig dome showed that the stresses would be highest in the inlet elbow. These stresses are caused mainly by thermal gradients, while the increased pressure required for testing under this Contract would have only a small effect as shown in Figure 25 and Table IV. For the test program sealed gas temperature of 922°K (1200°F), the inner radius (Location 7 in Figure 25) was calculated to be at 977.4°K (1300°F), while Location 1, which is about 5.08 cm (2 in) away was calculated to be 295.5°K (532°F) cooler. This gradient compresses the inner radius, resulting in extremely high compressive hoop stresses and localized yielding. Since the stresses are caused by the high thermal gradient, a heat shield in the inlet elbow would reduce the stresses, and was recommended and incorporated for a safer design. The minimum LCF life without the heat shield was estimated to be in excess of 10,000 cycles.

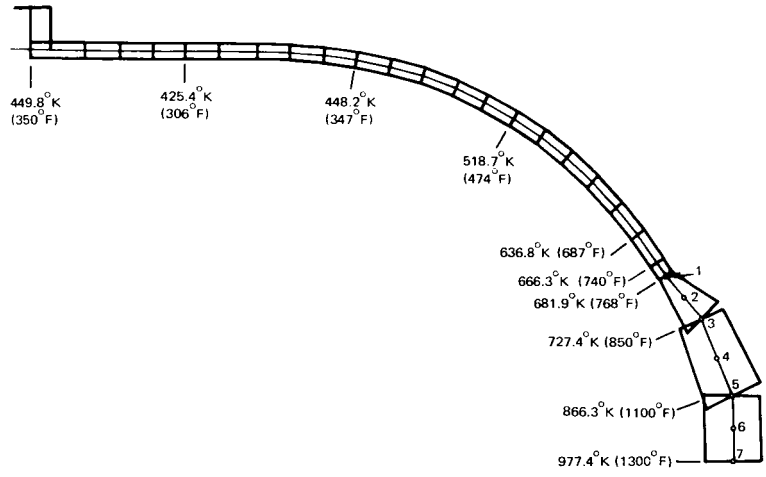

Figure 25 Thin Shell Model of Mainshaft Seal Rig Dome

TABLE IV

DOME STRESSES

Pressure N/cm²	Pressure lbs/in²	Location See Fig.	MERIDIONAL STRESS Max N/cm²	Max (lbs/in²)	Bending N/cm²	Bending (lbs/in²)	Membrane N/cm²	Membrane (lbs/in²)	CIRCUMFERENTIAL STRESS Max N/cm²	Max (lbs/in²)	Bending N/cm²	Bending (lbs/in²)	Membrane N/cm²	Membrane (lbs/in²)	0.2% Yield Stress N/cm²	0.2% Yield Stress (lbs/in²)
		1	12,641	(18,320)	9,136	(13,240)	3,443	(4,990)	16,167	(23,430)	5,955	(8,630)	10,212	(14,800)	23,460	(34,000)
		2	4,589	(6,650)	3,526	(5,110)	1,063	(1,540)	19,644	(28,470)	6,707	(9,720)	12,938	(18,750)	23,391	(33,900)
		3	4,747	(- 6,880)	3,988	(5,780)	759	(- 1,100)	28,559	(41,390)	11,454	(16,600)	17,105	(24,790)	23,253	(33,700)
		4	-12,717	(-18,430)	8,770	(12,710)	3,947	(- 5,720)	26,965	(39,080)	17,761	(25,740)	9,170	(13,290)	22,701	(32,900)
345	500	5	-21,832	(-31,640)	15,146	(21,950)	6,686	(- 9,690)	28,049	(40,650)	25,364	(36,760)	2,684	(3,890)	22,011	(31,900)
		6	19,389	(28,100)	11,558	(16,750)	-7,832	(-11,350)	42,525	(- 61,630)	29,987	(43,460)	-12,537	(-18,170)	21,666	(31,400)
		7	0	(0)	0	(0)	0	(0)	-76,493	(-110,860)	40,903	(59,280)	35,590	(-51,580)	20,907	(30,300)
		1	9,681	(14,030)	9,073	(11,700)	1,608	(2,330)	14,021	(20,320)	5,713	(8,280)	8,308	(12,040)	23,460	(34,000)
		2	4,402	(6,380)	4,216	(6,110)	186	(270)	18,809	(27,260)	7,142	(10,350)	11,668	(16,910)	23,391	(33,900)
		3	- 6,100	(- 8,840)	4,796	(6,950)	1,304	(- 1,890)	28,214	(40,890)	12,006	(17,400)	16,208	(23,490)	23,253	(33,700)
		4	-13,752	(-19,930)	9,356	(13,560)	-4,395	(6,370)	26,765	(39,790)	18,299	(26,520)	8,466	(12,270)	22,701	(32,900)
207	300	5	-22,708	(32,910)	15,511	(22,480)	7,197	(-10,430)	28,014	(40,600)	25,875	(37,500)	2,139	(3,100)	22,011	(31,900)
		6	19,879	(-28,810)	11,813	(17,120)	8,066	(- 11,690)	43,587	(- 63,170)	30,436	(44,110)	-13,151	(-19,060)	21,666	(31,400)
		7	0	(0)	0	(0)	0	(0)	77,887	(-112,880)	41,462	(60,090)	-36,425	(-52,790)	20,907	(30,300)

NOTES: These results are for the dome without the inlet elbow heat shield. An analysis of the structure with the heat shield shows a 15-percent decrease in maximum stresses.

3. Dome Flange Bolts

The original AMS-5735 material flange bolts have a high coefficient of thermal expansion, preventing a sufficiently high flange closing load at operating conditions of 449.8°K (350°F) and 345 N/cm^2 (500 psi) internal dome pressure. For this reason, the Contractor recommended changing the bolt material to AMS-6304, which has a lower coefficient of thermal expansion and a higher yield stress in the testing temperature range. The new bolts were analyzed for direct tensile stress, combined shear stress, and combined tensile stress. On the basis of this analysis and standard bolt criteria, a new assembly torque was selected to insure that the flanges would not separate and flange wedge loads should not be a problem. Table V lists the recommended torque and the accompanying stresses. The stresses are shown as a percent of 0.2-percent yield stress.

TABLE V
BOLT ANALYSIS RESULTS

Friction Factor	Assembly Torque m - kg	Assembly Torque (in - lbs)	Bolt Load Assembly N	Bolt Load Assembly (lbs)	Bolt Load Running N	Bolt Load Running (lbs)	Direct Tensile Stress (% Yield) Assembly	Direct Tensile Stress (% Yield) Running	Combined Tensile Stress (% Yield) Assembly	Combined Tensile Stress (% Yield) Running	Combined Shear Stress (% Yield) Assembly	Combined Shear Stress (% Yield) Running
0.10	4.03± .11	(350± 10)	32,246	(7,230)	34,610	(7,760)	68	84	75	93	41	51
0.15	4.03± .11	(350± 10)	22,300	(5,000)	24,396	(5,470)	47	60	56	70	33	40

NOTE: All Stresses and Loads are Maximum Values.

4. Duplex Bearing Support

A thin shell analysis of the duplex thrust bearing support indicated high bending stresses in the bearing housing support flange due to increased pressure, although this stress was still within the 0.2 percent yield stress. The maximum stress at any other point in the structure was within 41.4 X 10^3 N/cm^2 (60,000 psi), which is less than 60 percent of the 0.2 percent yield stress. The one-piece housing and support shown in Figure 26 was included in the modifications to provide a greater operating safety margin.

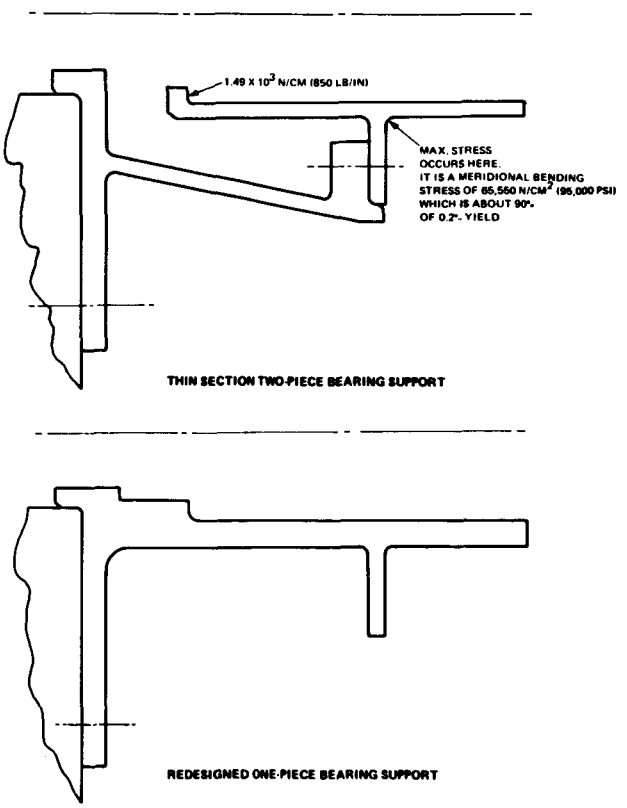

Figure 26 Duplex Bearing Support for the Mainshaft Seal Rig

B. PROCUREMENT AND MODIFICATION OF RIG HARDWARE

After the modifications discussed above were approved by NASA, the necessary detailed drawings were made and modifications undertaken. New parts were procured and existing parts from the rig transferred from Contract NAS3-7609 were reoperated as required. Since all test seal hardware for this program was to be supplied by NASA, no procurement other than rig parts was necessary.

VI. EXPERIMENTAL EVALUATION

A. PRELIMINARY DYNAMIC EXPERIMENTAL EVALUATION (TASK III)

This section describes the work done under Task III of the program which was directed to obtaining measurements of gas-film thickness during dynamic rig testing of a gas-film seal design.

NASA furnished two (2) seal assemblies which were similar to the wide-pad seal design, CF-847650, successfully evaluated in Contract NAS3-7609. Each seal assembly was received with four (4) capacitance type proximity probes installed in the carbon nosepiece. Each probe was located within a Rayleigh pad as shown in Figure 27.

Experimental evaluation of both seals was halted after an abbreviated test program. Reliable gas-film thicknesses could not be determined because of probe failures shortly after initiation of testing.

1. Instrumented Seal Test

The first instrumented test seal supplied by NASA was inspected by the Contractor and it was noted that the seal dam on this seal was damaged with localized distress as much as 6.35 microns (0.25 mils) deep. From the nature of the damage, it appeared that it occurred during installation and calibration of the proximity probes at NASA. It was decided to use the alternate instrumented seal supplied by NASA since the damage to the sealing dam might influence the gas-film thickness.

During inspection and assembly of the alternate instrumented seal assembly, the vinyl sheathing on the four proximity probe leads cracked. Examination of the leads revealed that they were brittle at the probes, apparently because of the heat applied to them during the probe installation. The leads were then covered with a rubber compound to repair the vinyl sheathing. Recalibration of the four probes with the Contractor's readout equipment revealed that 3 of the 4 probes were still in good condition. The slope of the calibration curves obtained by the Contractor was the same as that obtained by NASA. However, the curves did shift because of the difference in readout equipment.

As installed in the test rig, the seal seat axial runout was measured to be 25.4 microns (1.0 mils) and it was flat to within 0.5 microns (0.02 mils) as measured with an optical flat. A static air leakage calibration was completed on the seal assembly with the bench equipment and procedure described in Appendix B of this report. The seal was installed in the rig and two (2) Bently-Nevada proximity probes were installed and calibrated, one to measure shaft axial motion and the other for use as a phase reference. Figure 28 indicates the location of the Bently-Nevada probes with the rig pressure dome removed. Final assembly of the rig in the test facility (see Appendix B) was completed.

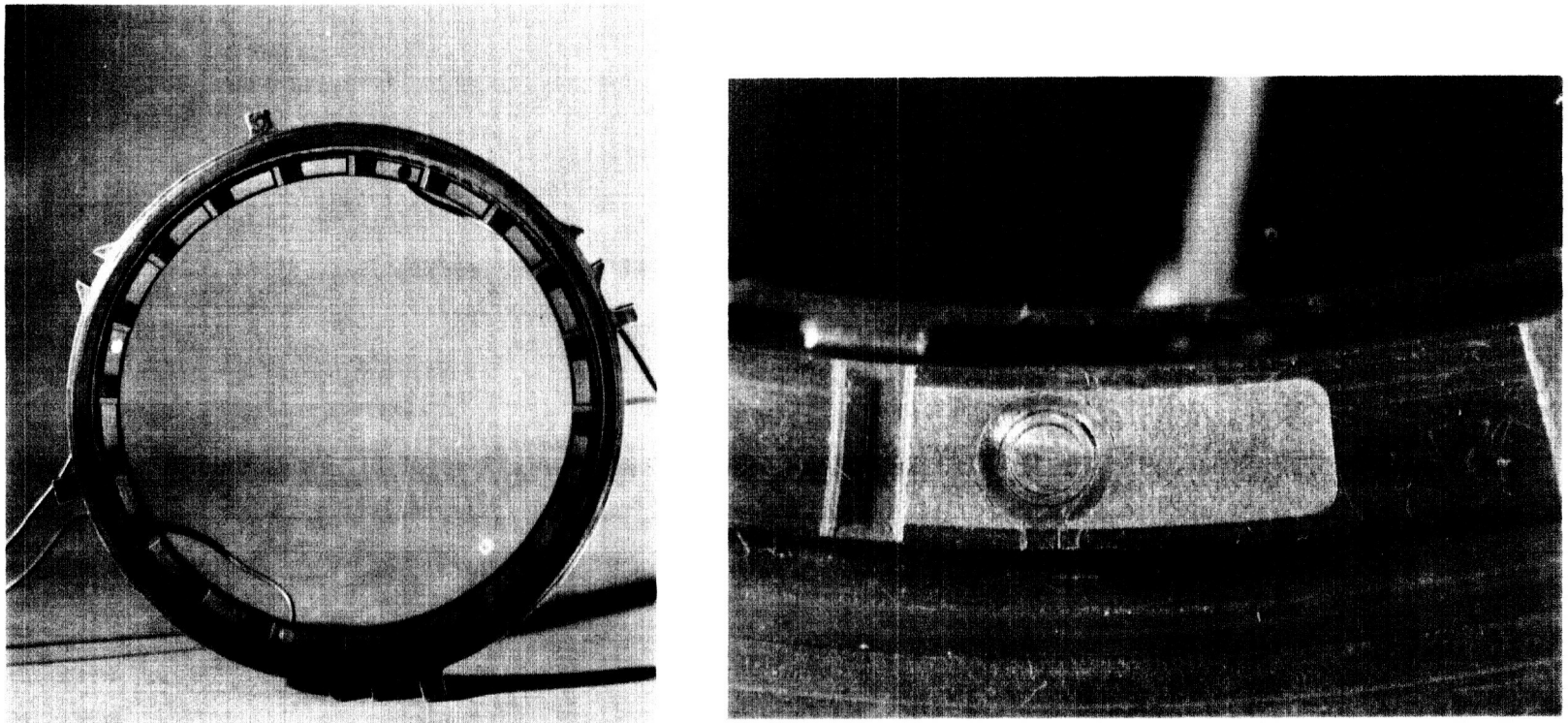

Figure 27 Carbon Nosepiece With Four Capacitance Proximity Probes Installed Within Rayleigh Pads to Measure Gas-Film Thickness (Left), Closeup of Proximity Probe and Rayleigh Pad (Right) (CN-32162, CN-33040)

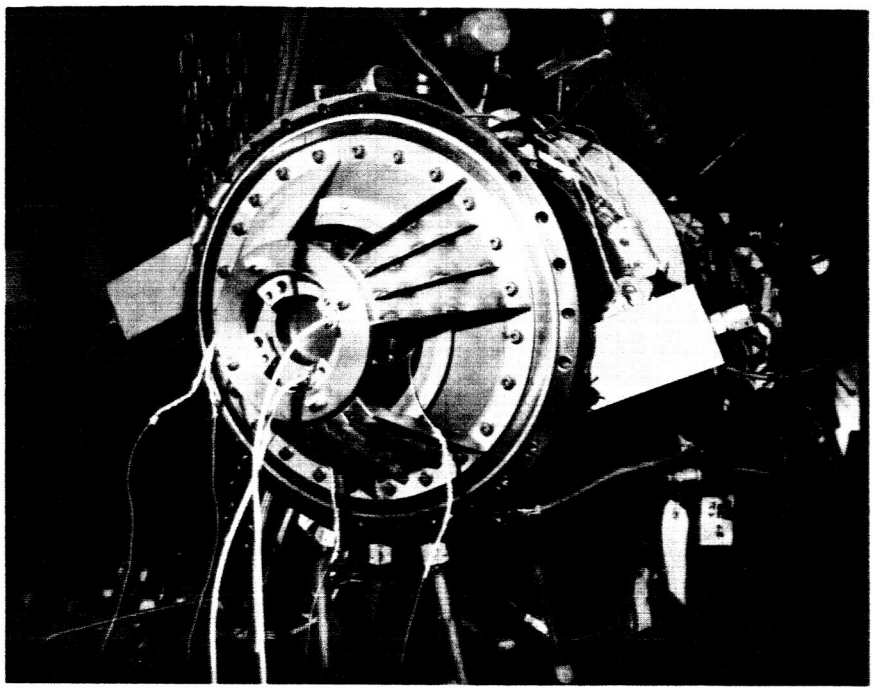

Figure 28 Seal and Hub End of Test Rig Showing Locations of Bently-Nevada Proximity Probes to Measure Shaft Axial Motion and Phase Reference (X-36966)

Immediately after test start-up, the proximity probes installed to measure gas-film thickness stopped functioning properly. The seal was removed from the rig and inspection of the probe leads revealed that they were in poor condition. In addition, the face of the carbon nosepiece was found covered with carbon wear particles. At this time, it was decided to install the alternate instrumented nosepiece for testing.

The alternate instrumented nosepiece was installed in the seal assembly and a static air leakage calibration completed. The static leakage was determined to be acceptable. Again the two (2) Bently-Nevada proximity probes were mounted and calibrated along with the four (4) transducers on the seal nosepiece. The seal was tested at a sliding speed of 91.4 m/sec (300 ft/sec) and seal pressure differentials of 34.5, 69, 104, 138 and 172 N/cm^2 (50, 100, 150, 200, and 250 psi) with room temperature air.

During the testing, the operation of the four probes on the nosepiece was erratic. All four probes were operational at the beginning of the test, but two showed very large zero shifts and erratic signals. A third probe showed a large zero shift on the first acceleration, the fourth probe yielded acceptable data for a short period at the first steady state point, but then experienced a large zero shift and a decay in the dynamic portion of the signal. Analysis of the measurements made with the fourth transducer showed a 1E amplitude of 7.62 microns (0.30 mils) peak-to-peak at the steady-state speed of 91.29 m/sec (299.5 ft/sec) with 69.0 N/cm^2 (100 psi) pressure differential across the seal. The Bently-Nevada probe measuring shaft axial motion showed 1E amplitudes of 60.96 microns (2.4 mils) and 37.08 microns

(1.46 mils) peak-to-peak at the same running conditions. Since only minimum data was obtained with the proximity probes and the repeatability of the instrumentation was not established, no further analysis was attempted.

2. Failure Investigation of Probes

An investigation into the failures of the three-element NASA capacitance probes was conducted and it was concluded that the failures were attributed primarily to the type of leadwire used and the technique employed in potting the probes and leadwires into the carbon seals. The leadwire coating appeared to be polyvinyl chloride, which is rated to 355°K (180°F), but rig air temperatures in the area of the leadwires exceeded 366°K (200°F). For the first seal tested, the as-received condition of the leadwire in the area of the potting compound indicated that the leadwires were probably overtemperatured in the cure cycle for the potting compound. The wire was very brittle, and any movement or bending of the wire caused cracking in the outer insulation and in the outer shield. In an attempt to protect the brittle area, it was coated.

A post-test resistance check of the leadwires from the nosepiece of the first instrumented seal tested indicated a short across the two inner elements (probe capacitive plate and guard ring) of all the probes. One probe was shorted by a metallic particle across the two inner elements, but the other transducer faces appeared to be in good condition. It was not possible to determine exactly where the short occurred without parting the leadwire from the transducer, but it was apparent from the condition of the leadwire that it was the source of failure.

Inspection of the transducer from the second seal nosepiece tested indicated a short between the two inner conductors on all transducers. The probe leadwires for this seal were not brittle, but it was judged that they were the primary cause for failure. The transducer faces showed evidence of a physical breakdown of the insulating material between the three elements; this would have caused a zero shift and a change in transducer sensitivity, but probably would not have caused a direct short between the elements.

B. ELEVATED TEMPERATURE TESTING (TASK IV)

In Task IV, elevated temperature testing was conducted on the gas-film seal design analyzed under Task I. Test hardware was supplied by NASA. A total of 136 hours of testing was completed on one seal noisepiece. Test conditions included sliding speeds from 107 to 175 m/sec (350 to 575 ft/sec), seal pressures differentials from 34.5 to 345 N/cm^2 (50 to 500 psi), and seal gas temperatures from 366 to 922°K (200 to 1200°F). Testing was terminated when a rapid increase in leakage occurred as the result of a seal rub while running at a sliding speed of 137 m/sec (450 ft/sec), a pressure differential of 207 N/cm^2 (300 psi), and a gas temperature of 922°K (1200°F).

1. Pre-Test Assembly and Modification

The test rig was modified for high speed, pressure, and temperature operation prior to this part of the program, as described in Section II. Initially, the test rotor was assembled to the configuration of Figure 29 using a new "thin-section" seal seat furnished by NASA. Al-

though seal seat flatness was satisfactory before assembly, torquing the hub locking nut to a normal value of 115.25 m-kg (10,000 in-lb) induced an out-of-flatness of 12.7 microns (0.5 mils). Refinishing the hub components and reassembly did not significantly reduce the amount of distortion when the same torque was applied. Inspection after reassembly with a reduced locking torque of 69.15 m-kg (6000 in-lb) revealed a saddle-shaped distortion. This was verified by F.I.R. of the squareness of the seal seat face with the hub centerline. The F.I.R was 20.3 microns (0.8 mils) and a plot of the circumferential variation revealed that the shape of the resulting curve was bimodal, indicating a seal seat face out-of-flatness superimposed on the normal out-of-squareness.

The seal seat was then removed from the piloting spacer, and the hub was reassembled without the seal seat using a torque of 69.15 m-kg (6,000 in-lb). Runout readings of the rear spacer, which acts as a stop for the seal seat, indicated a bimodal distortion, thus indicating that clamping of the hub components resulted in distortion of the hub components.

Assembly of the rig was next attempted with the rear shaft spacer configuration shown in Figure 30. With a locking nut torque of 115.25 m-kg (10,000 in-lb), however, distortion was again encountered. F.I.R. runout of the seat face was 20.3 microns (0.8 mils). Reducing the locking nut torque to 82.98 m-kg (7,200 in-lb), decreased the runout to 12.7 microns (0.5 mils), but distortion of the seal seat face was still present.

At this point, it was decided to rework the hub components in an attempt to reduce the loads caused by the component fits and thus reducing seal seat distortion. The seal seat was relapped flat to within 0.5 microns (0.02 mils). Also, the O.D. of the shaft spacer was reduced to decrease the nominal fit between the seal seat and shaft spacer from an interference fit of 0.0254 - 0.0762 mm (0.001-0.003 inch) to a loose fit of 0.0000-0.0127 mm (0.0000-0.0005 inch) and the I.D. of the shaft spacer was increased 0.0254 mm (1.0 mil), resulting in a loose fit when installed on the hub.

Subsequent assembly of the rotor with a torque of 115.25 m-kg (10,000 in-lb) revealed that no improvement resulted from this work.

It was agreed with the NASA Project Manager to return to the wide seat configuration shown in Figure 31. The assembly was locked with a torque of 115.25 m-kg (10,000 in-lb), and an optical flatness reading indicated the seal seat face was flat within 0.5 microns (0.02 mils).

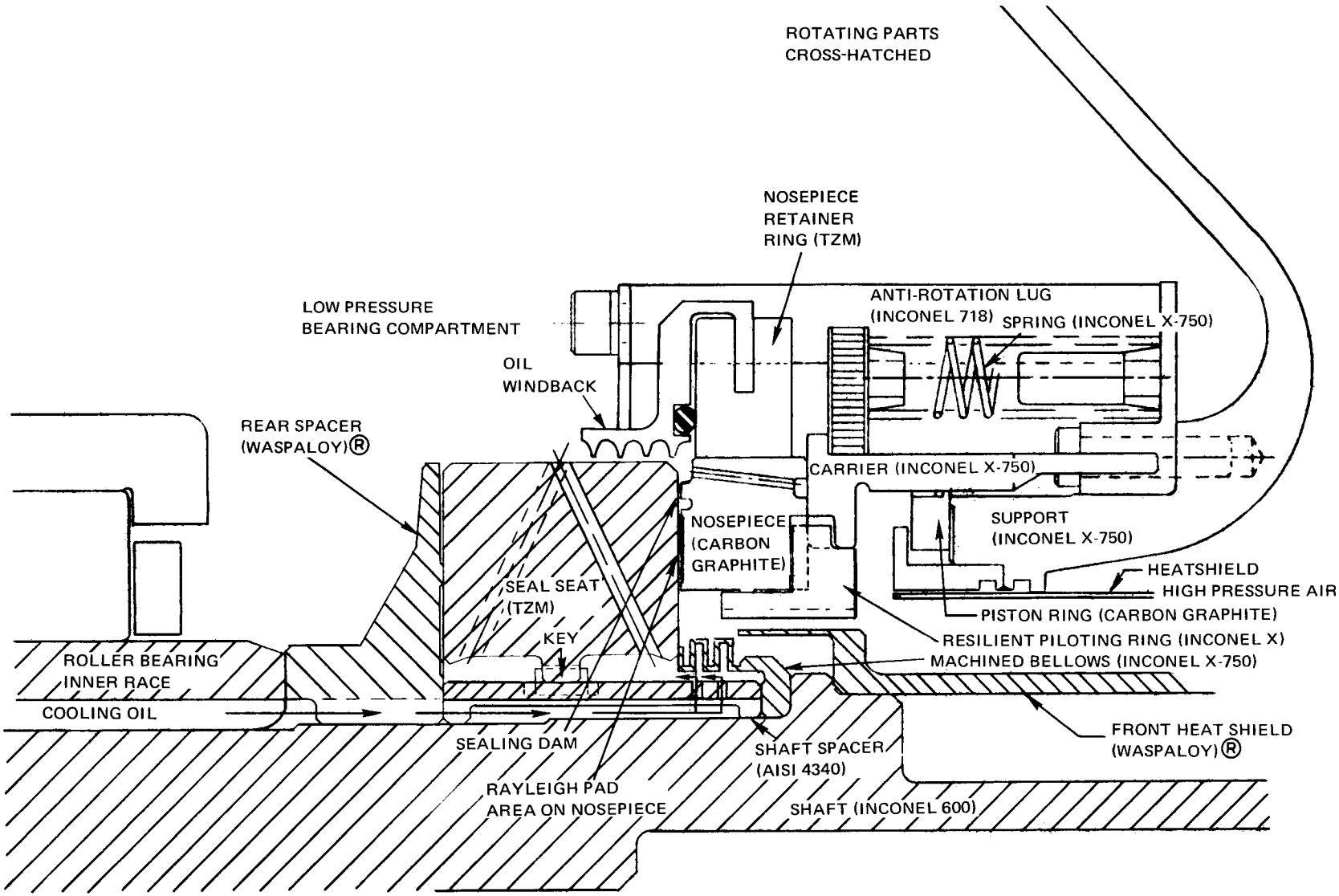

Figure 29 Initial Hub and Seal Assembly for Elevated Temperature Testing Showing Small Diameter Narrow Seal Seat, One Piece Rear Spacer, and Oil Windback

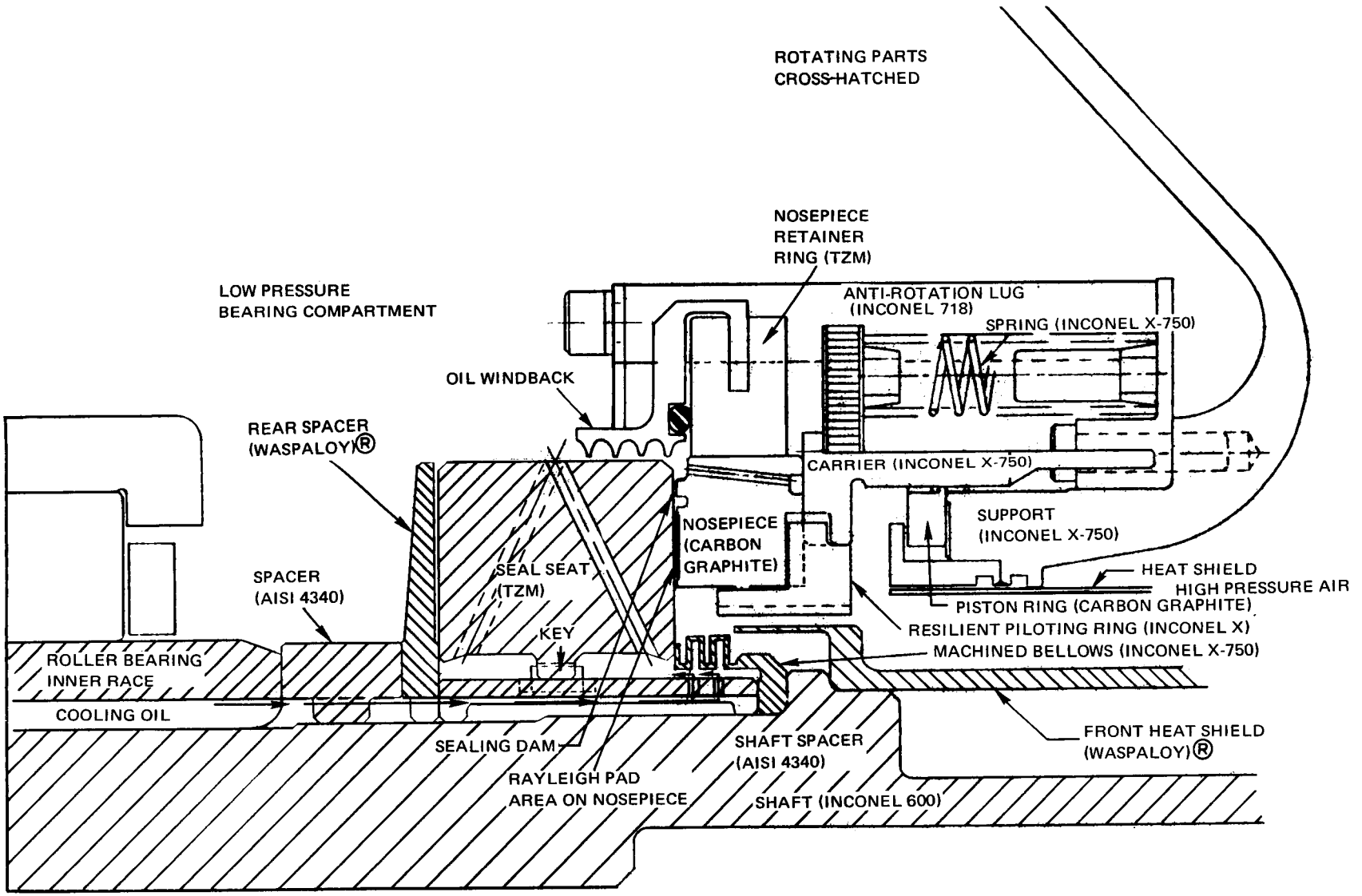

Figure 30 Hub and Seal Assembly the Same as Figure 29 Except for Alternate Two-Piece Seal Seat Spacer

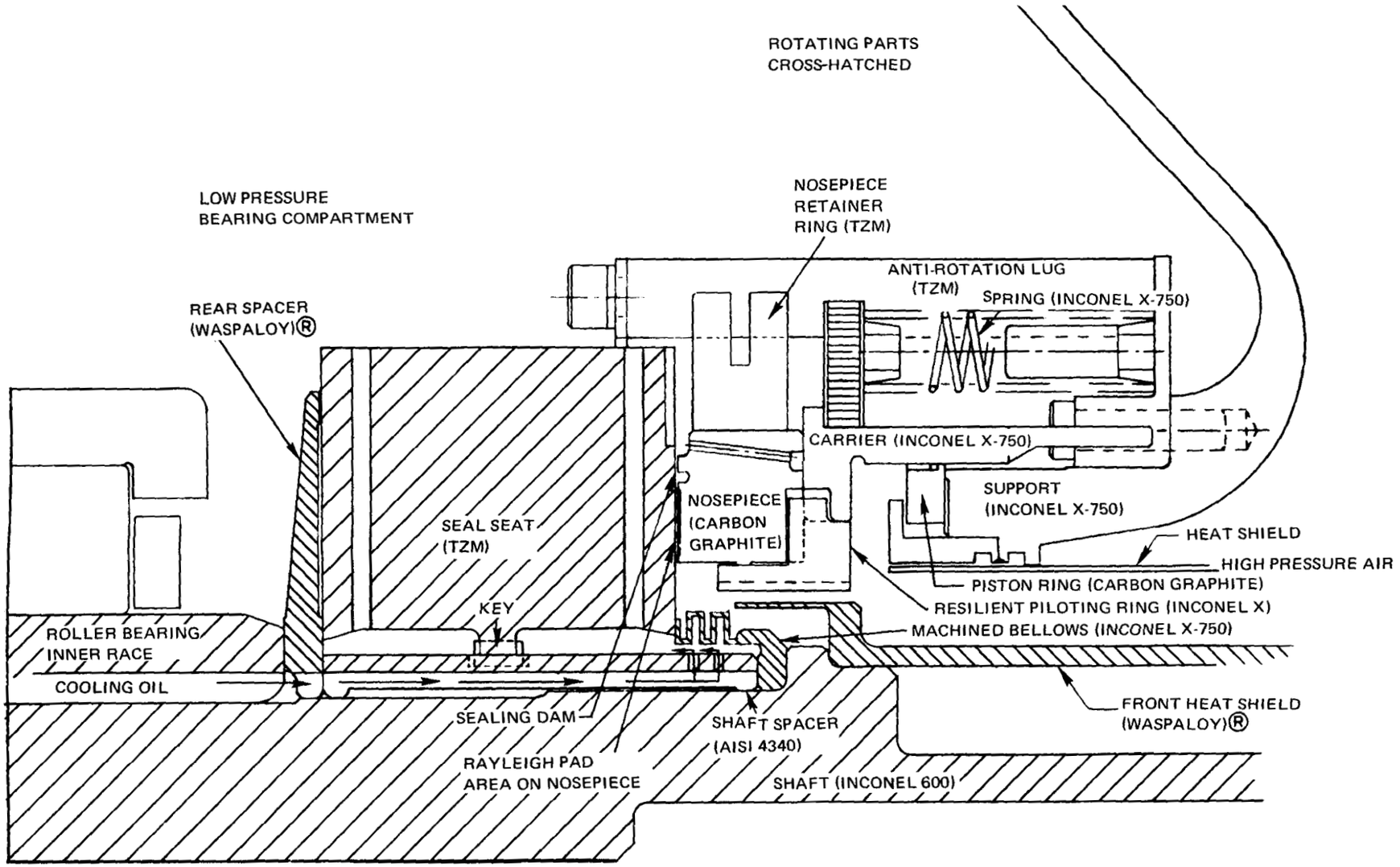

Figure 31 Final Hub and Seal Assembly Configuration With Large Diameter Wide Seal Seat Used During Elevated Temperature Testing and During Elevated Temperature Endurance Testing

The F.I.R. runout of the seat was 17.78 microns (0.7 mils), with a sinusoidal variation which indicated that the seal seat face was flat.

The rotor assembly was then completed and balanced to within 7.2 gm-cm (0.1 oz-in). Assembly of the rig was completed. The test seal assembly had a total spring force of 118N (26.5 lb) at the seal operating position.

Three (3) changes were made to the NASA supplied test seal assembly prior to its installation into the rig. Utilization of the seal seat configuration shown in Figure 31 required two changes to the seal assembly shown in Figures 29 and 30. The larger seal seat necessitated removal of the windback from the seal nosepiece assembly and material was removed from the I.D. of the retainer ring to permit the ring to clear the O.D. of the seal seat when installed. The remaining change was made to the seal carrier. The venting capacity of the annulus in the carbon nosepiece at the nosepiece/carrier mating faces was increased by machining six (6) bleed slots in the carrier. The bleed slots connected the annulus with the low pressure side of the carrier.

A profile trace was made across the face of the carbon seal nosepiece prior to testing and is shown in Figure 32.

2. Seal Test Evaluation

The test rig was installed in the test facility described in Appendix B. A static leakage calibration was performed at pressure differentials up to 206.8 N/cm^2 (300 psi) prior to dynamic testing. The calibration results are shown in Figure 33. A dynamic test run was then completed at the conditions given in Table VI.

TABLE VI
DYNAMIC TEST RUN CONDITIONS

Time	Sliding Speed		Seal Pressure		Air Temperature		Oil-In Temperature		Actual Total Air Leakage	
hrs	m/sec	(ft/sec)	N/cm^2	(psi)	°K	(°F)	°K	(°F)	scms x 10^3	(scfm)
5.0	121.9	(400)	68.9	(100)	588.7	(600)	394.3	(250)	2.2	(4.7)
5.0	121.9	(400)	68.9	(100)	810.9	(1000)	394.3	(250)	2.0	(4.2)
5.0	121.9	(400)	103.4	(150)	588.7	(600)	394.3	(250)	4.5	(9.6)
5.0	121.9	(400)	103.4	(150)	810.9	(1000)	394.3	(250)	3.2	(6.9)
5.0	121.9	(400)	137.9	(200)	810.9	(1000)	394.3	(250)	3.8	(8.0)
5.0	121.9	(400)	137.9	(200)	588.7	(600)	394.3	(250)	5.0	(10.6)
5.0	121.9	(400)	206.8	(300)	588.7	(600)	394.3	(250)	8.6	(18.2)
15.0	121.9	(400)	137.9	(200)	588.7	(600)	394.3	(250)	5.4	(11.5)
5.0	137.2	(450)	206.8	(300)	810.9	(1000)	394.3	(250)	9.4	(19.9)

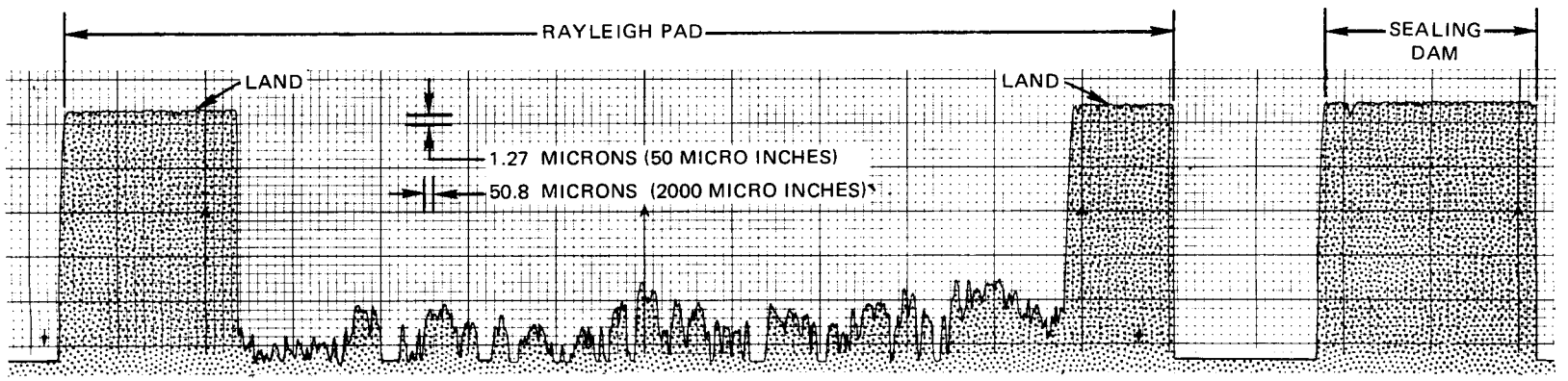

Figure 32 Representative Profile Trace Taken Radially Across the Face of the Carbon Nosepiece in New Condition Before Elevated Temperature Testing

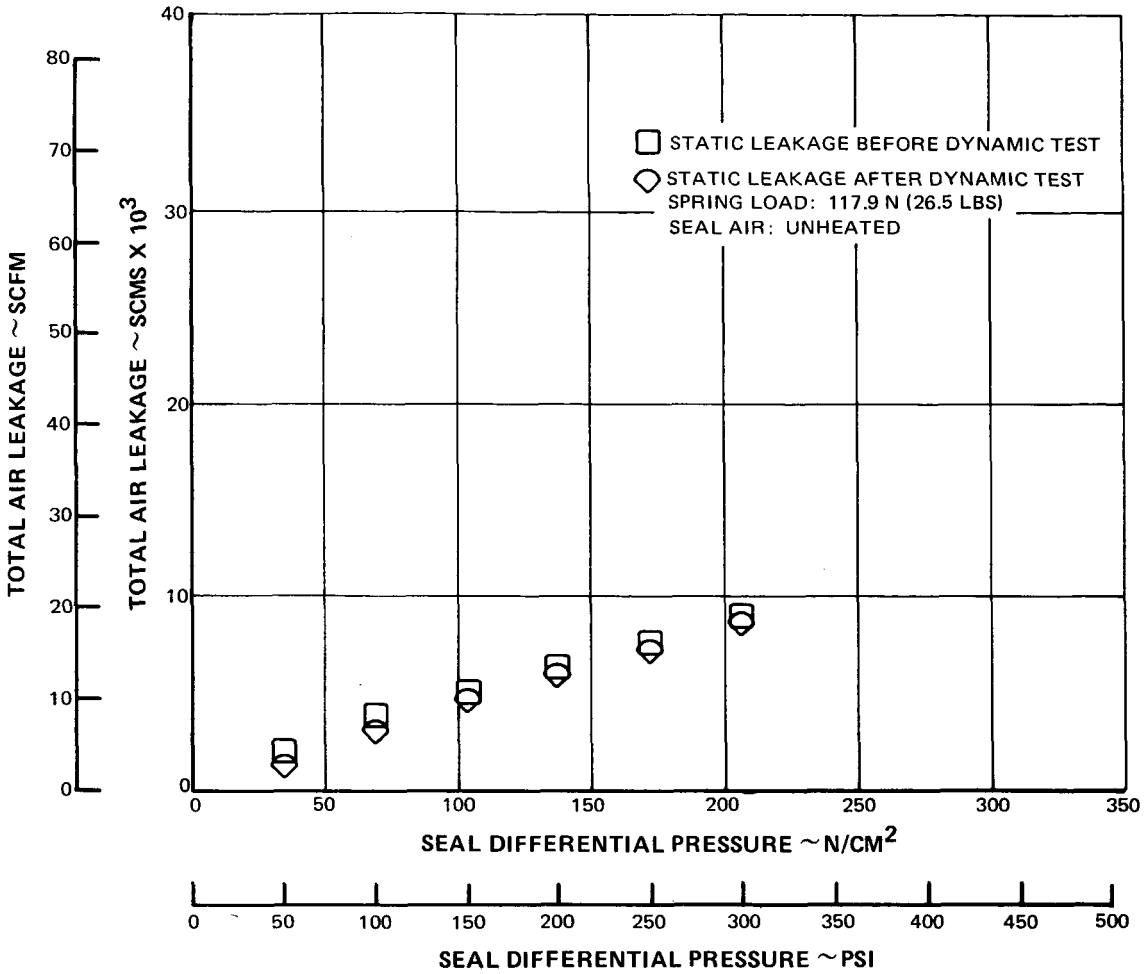

Figure 33 Static Seal Leakage Calibration for Elevated Temperature Evaluation

A post-test static leakage calibration was made at incremental pressure differentials to 206.8 N/cm^2 (300 psi) without removing the seal from the rig. The results shown in Figure 33, indicate a slight reduction in static leakage when compared to the values recorded prior to dynamic testing.

At this time, it was decided to reduce the total seal closing force, which is the sum of the hydraulic closing force and the spring force, by reducing the total spring load. With a smaller closing force, a thicker seal-film would result, minimizing chances of a seal rub at the combinations of high operating pressure and lower speed to be attempted in subsequent testing. The test seal assembly was removed from the rig and visual inspection of the seal assembly hardware and seat showed that both were in good condition. The spring force in the test seal was reduced to 71.4 N (16.0 lb) from the previous force of 118N (26.5 lb).

After reinstalling the seal in the rig, a static leakage calibration was completed, and the measurements are presented in Figure 34. A dynamic test run was then made at the combinations presented in the Table VII.

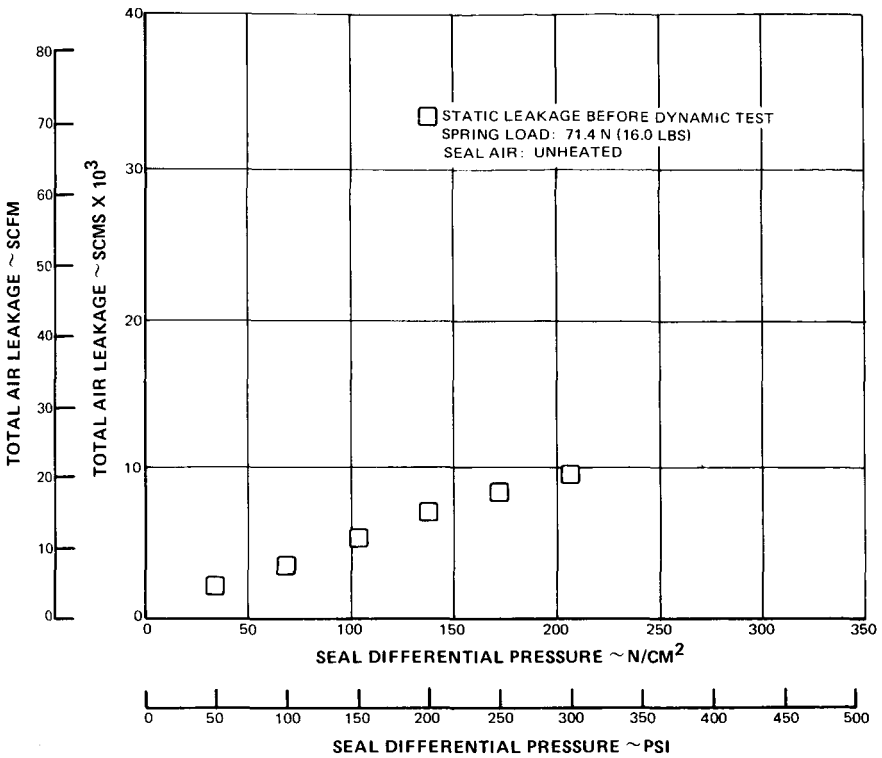

Figure 34 Static Seal Leakage Calibration for Elevated Temperature Evaluation

TABLE VII
DYNAMIC TEST RUN COMBINATIONS

Time	Sliding Speed		Seal Pressure		Air Temperature		Oil-In Temperature		Actual Total Air Leakage	
hrs.	m/sec	(ft/sec)	N/cm^2	(psi)	°K	(°F)	°K	(°F)	scms x 10^3	(scfm)
1.0	121.9	(400)	207	(300)	588.7	(600)	394.3	(250)	8.2	(17.3)
1.0	121.9	(400)	224	(325)	588.7	(600)	394.3	(250)	10.2	(21.7)
1.0	121.9	(400)	241	(350)	588.7	(600)	394.3	(250)	10.9	(23.3)
1.0	121.9	(400)	258	(375)	588.7	(600)	394.3	(250)	11.7	(25.1)
1.0	121.9	(400)	275	(400)	588.7	(600)	394.3	(250)	14.0	(30.0)
2.0	121.9	(400)	275	(400)	348.7	(200)	394.3	(250)	19.3	(41.4)
1.0	121.9	(400)	293	(425)	348.7	(200)	394.3	(250)	21.0	(45.0)
1.0	106.4	(350)	293	(425)	348.7	(200)	394.3	(250)	21.5	(46.0)
2.0	106.4	(350)	310	(450)	348.7	(200)	394.3	(250)	22.3	(47.7)
2.0	106.4	(350)	327	(475)	348.7	(200)	394.3	(250)	23.4	(50.0)
2.0	106.4	(350)	344	(500)	348.7	(200)	394.3	(250)	24.9	(53.4)
0.5	106.4	(350)	344	(500)	348.7	(200)	394.3	(250)	24.3	(52.0)
0.5	121.9	(400)	344	(500)	348.7	(200)	394.3	(250)	25.0	(53.5)
0.5	121.9	(400)	344	(500)	477.2	(400)	294.3	(250)	25.7	(55.0)
0.5	137.2	(450)	344	(500)	533.0	(500)	394.3	(250)	25.7	(55.0)

Following the last condition noted in Table VII, the seal sliding velocity was increased to 152.4 m/sec (500 ft/sec) while holding the other test conditions constant. A rapid increase in air leakage to a volume of about 33 x 10^{-3} scms (70 scfm) resulted in termination of the test. A post-test static leakage calibration was not performed at this time.

Post-test inspection of the test rig and seal hardware (total time in Task IV testing was now 95.0 hours) revealed that the increase in air leakage during test was the apparent result of two (2) component failures in the rig cover assembly.

One failure was in the weld of the rig cover bleed fitting which accounted for a slight increase in the air leakage measured. The other failure was a break in the air manifold, which directs the heated air toward the seal. This break allowed the manifold to rub against the seal rotor and debris generated damaged the seal and apparently caused the increased seal air leakage.

Profile traces across the face of the carbon nosepiece, Figure 35, showed that the seal dam received most of the damage from the debris. In some areas, it was worn as much as 12.7 microns (0.5 mils) below the level of the original surface. The Rayleigh pads were in good condition, having maintained their original depth of 35.6 microns (1.4 mils). The condition of the carbon nosepiece is shown in Figure 36.

The seal dam on the carbon piston ring also was severely worn, with some areas 38.2 microns (1.5 mils) below the original surface. The remainder of the piston ring was in good condition, with no evidence of oxidation or wear. The carrier surface, which mates with the carbon piston ring, was in good condition except at the location of the piston-ring gap. At the gap, the aluminum oxide hardcoat had been eroded away, exposing the base material as shown in Figure 37. The seal seat face was in good condition, with no indications of distress.

The seal assembly was rebuilt after the carbon nosepiece was relapped to improve the condition of the seal dam. The average depth of the Rayleigh pads was reduced from 35.6 microns (1.4 mils) to 25.4 microns (1.0 mils). A profile trace of the relapped carbon nosepiece is shown in Figure 38. A new seal carrier made of TZM material, and having the same dimensions as the previous carrier, was furnished by NASA. Since the new carrier would result in reduced radial differential thermal growth between the carrier and the carbon nosepiece, which would reduce the hydraulic closing force, the spring force was increased to its original value of 118N (26.5 lb). To increase the durability of the secondary seal, the carbon piston ring was replaced with a ring made of Haynes Alloy 25.

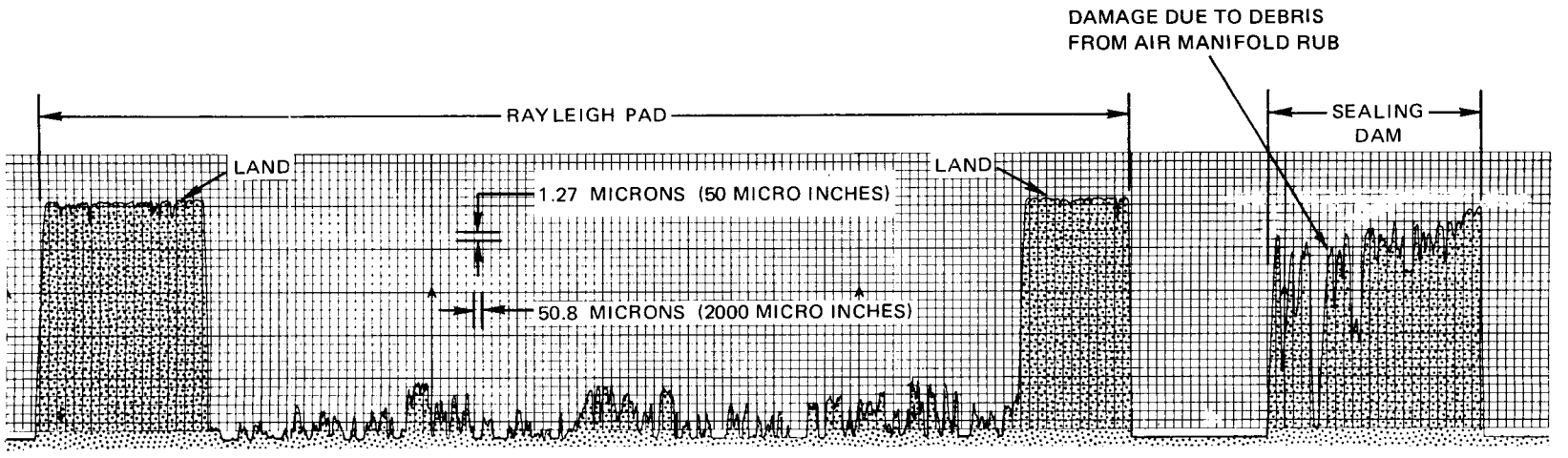

Figure 35 Results of Air-entrained Debris, Representative Profile Trace Taken Radially Across the Face of the Carbon Nosepiece; Rayleigh Pad, No Wear; Seal Dam, 12.7 Microns (0.5 mils) Wear Maximum; Total Time, 95 Hours

Figure 36 Carbon Nosepiece After 95 Hours at Elevated Temperature Testing (XPN-30630)

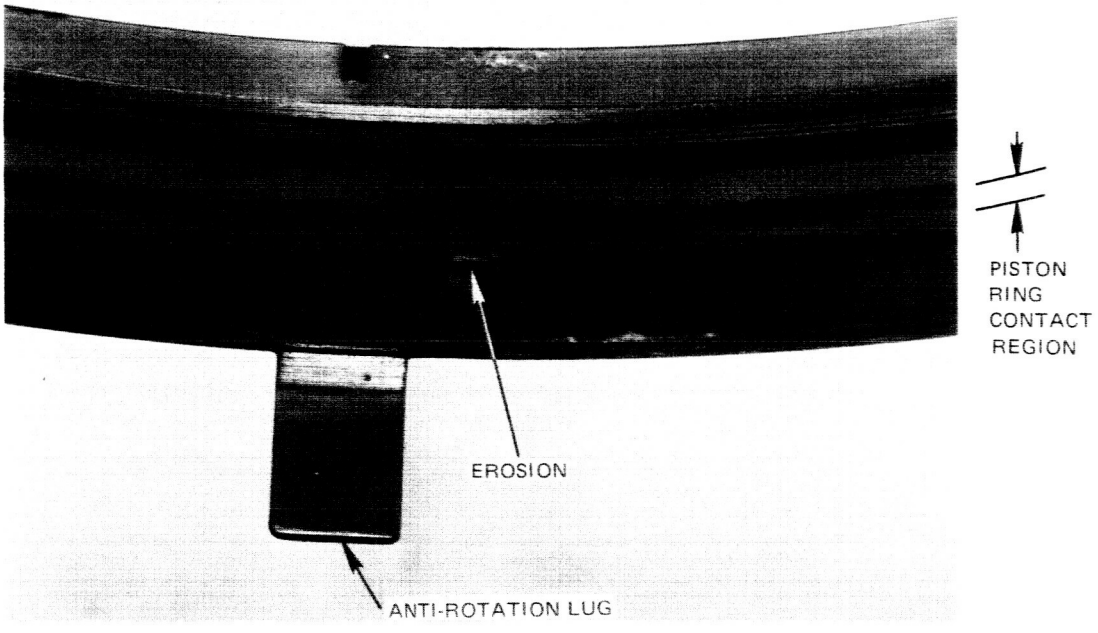

Figure 37 Seal Carrier Showing Erosion of Aluminum Oxide Coating in Area of Piston Ring Gap After 95 Hours of Elevated Temperature Testing (XPN-36434)

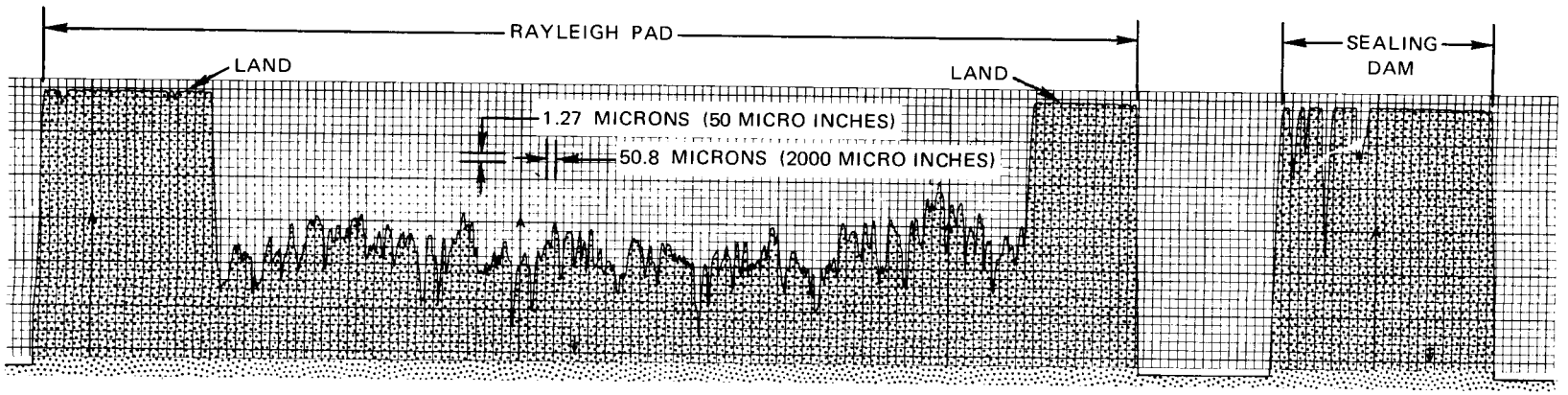

Figure 38 Representative Profile Trace Taken Radially Across the Face of the Carbon Nosepiece After Lapping the Face Shown in Figure 35 to Continue the Elevated Temperature Testing

The seal assembly was installed in the rig. A static leakage test was performed and the results found acceptable. The test program, Table VIII, was then successfully completed.

TABLE VIII
TEST PROGRAM

Time	Sliding Speed		Seal Pressure		Air Temperature		Oil-In Temperature		Actual Total Air Leakage	
hrs	m/sec	(ft/sec)	N/cm^2	(psi)	°K	(°F)	°K	(°F)	scms x 10^{-3}	(scfm)
2.0	111	(365)	207	(300)	700	(800)	394	(250)	15.0	(31.9)
2.0	111	(365)	224	(325)	700	(800)	394	(250)	16.5	(34.9)
2.0	111	(365)	241	(350)	700	(800)	394	(250)	17.8	(37.8)
2.0	111	(365)	259	(375)	700	(800)	394	(250)	18.8	(39.9)
2.0	111	(265)	275	(400)	700	(800)	394	(250)	19.6	(41.5)
2.0	122	(400)	275	(400)	700	(800)	394	(250)	26.6	(56.4)
8.0	122	(400)	293	(425)	700	(800)	394	(250)	27.8	(59.0)
1.0	137	(450)	207	(300)	811	(1000)	394	(250)	17.2	(36.5)
0.5	152	(500)	207	(300)	811	(1000)	394	(250)	17.5	(37.0)
0.5	160	(525)	207	(300)	811	(1000)	394	(250)	16.5	(35.0)
0.75	168	(550)	207	(300)	811	(1000)	394	(250)	16.5	(35.0)
0.25	175	(575)	207	(300)	811	(1000)	394	(250)	17.9	(38.0)

Having established that the gas-film seal being evaluated was capable of operation at pressures up to 345 N/cm^2 (500 psi) and sliding speeds up to 175 m/sec (575 ft/sec), operation at an air temperature of 922°K (1200°F) was attempted. The specific speed and pressure combination attempted are presented in Table IX

TABLE IX
SPECIFIC SPEED AND PRESSURE COMBINATIONS

Sliding Speed		Seal Pressure	
m/sec	(ft/sec)	N/cm^2	(psi)
107	(350)	207	(300)
137	(450)	207	(300)

Testing was satisfactory at the first condition above with the seal leakage at 18.4 x 10^{-3} scms (39.0 scfm). The seal sliding speed was then increased to the level in the second condition. As the speed was stabilizing, the air leakage suddenly increased to more than 35.4 x 10^{-3} scms (75 scfm). Reducing the sliding speed to 107 m/sec (350 ft/sec) and the seal pressure differential to 93 N/cm^2 (135 psi) resulted in stable operation, but the air leakage was approximately 30 percent less than had been measured previously at the same conditions. Such a reduction indicated a possibility that the seal seat was rubbing on the carbon nosepiece. Testing was discontinued and the seal was removed from the test rig.

Inspection of the seal nosepiece revealed that rubbing had occurred as indicated in the profile trace across the seal face shown in Figure 39. The face of the nosepiece had worn approximately 20.4 microns (0.8 mil) with near obliteration of the Rayleigh pads which were an average of 25.4 microns (1.0 mil) deep at the start of the test. Five recesses in particular were almost entirely removed. They were in two areas: one was located over an anti-rotation pin and included four of the five recesses, while the other was located approximately 2.6 radians (150°) away as shown in Figure 40. The profile traces indicate that wear resulted from a rocking motion of the nosepiece. The face of the nosepiece was out of flat by 43.2 microns (1.7 mils) with the rear side out of flat by 28.0 microns (1.1 mils). Before testing, both sides of the nosepiece had been flat within 0.5 micron (0.02 mil). The Haynes Alloy 25 piston ring, Figure 41, no longer had a free gap, indicating that the ring had been overstressed by overexpansion during the test. The seal seat was smeared from contact with the nosepiece, as shown in Figure 42, but was in generally good condition. The remaining seal components were in good condition with no visible signs of distress.

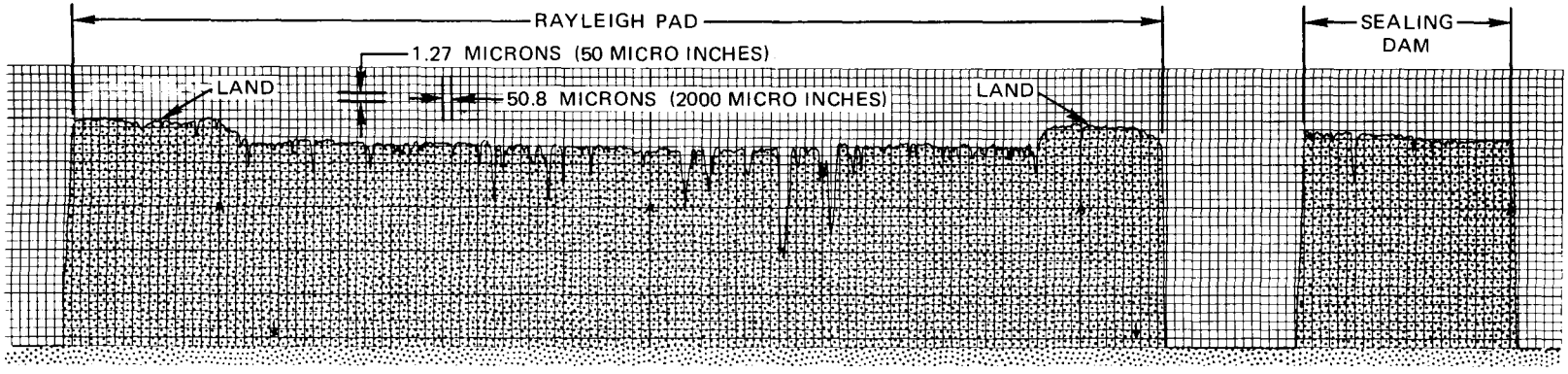

Figure 39 Representative Profile Trace Taken Radially Across the Face of the Carbon Nosepiece at Completion of Elevated Temperature Testing. Total Time on Nosepiece 136 Hours

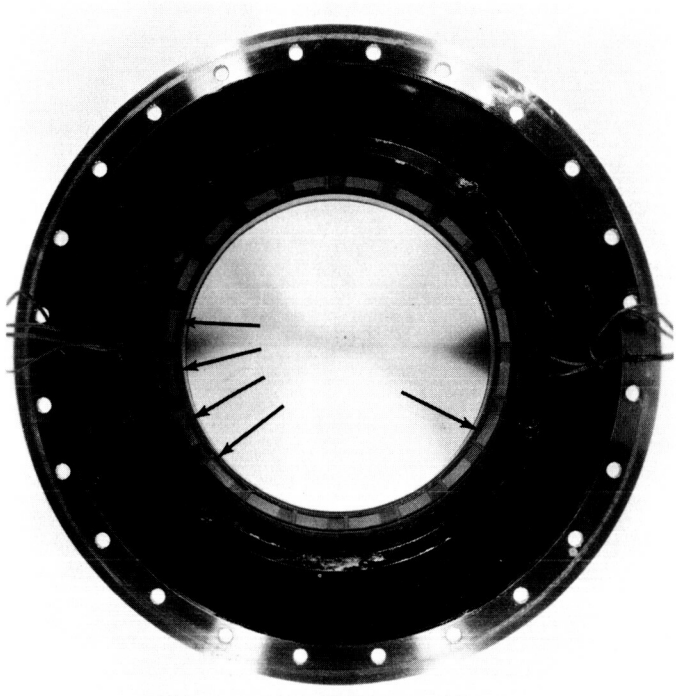

Figure 40 Seal Assembly Showing Wear of Rayleigh Pad on Carbon Nosepiece. Total Time on Nosepiece 136 Hours (CN-34394)

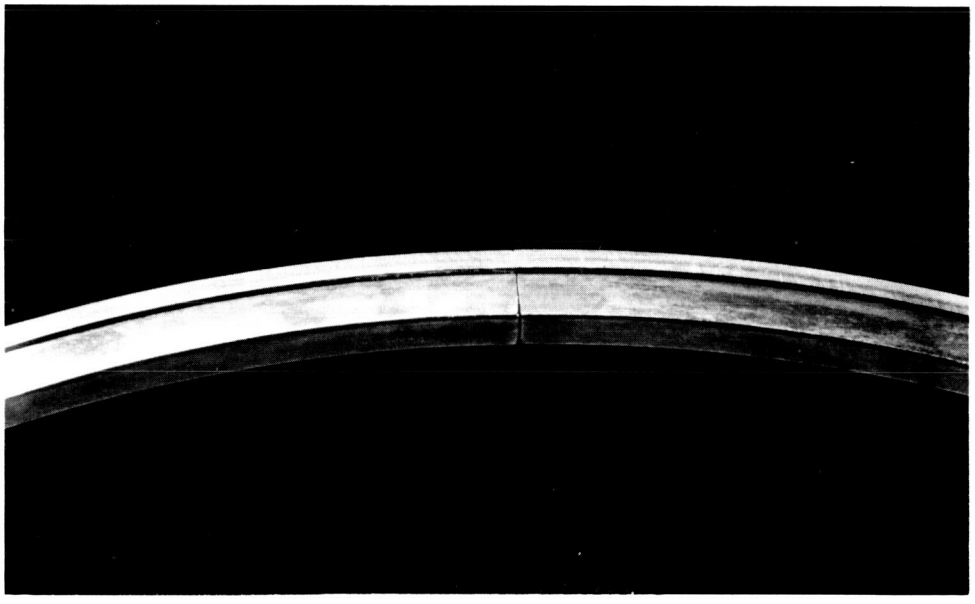

Figure 41 Haynes Alloy 25 Secondary Seal Piston Ring Showing Closed Gap. Total Time of 41 Hours on Piston Ring at Elevated Temperature Conditions (XPN-36435)

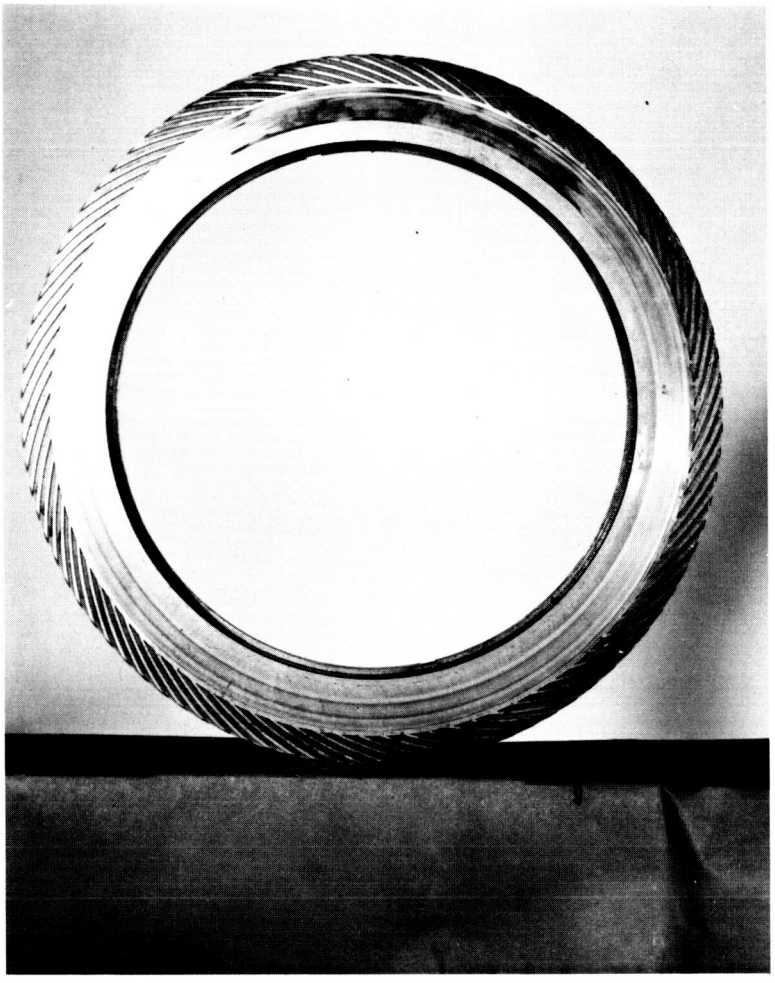

Figure 42 Seal Seat After 136 Hours of Testing (XPN-32372)

Analysis of the test results indicated that insufficient piston ring operating gap or binding at the anti-rotation pins caused the rubbing contact between the carbon seal face and seal seat.

A Haynes Alloy 25 piston ring, identical to the one used in the last series of elevated temperature testing was subjected to temperatures of 589°K (600°F) for 12 hours, 700°K (800°F) for 4 hours, and 830°K (1035°F) for 4 hours by NASA. No change in piston ring free gap was observed, indicating that the change in free gap observed during the elevated temperature test was caused by overstressing (ends of piston ring butted together) and was not due to relaxation of residual stress. This indication is supported by the physical properties of the materials. The coefficient of expansion of the Haynes Alloy 25 material used in the piston ring is 13.6×10^{-6} cm/cm/°K (7.6×10^{-6} in/in/°F), while the coefficient of expansion of the TZM carrier material is 5.9×10^{-6} cm/cm/°K (3.3×10^{-6} in/in/°F). Hence, the piston ring will expand more rapidly due to temperature than the carrier which contains it.

The installed gap of the Haynes Alloy 25 piston ring at room temperature was 0.175 cm (0.069 in). Using the measured carrier temperature of 530°K (495°F) at the 922°K (1200°F) air temperature condition, a piston ring temperature of 644°K (700°F) was calculated to close the gap.

The rubbing contact experienced by the nosepiece probably resulted in localized heat generation at the two points of maximum wear and hence, local distortion. The rocking mode of nosepiece wear, together with the angular relation of the worn areas to the four (4) anti-rotation pins indicated that binding of the anti-rotation pins in combination with piston ring secondary seal friction was the most probable cause for the rubbing observed.

The seal failure resulted in the termination of the Task IV elevated temperature testing. During this phase of the gas-film seal evaluation, a total of 136 hours of testing was completed on the Task I seal design, of which 95 hours were at Contract conditions.

C. EVALUATION OF EFFECTS OF AXIAL RUNOUT (TASK VI)

Under Task VI, the Contractor conducted seal dynamic tests on the Task I seal design to evaluate the effects of axial seal seat runout on seal performance. For these tests, the seal seat was installed in the test rig so that the resulting hand-turned axial seal seat runout was 57.15 microns (2.25 mils). The normal assembly requirement for axial seal seat runout is less than or equal to 25.4 microns (1 mil). The seal shown in Figure 43 ran successfully at sliding speeds from 91.4 to 152.4 m/sec (300 to 500 ft/sec) and pressure differentials from 34.5 to 345 N/cm^2 (50 to 500 psi). Tests were conducted with air at the compressor discharge temperature and with a nominal oil-in temperature of 394.1°K (250°F). Sealing was consistently good, with the seal leakage rates below predicted values in most instances. Wear on the faces of the seal nosepiece and seal seat were observed after test completion.

1. Seal Evaluation

The test rig shaft was assembled with seal seat spacer parts which had been altered to obtain an axial seal seat runout of 50.8 to 76.2 microns (2.0 to 3.0 mils). As mounted on the rig hub, the seal seat was found to be flat within 0.5 microns (0.02 mils), and the maximum axial runout was 63.5 microns (2.5 mils). The shaft assembly was then completed and balanced to within 3.6 gm-cm (0.05 oz-in). The axial seal seat runout was 57.15 microns (2.25 mils) with the shaft assembly mounted in the rig.

The seal design shown in Figure 43 was used in the initial assembly. It was essentially the same as the Task I seal design except a total spring force of 81.4N (18.25 lb) was used instead of the 111N (25 lb) value recommended in the Seal Design Analysis section, to allow a large operating seal gas-film and minimize chances of a seal rub with the seal test runout.

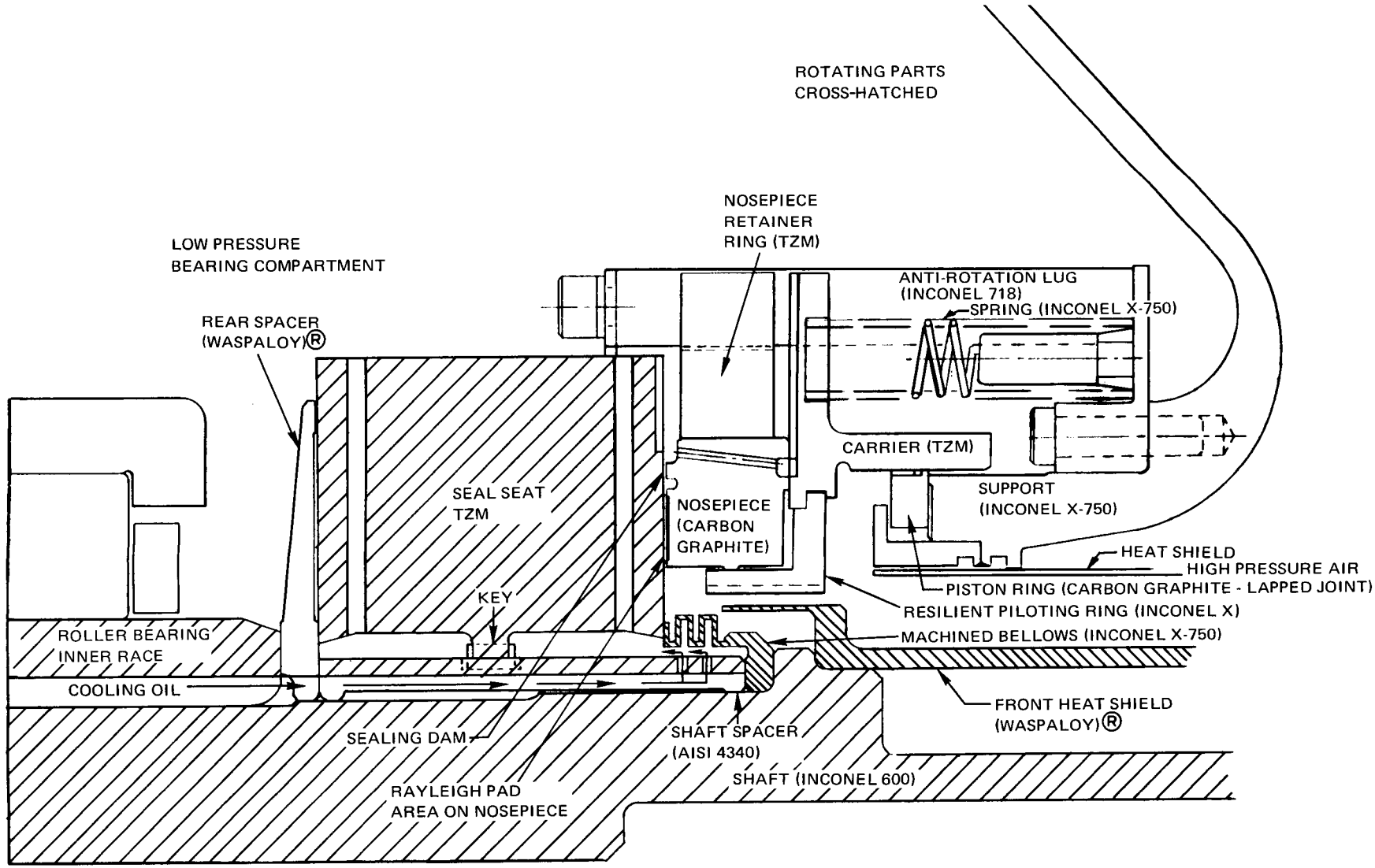

Figure 43 Hub and Seal Assembly Configuration as Used During Axial Seal Seat Runout Testing and During First Part of Contaminated Air Testing

The secondary seal used was a lapped-joint carbon piston ring as shown in Figure 44. A profile trace across the face of the nosepiece in the pre-test condition is shown in Figure 45. With the rig installed for test, a static leakage calibration was performed at incremental pressures up to 206.8 N/cm^2 (300 psi). The results which were higher than obtained during Task IV, are shown in Figure 46. Dynamic testing was initiated, with unheated air and an oil-in temperature of 394.3°K (250°F), and then continued for 19 hours at the conditions in Table X.

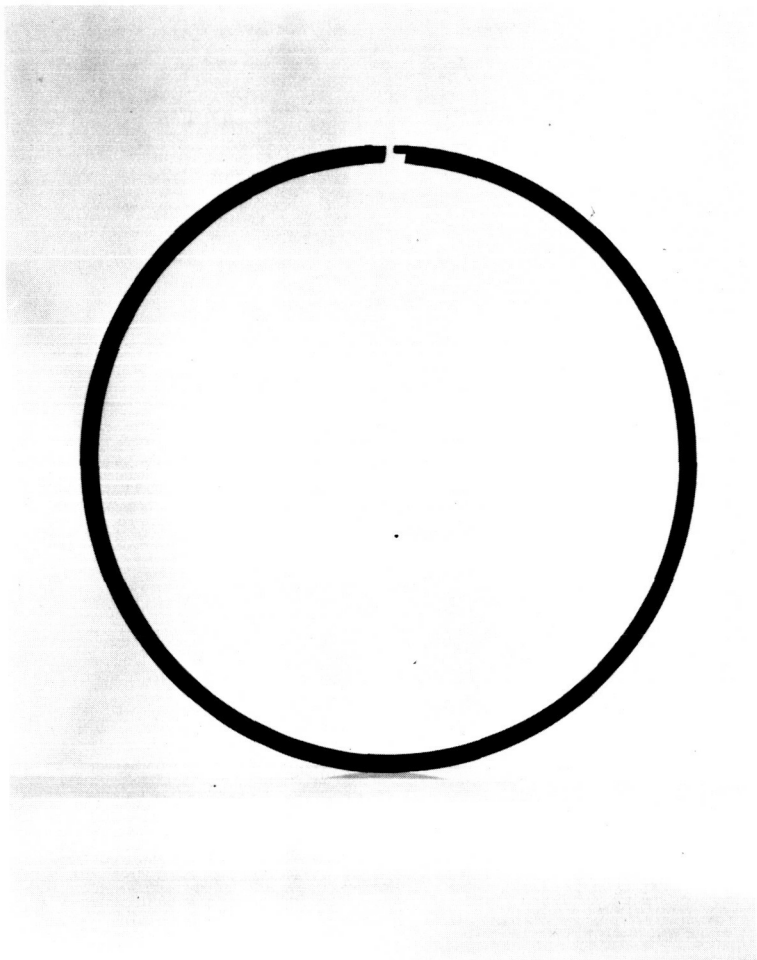

Figure 44 Lapped-Joint Carbon Secondary Seal Piston Ring Used During Axial Seal Seat Runout Testing (XPN-36572)

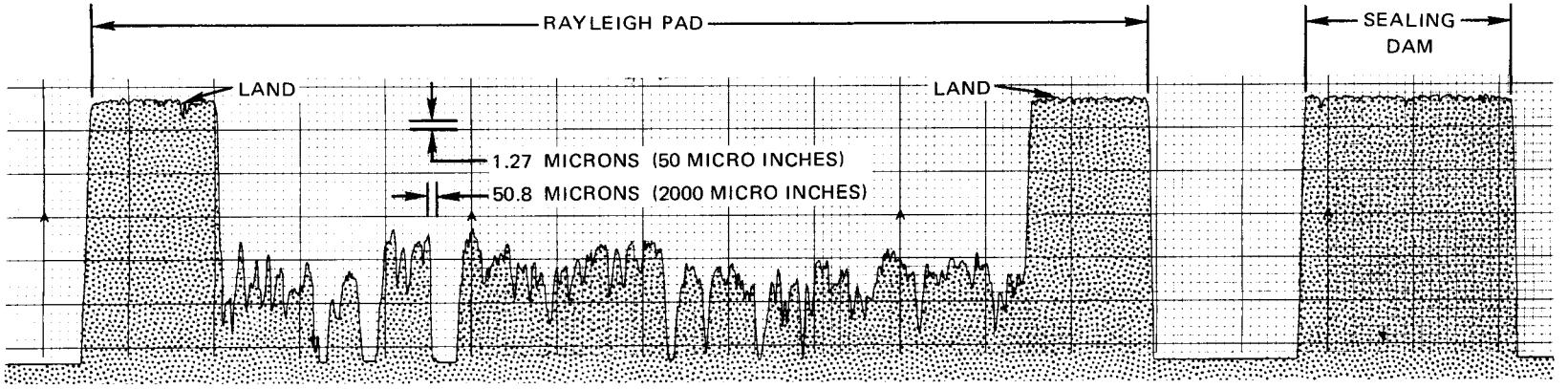

Figure 45 Representative Profile Trace Taken Radially Across the Face of the Carbon Nosepiece in New Condition Before Axial Seal Seat Runout Testing

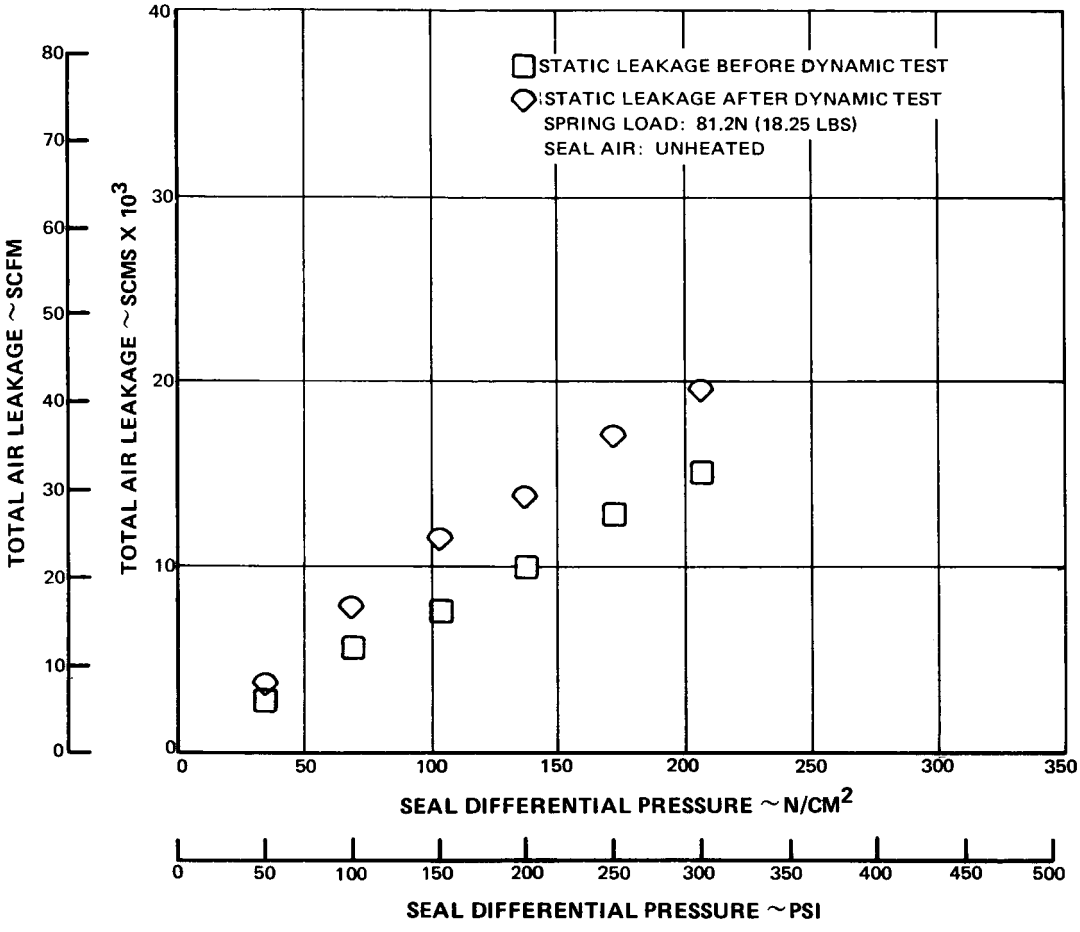

Figure 46 Static Seal Leakage Calibration for Axial Seal Seat Runout Test

TABLE X
INITIAL DYNAMIC TEST CONDITIONS

Seal Sliding Speed		Seal Differential Pressure	
m/sec	(ft/sec)	N/cm^2	(psi)
91.4	(300)	34.5 - 206.8	(50-300)
106.7	(350)	34.5 - 344	(50-500)
121.9	(400)	34.5 - 206.8	(50-300)

Data obtained at the three speed conditions are shown in Figures 47, 48, and 49, respectively. At each speed setting, the leakage initially observed was substantially the same as the pre-test static leakage. As testing progressed, leakage increased to the maximum rates shown. As a result of the progressive increase in leakage, dynamic testing was interrupted for inspection of the test seal.

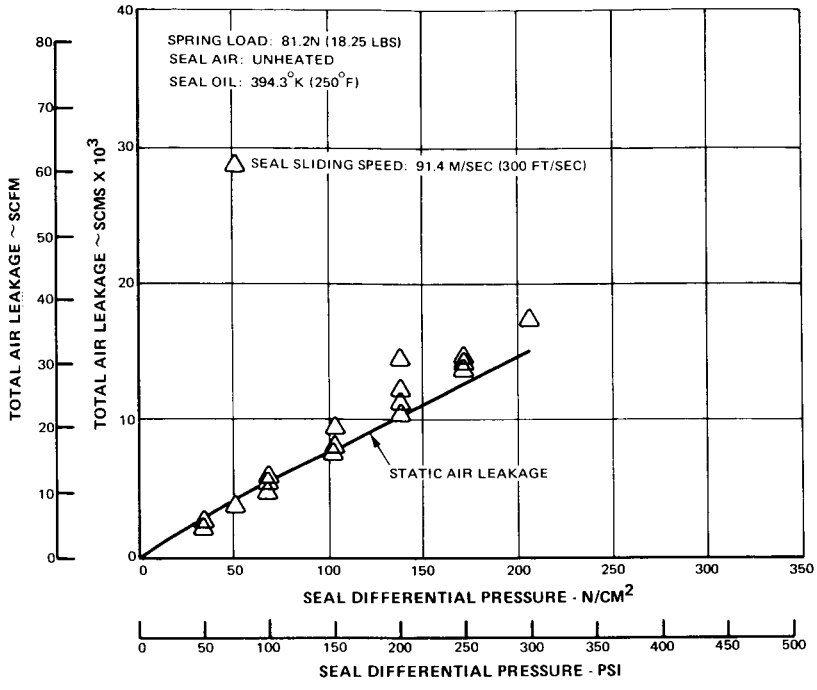

Figure 47 Performance Calibration for Axial Seal Seat Runout Test – 91 m/sec (300 ft/sec)

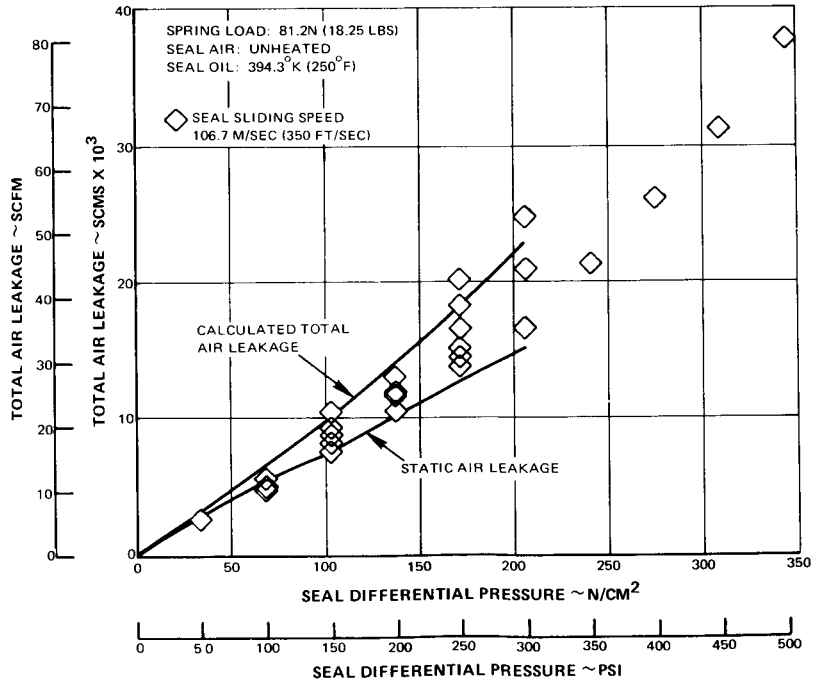

Figure 48 Performance Calibration for Axial Seal Seat Runout Test – 106.7 m/sec (350 ft/sec)

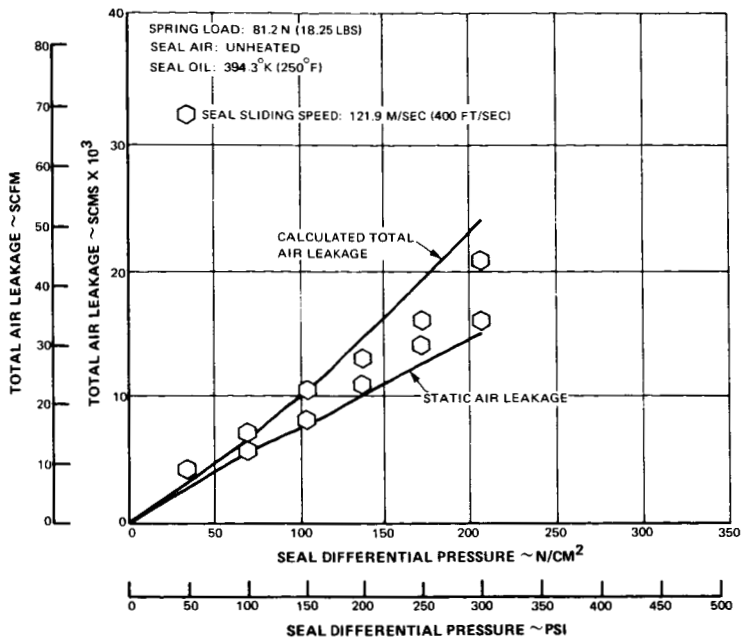

Figure 49 Performance Calibration for Axial Seal Seat Runout Test – 121.9 m/sec (400 ft/sec)

Prior to removing the test seal assembly for inspection, a static leakage test was performed at incremental pressures up to 206.8 N/cm^2 (300 psi). The results are shown in Figure 46 and indicate an approximate 22 percent increase in the leakage rates over the values obtained prior to the dynamic test. Inspection of the seal assembly revealed evidence that the piston ring sealing dam was not making complete circumferential contact with the base of the seal carrier. This accounted for the higher static leakage obtained prior to dynamic testing. All other details in the seal assembly appeared in satisfactory condition, with no evidence of distress or deterioration. No apparent reason was found for the increase in the static and dynamic leakage experienced in these tests. The same seal assembly was reinstalled in the test rig without modifications of the seal assembly or seal seat runout.

Testing was resumed after first completing a static leakage calibration up to 345 N/cm^2 (500 psi). As shown in Figure 50, the leakage was unchanged in the range of 68.9 to 206.8 N/cm^2 (100 to 300 psi) from the values recorded prior to removing the seal from the rig. Dynamic testing continued with unheated air and an oil-in temperature of 394.3°K (250°F). Ten (10) hours of testing was completed at the conditions shown in Table XI.

TABLE XI
ADDITIONAL DYNAMIC TEST CONDITIONS

Seal Sliding Speed		Seal Differential Pressure	
m/sec	(ft/sec)	N/cm^2	(psi)
106.7	(350)	34.5-276.0	(50-400)
121.9	(400)	137.9-276.0	(200-400)
137.2	(450)	46.2-276.0	(67-400)
152.4	(500)	68.9 -276.0	(100-400)

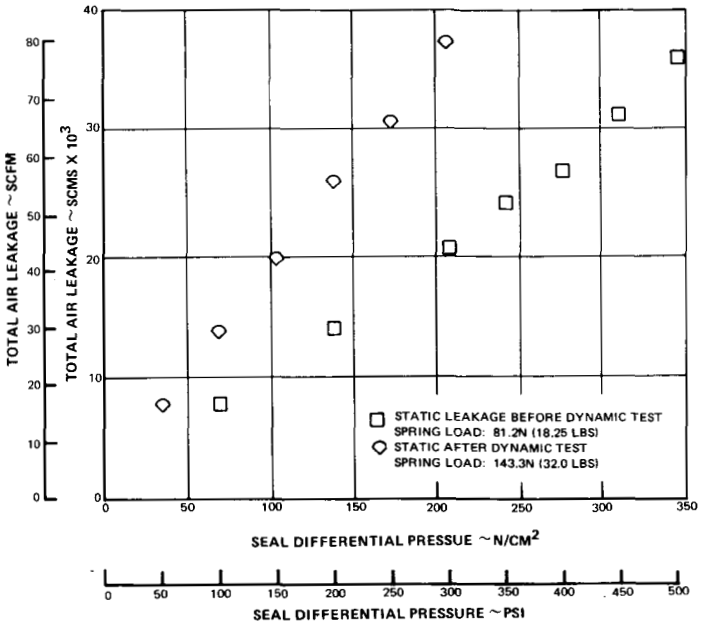

Figure 50 Static Seal Leakage Calibration for Axial Seal Seat Runout Test

The leakages from the above testing are presented in Figure 51 through 54. At the higher levels of differential pressure, the measured leakage was slightly less than predicted*. Conversely, at low pressures and high speeds the measured leakage was somewhat higher than predicted. The latter occurred because total seal closing force was marginal with the reduced spring load. The nosepiece could not follow the seal seat runout and the effective seal gap was increased.

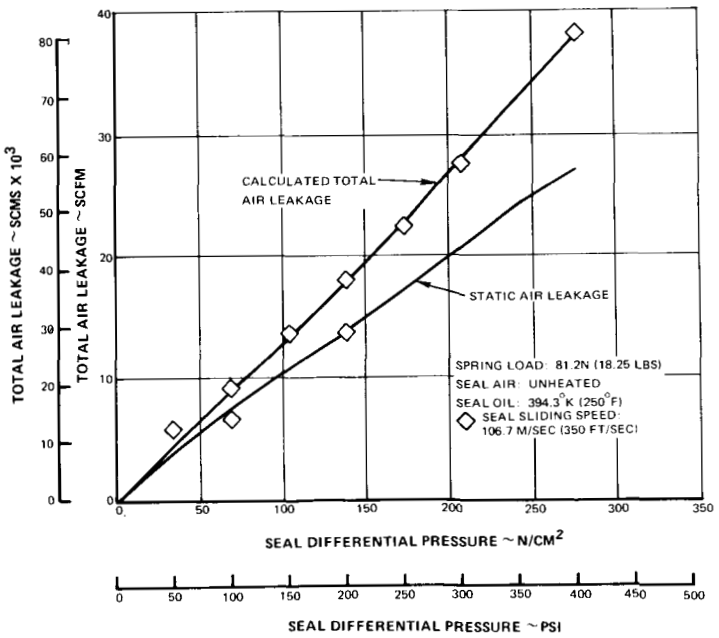

Figure 51 Performance Calibration for Axial Seal Seat Runout Test – 106.7 m/sec (350 ft/sec)

*predicted by adding the pre-test static air leakage (Fig. 49) to predicted dynamic leakage effects calculated in Section IV.

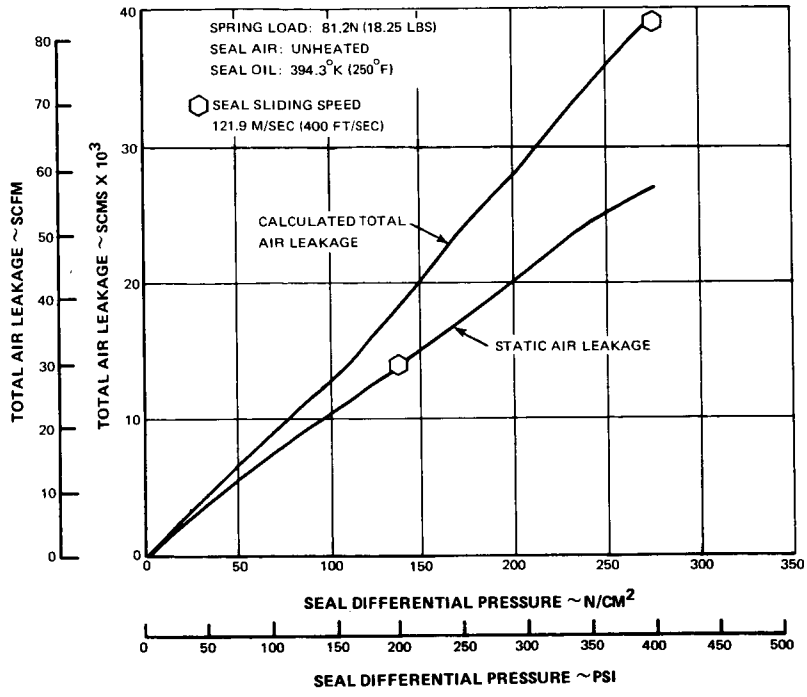

Figure 52 Performance Calibration for Axial Seal Seat Runout Test – 121.9 m/sec (400 ft/sec)

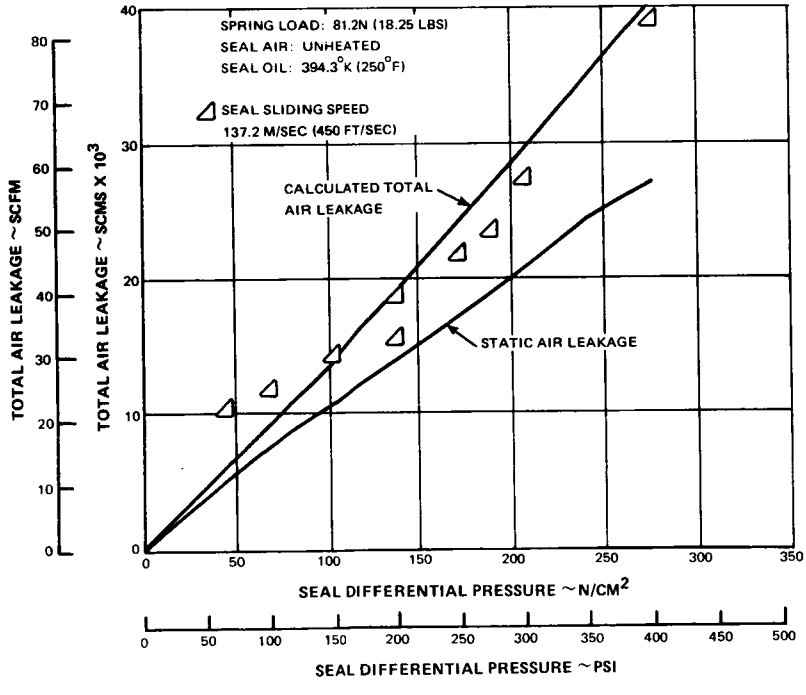

Figure 53 Performance Calibration for Axial Seal Seat Runout Test – 137.2 m/sec (450 ft/sec)

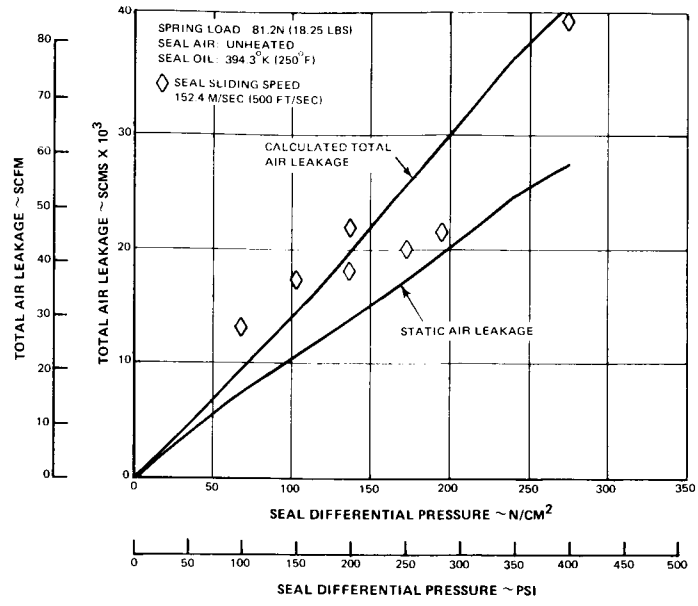

Figure 54 Performance Calibration for Axial Seal Seat Runout Test - 152.4 m/sec (500 ft/sec)

Post-test inspection of the seal showed it to be in good condition except for one shallow scratch across the nosepiece sealing dam.

In an attempt to improve sealing at low-pressure/high-speed conditions, the total seal spring force was increased to 137.9 N (31.0 lb) by increasing the number of springs. Testing was resumed and four (4) additional calibration points were completed. With the increased spring force, a slight improvement was realized in that it was possible to operate down to 34.5 N/cm^2 (50 psi) pressure differential at a seal speed of 137.2 m/sec (450 ft/sec). With the lower spring force, it was not possible to conduct testing below 46.2 N/cm^2 (67 psi) at that speed without erratic sealing performance.

A static leakage calibration following the four (4) dynamic test points indicated, as shown in Figure 50, a linear leakage rate from 0.014 scms (29 scfm) at 68.9 N/cm^2 (100 psi) to 0.0375 scms (79.5 scfm) at 206.8 N/cm^2 (300 psi). A subsequent bench test of the seal assembly indicated only small amounts of leakage across the face of the seal and by the piston ring. The primary static leakage path was located at the interfaces of the rear of the seal nosepiece and the seal carrier.

Inspection of the seal assembly indicated that the carbon nosepiece had shifted in its carrier, apparently during running. A polar profile trace showed that the back side of the nosepiece was out of flat by 152.4 microns (6 mils). Profile traces, Figure 55, across the front side of the nosepiece showed significant wear at the inner edge of the Rayleigh pads and at the outer edge of the sealing dam. The seal seat, Figure 56, was examined with an otpical flat, and although it displayed indications of seal contact, it was found to be flat within 0.5 micron (0.02 mils).

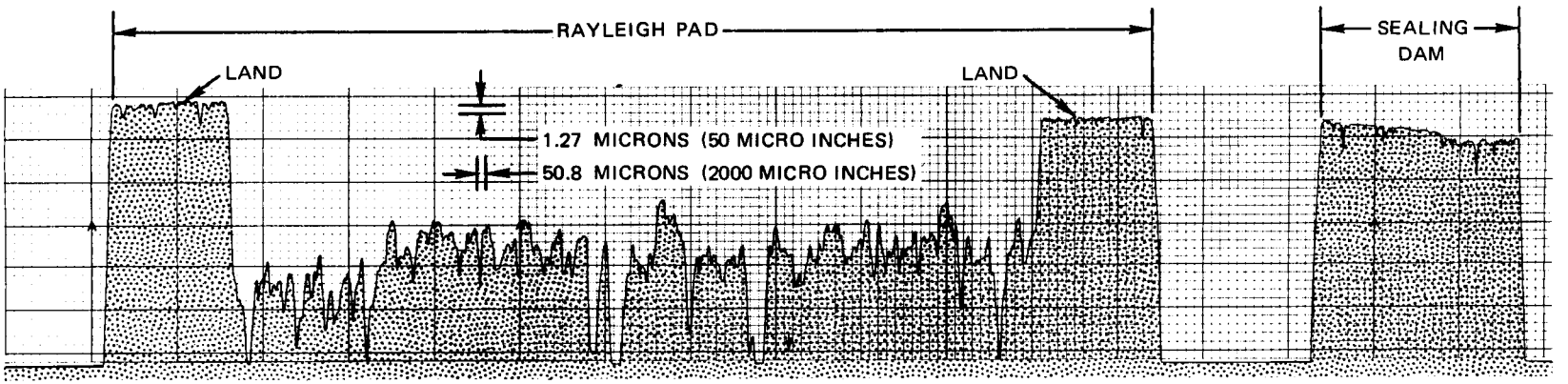

Figure 55 Representative Profile Trace Taken Radially Across the Face of the Carbon Nosepiece at Completion of Axial Seal Seat Runout Testing. Total Time on Nosepiece 31.5 Hours

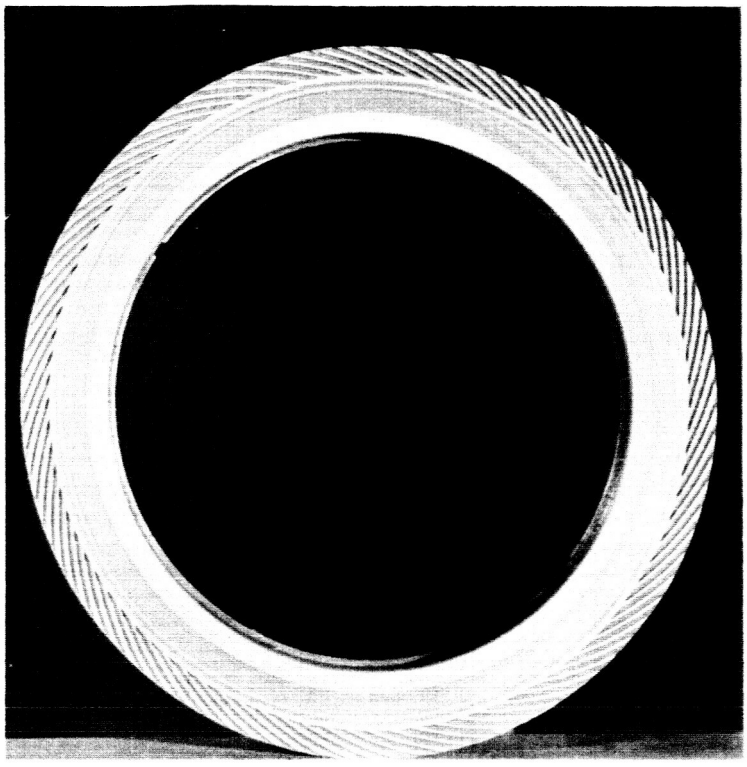

Figure 56 Seal Seat After 31.5 Hours of Testing With Axial Seal Seat Runout (XPN-33380)

The thirty-seven (37) combinations of speed and pressure documented with the 81.44 (18.25 lb) spring force and the four (4) test combinations completed with the increased spring force are presented in Tables XII and XIII, respectiyely.

TABLE XII

AXIAL SEAL SEAT RUNOUT TEST CONDITIONS AND RESULTS WITH A SPRING FORCE OF 81.4N (18.25 lb)

Point No.	Time hrs.	Sliding Speed m/sec	(ft/sec)	Seal Pressure N/cm^2	(psi)	Actual Total Air Leakage scms x 10^3	(scfm)
1	.25	91.4	(300)	34.5	(50)	2.60	(5.5)
2	.25	106.7	(350)	34.5	(50)	2.60	(5.5)
3	.25	121.9	(400)	34.5	(50)	4.25	(9.0)
4.	.25	137.2	(450)	46.2	(67)	10.15	(21.5)
5.	.25	91.4	(300)	68.9	(100)	5.19	(11.0)
6	.25	106.7	(350)	68.9	(100)	5.19	(11.0)
7.	.25	121.9	(400)	68.9	(100)	5.66	(12.0)
8	.25	137.2	(450)	68.9	(100)	11.58	(24.5)
9	.25	152.4	(500)	68.9	(100)	13.22	(28.0)
10	.25	91.4	(300)	103.4	(150)	8.02	(17.0)
11	.25	106.7	(350)	103.4	(150)	8.02	(17.0)
12	.25	121.9	(400)	103.4	(150)	8.02	(17.0)
13	.25	137.2	(450)	103.4	(150)	13.92	(29.5)
14	.25	152.4	(500)	103.4	(150)	17.23	(36.5)
15	.25	91.4	(300)	137.9	(200)	11.09	(23.5)
16	.25	106.7	(350)	137.9	(200)	10.62	(22.5)
17	.25	121.9	(400)	137.9	(200)	10.86	(23.0)
18	.25	137.2	(450)	137.9	(200)	15.34	(32.5)
19	.25	152.4	(500)	137.9	(200)	17.70	(37.5)
20	.25	91.4	(300)	172.4	(250)	14.17	(30.0)
21	.25	106.7	(350)	172.4	(250)	13.69	(29.0)
22	.25	121.9	(400)	172.4	(250)	14.16	(30.0)
23	.25	137.2	(405)	172.4	(250)	21.71	(46.0)
24	.25	152.4	(500)	172.4	(250)	19.82	(42.0)
25	.25	137.2	(450)	189.7	(275)	23.36	(49.5)
26	.25	91.4	(300)	206.8	(300)	17.23	(36.5)
27	.25	106.7	(350)	206.8	(300)	16.52	(35.0)
28	.25	121.9	(400)	206.8	(300)	16.05	(34.0)
29	.25	137.2	(450)	206.8	(300)	27.14	(57.5)
30	.25	152.4	(500)	206.8	(300)	22.18	(47.0)
31	.25	106.7	(350)	241	(350)	21.24	(45.0)
32	.25	106.7	(350)	275	(400)	25.96	(55.0)
33	.25	121.9	(400)	275	(400)	38.94	(82.5)
34	.25	137.2	(450)	275	(400)	39.18	(83.0)
35	.25	152.4	(500)	275	(400)	39.41	(83.5)
36	.25	106.7	(350)	310	(450)	31.15	(66.0)
37	.25	106.7	(350)	344	(500)	37.76	(80.0)

TABLE XIII

AXIAL SEAL SEAT RUNOUT TEST CONDITIONS AND RESULTS WITH A SPRING FORCE OF 138.3 N (31 lb)

Point No.	Time hrs.	Sliding Speed m/sec	(ft/sec)	Seal Pressure N/cm^2	(psi)	Actual Total Air Leakage scms x 10^3	(scfm)
38	.25	10.67	(350)	68.9	(100)	9.44	(20.0)
30	.25	137.2	(450)	34.5	(50)	7.70	(16.5)
40	.25	137.2	(450)	68.9	(100)	11.09	(23.5)
41	.25	137.2	(450)	137.9	(200)	21.00	(44.5)

The data indicates that the seal design can function satisfactorily at the maximum seal seat axial runout expected in present carbon face seal applications.

D. EFFECTS OF AIR-ENTRAINED DIRT (TASK VII)

Task VII of this program was directed to evaluating the effects of air-entrained dirt on the NASA seal design. A dirt metering device was designed, built, and installed on the test rig. Two tests were performed on NASA furnished seal hardware, at sliding speeds from 91.4 to 137.2 m/sec (300 to 450 ft/sec), differential pressures from 68.9 to 206.8 N/cm^2 (100 to 300 psi), and sealed gas temperatures from 369 to 643°K (205 to 699°F). Although wear was generated on the seal nosepiece, satisfactory overall performance with the absence of erratic sealing demonstrated that the design is not abnormally sensitive and has tolerance to air-entrained dirt.

1. Provision For Air-Entrained Dirt

A metering device was designed and built by the Contractor to introduce dirt into the seal pressurizing air. The device was mounted on the test rig cover and connected to the air inlet line as shown in Figure 57. Dirt was supplied by a motor driven, calibrated feed screw, as shown in Figure 58, at approximately 3.5 gr/hr (0.125 oz/hr) into the seal pressurizing air. Previous P&WA™ tests on positive-contact mainshaft face seals, approximately the same size as the gas-film seal, indicated that 3.5 gr/hr (0.125 oz/hr) of crushed quartz in the seal pressurizing air was sufficient to cause measurable seal wear in a 10-hour period.

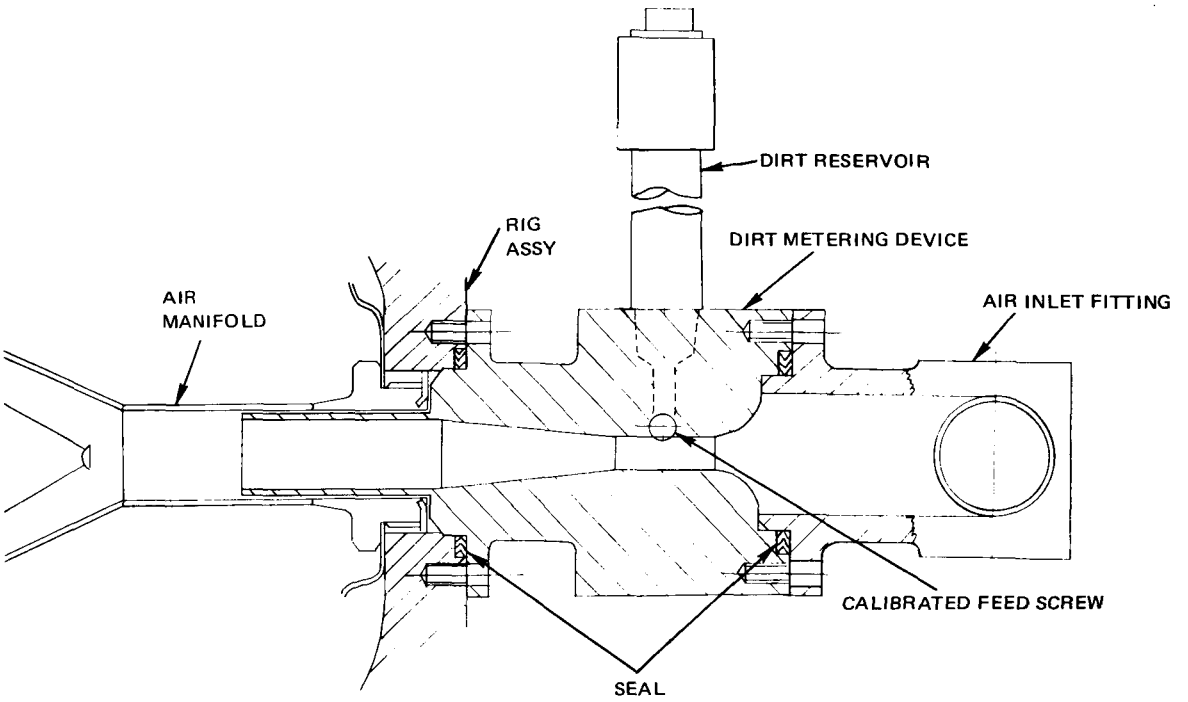

Figure 57 Test Setup Contaminant Injector

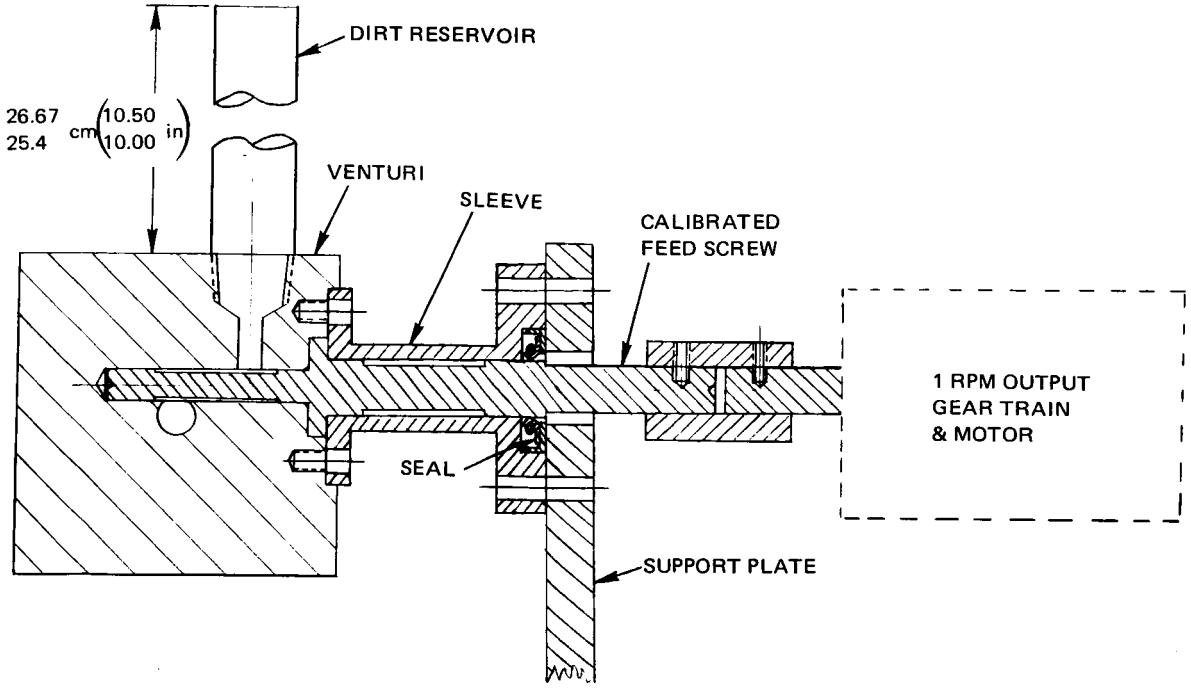

Figure 58 Assembly and Test Setup Contaminant Injector

The dirt contaminant used in this program is commercially known as "Arizona Road Dust - AC Fine", manufactured by AC Sparkplug Division of General Motors Corporation, and is classified as an air cleaner test dust. The specification for the dirt particle size distribution is given in Table XIV.

TABLE XIV

DIRT PARTICLE SIZE DISTRIBUTION

Micron Size	Percent
0-5	39±2
5-10	18±3
10-20	16±3
20-40	18±3
40-80	9±3

2. Test Seal Evaluation

The test rig rotor and test seal were assembled as shown in Figure 43. The seal seat was flat within 0.5 microns (0.02 mils) and in the assembled rig it had a runout of 15.2 microns (0.60 mils). The rotor assembly was balanced to within 3.95 gm-cm (.055 oz-in). The gas-film seal from the axial seal seat runout test was assembled with a new carbon nosepiece, and was installed with a total spring force of 82.5N (18.5 lbs) at the seal operating position. A profile trace across the face of the nosepiece in the new condition is shown in Figure 59.

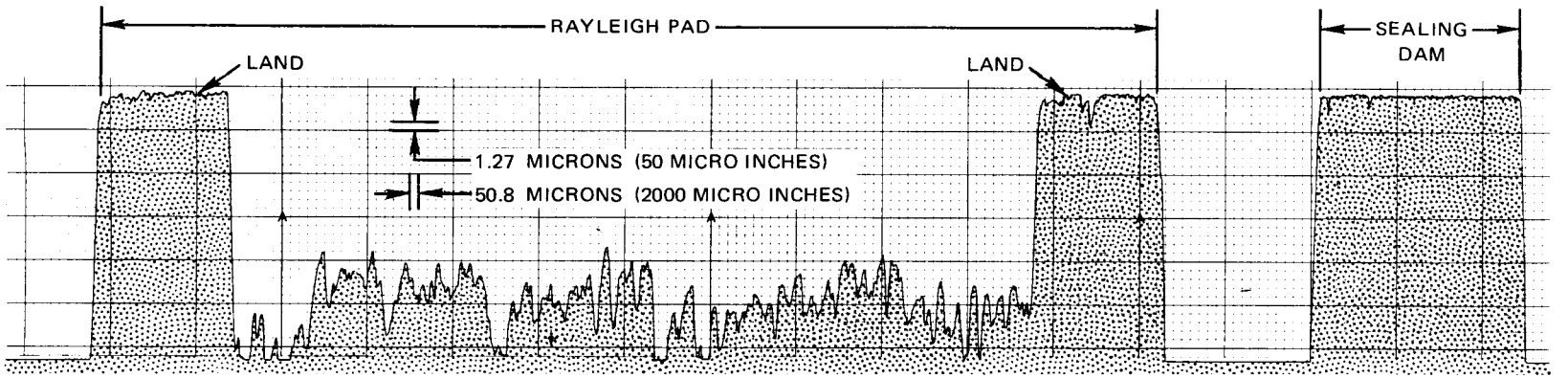

Figure 59 Representative Profile Trace Taken Radially Across the Face of the Carbon Nosepiece in New Condition Before First 10.5 Hours of Contaminated Air Testing

A static seal leakage calibration was performed at incremental pressures up to 206.8 N/cm^2 (300 psi). The results, which are presented in Figure 60, indicated that leakage was lower than that obtained prior to Task VI testing. Dynamic testing was initiated, with contaminate introduced into the seal pressurizing air at a rate of 3.5 gm/hr (0.125 oz/hr). After 4.5 hours of evaluation, the test was interrupted for repair of the dirt metering device. Testing was resumed and again interrupted, after 1.75 hours, to repair the compressor which supplies the high pressure air. The test was again resumed and continued for an additional 4.25 hours. At that time, the rig thrust bearings failed and the test was terminated. During test, no indications of erratic seal performance were observed. Specific conditions and leakages for the accumulated 10.5 hours of testing are summarized in Table XV.

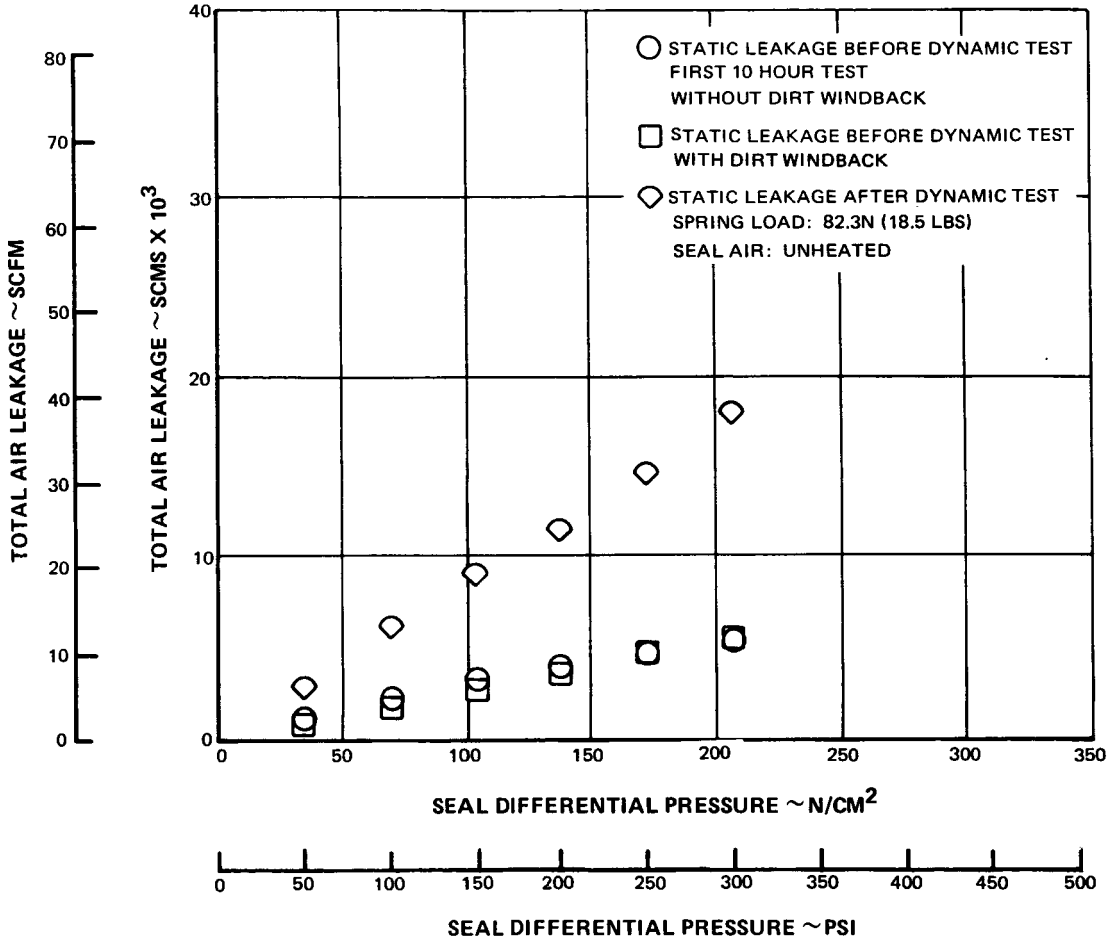

Figure 60 Static Seal Leakage Calibration for Evaluation of the Effects of Air-Entrained Dirt

TABLE XV

EVALUATION OF EFFECTS OF AIR-ENTRAINED CONTAMINANT TEST CONDITIONS AND MEASURED AIR LEAKAGE RATES WITHOUT DIRT WINDBACK

Time		Sliding Speed		Seal Pressure		Air Temp.		Total Air Leakage	
hrs	total hrs	m/sec	(ft/sec)	N/cm^2	(psi)	°K	(°F)	scms x 10^3	(scfm)
0.25	0.25	106.7	(350)	68.9	(100)	369	(205)	2.5	(5.2)
0.25	0.50	106.7	(350)	137.9	(200)	419	(295)	5.9	(12.6)
0.25	0.75	106.7	(350)	206.8	(300)	510	(459)	9.2	(19.4)
0.25	1.00	137.2	(450)	206.8	(300)	602	(625)	9.6	(20.3)
0.50	1.50	137.2	(450)	206.8	(300)	643	(699)	9.2	(19.4)
0.50	2.00	137.2	(450)	206.8	(300)	632	(679)	9.2	(19.4)
0.50	2.50	137.2	(450)	206.8	(300)	619	(656)	9.2	(19.4)
0.50	3.00	137.2	(450)	206.8	(300)	614	(646)	9.3	(19.8)
0.50	3.50	137.2	(450)	206.8	(300)	600	(620)	9.9	(21.0)
0.25	3.75	106.7	(350)	206.8	(300)	538	(510)	9.2	(19.4)
0.25	4.00	91.4	(300)	206.8	(300)	503	(446)	8.9	(18.8)
0.25	4.25	91.4	(300)	206.8	(300)	489	(422)	8.9	(18.8)
0.25	4.50	91.4	(300)	155.0	(225)	461	(372)	5.6	(12.0)
0.25	4.75	106.7	(350)	68.9	(100)	416	(290)	7.5	(15.8)
0.25	5.00	106.7	(350)	137.9	(200)	505	(450)	9.7	(20.6)
0.25	5.25	106.7	(350)	206.8	(300)	602	(625)	11.0	(23.2)
0.50	5.75	137.2	(450)	206.8	(300)	638	(689)	12.4	(26.2)
0.50	6.25	137.2	(450)	206.8	(300)	630	(675)	12.7	(27.0)
0.25	6.50	91.4	(300)	68.9	(100)	393	(248)	5.4	(11.5)
0.25	6.75	106.7	(350)	137.9	(200)	463	(375)	11.2	(23.8)
0.25	7.00	106.7	(350)	206.8	(300)	619	(655)	16.1	(34.2)
0.50	7.50	137.2	(450)	206.8	(300)	663	(735)	16.1	(34.2)
0.50	8.00	137.2	(450)	206.8	(300)	627	(670)	17.9	(38.0)
0.50	8.50	137.2	(450)	206.8	(300)	605	(630)	17.2	(36.5)
0.50	9.00	137.2	(450)	206.8	(300)	596	(614)	17.9	(38.0)
0.50	9.50	137.2	(450)	206.8	(300)	590	(604)	17.9	(38.0)
0.50	10.00	137.2	(450)	206.8	(300)	589	(602)	17.9	(38.0)
0.50	10.50	137.2	(450)	206.8	(300)	650	(612)	17.9	(38.0)

While the rig bearing was being replaced, the test seal assembly was removed from the rig for a static leakage test in the bench fixture. The leakage rate had increased from the pre-test value of 0.0015 scms (3.2 scfm) at 55.2 N/cm^2 (80.0 psi) to 0.0021 scms (4.5 scfm) at 20.7 N/cm^2 (30 psi). The leakage appeared to be equally divided among the seal face, the piston ring, and the interfaces of the nosepiece and carrier. All of the seal components were in good condition as shown in Figures 61 and 62. After the hub assembly was removed from the rig, but with the seal seat still on the hub, an optical flatness check of the seal seat showed it to be flat within 0.5 microns (0.02 mils). A profile trace across the carbon nosepiece, Figure 63, showed wear up to 11.43 microns (0.45 mils) across the Rayleigh pads and up to 34.3 microns (1.35 mils) at the inner edge of the sealing dam. A photograph of the nosepiece is shown in Figure 64.

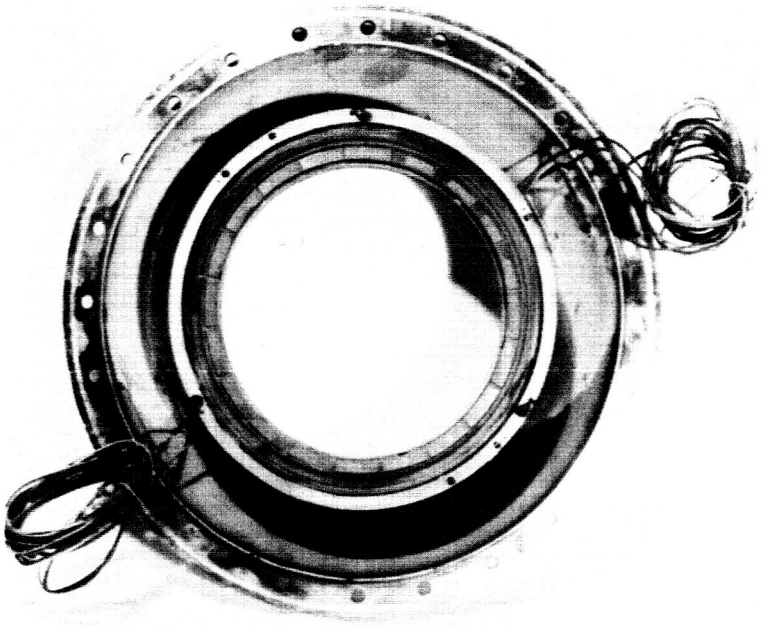

Figure 61 Seal Assembly After Completing First 10.5 Hours Contaminated Air Test. Total Time on Seal 11 Hours (XPN-33887)

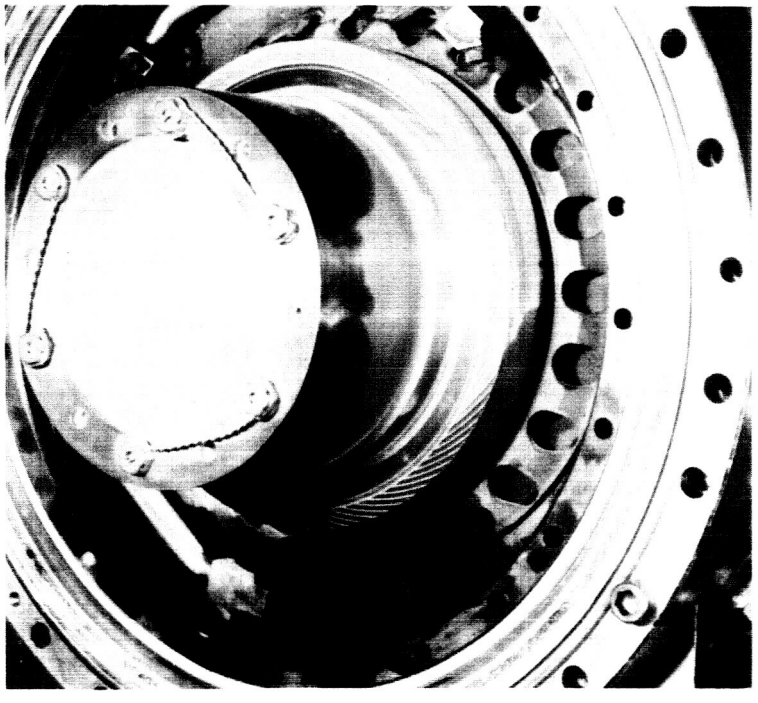

Figure 62 Seal Seat After Completing First 10.5 Hour Contaminated Air Test. Total Time on Seal Seat 11 Hours (XPN-33889)

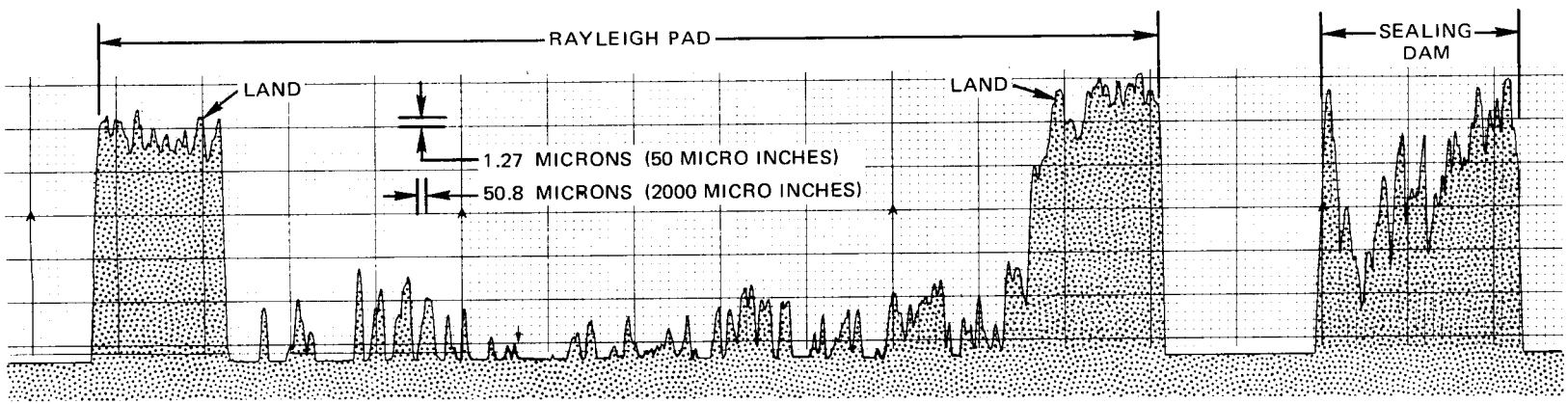

Figure 63 Representative Profile Trace Taken Radially Across the Face of the Carbon Nosepiece at Completion of First 10.5 Hours of Contaminated Air Testing. Total Time on Nosepiece 11 Hours

Figure 64 Seal Nosepiece After Completing First 10.5 Hours Contaminated Air Test. Total Time on Seal 11 Hours (XPN-36569)

The seal assembly was rebuilt with a new seal nosepiece and a new carbon piston ring secondary seal. A profile trace of this nosepiece in the new condition is shown in Figure 65. Dirt rejection hardware (refered to as "dirt windback") designed and supplied by NASA was installed in the rig as shown in Figure 66. The dirt windback consisted of a stationary helix attached to the seal support housing, and a rotating helix mounted on the hub assembly. Seal pressurizing air passed through and between the two parts of the windback. The intent of the windback design was to remove air-entrained dirt particles before they reached the sealing surfaces.

A static leakage calibration was preformed on the rebuilt seal assembly at incremental pressures up to 206.8 N/cm^2 (300 psi) in the rig. These results are shown in Figure 60 and are approximately the same as the static leakage calibration results obtained prior to the first 10.5 hours of testing without the dirt windback.

The second dynamic test was initiated with dirt fed into the seal pressurizing air at a rate of 3.5 g/hr (0.125 oz/hr). The test was interrupted after 4.25 hours to repair the contaminant reservoir pressurizing line. Testing then continued without further interruption until completion with a total of 11.5 hours of testing accrued. The test conditions and leakage results, which were again obtained without erratic sealing, are summarized in Table XVI. Prior to removing the test seal from the rig, a static seal leakage calibration was performed at incremental pressures up to 206.8 N/cm^2 (300 psi). As shown in Figure 60, the static calibration indicated a deterioration in static sealing during the course of testing with the dirt windback. With 206.8 N/cm^2 (300 psi) differential pressure, the leakage increased from the pre-test level of 0.005 scms (11.5 scfm) to the post-test level of 0.018 scms (38.0 scfm).

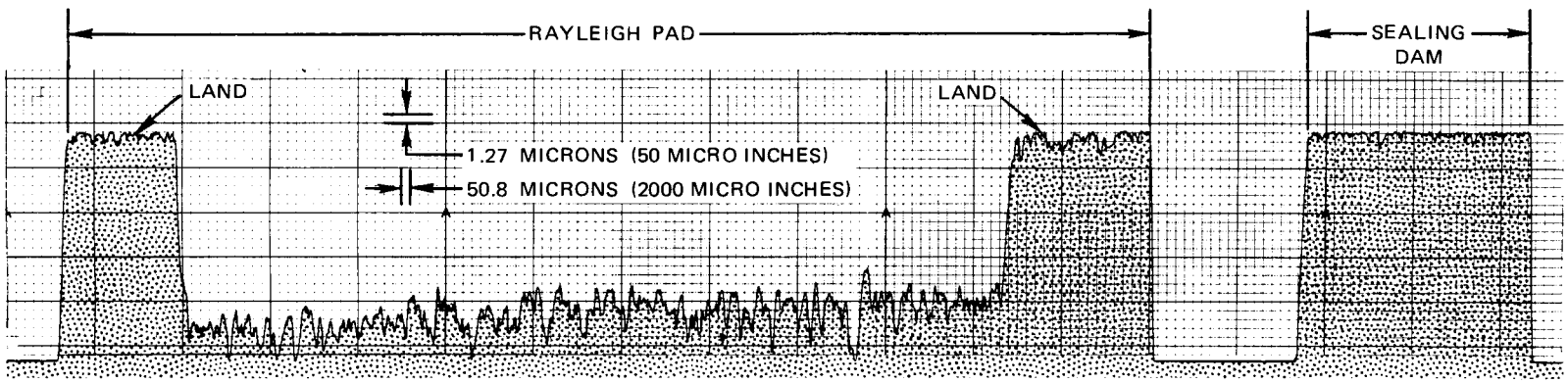

Figure 65 Representative Profile Trace Taken Radially Across the Face of the Carbon Nosepiece in the New Condition Before the Second Contaminated Air Test

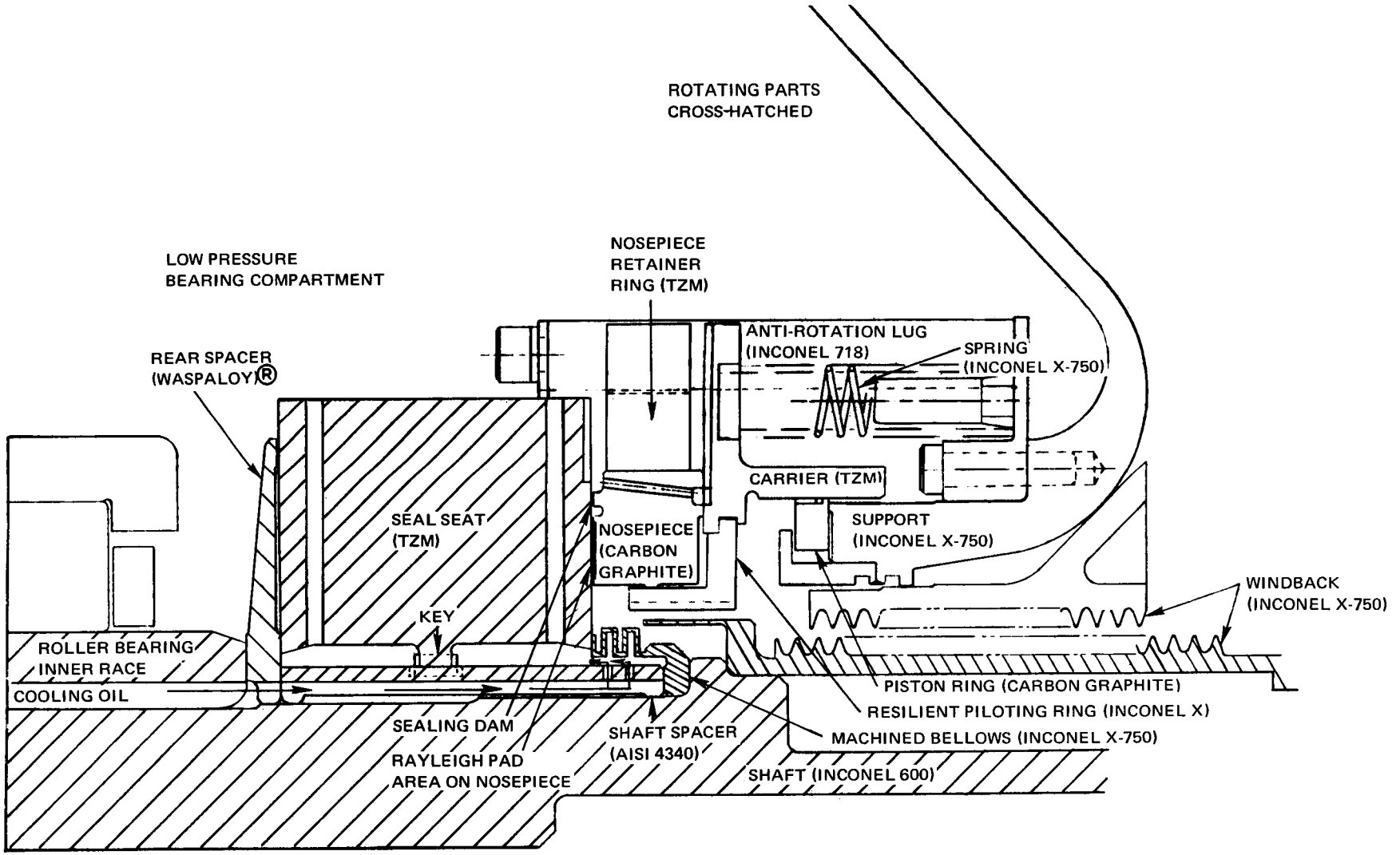

Figure 66 Hub and Seal Assembly Configuration as Used During Second Part of Contaminated Air Testing Showing Dirt Windback

TABLE XVI

TEST CONDITIONS AND MEASURED AIR LEAKAGE RATES FROM THE SECOND TASK VII CONTAMINATED AIR TEST WITH DIRT WINDBACK EMPLOYED

Time		Sliding Speed		Seal Pressure		Air Temp.		Total Air Leakage	
hrs	total hrs	m/sec	(ft/sec)	N/cm^2	(psi)	°K	(°F)	scms x 10^3	(scfm)
.25	.25	121.9	(400)	103.4	(150)	406	(271)	6.5	(13.8)
.25	.50	121.9	(400)	137.9	(200)	454	(357)	8.9	(18.8)
.25	.75	121.9	(400)	206.8	(300)	513	(464)	13.7	(29.0)
.25	1.00	137.2	(450)	206.8	(300)	590	(603)	15.2	(32.2)
.25	1.25	137.2	(450)	206.8	(300)	608	(635)	15.2	(32.3)
.50	1.75	137.2	(450)	206.8	(300)	597	(615)	14.9	(31.6)
.50	2.25	137.2	(450)	206.8	(300)	594	(610)	15.1	(32.0)
.50	2.75	137.2	(450)	206.8	(300)	594	(610)	15.2	(32.2)
.50	3.25	137.2	(450)	206.8	(300)	596	(613)	15.4	(32.6)
.50	3.75	137.2	(450)	206.8	(300)	596	(614)	15.9	(33.6)
.50	4.25	137.2	(450)	206.8	(300)	595	(611)	159	(33.6)
.25	4.50	121.9	(400)	68.9	(100)	411	(281)	7.1	(15.0)
.25	4.75	121.9	(400)	137.9	(200)	516	(470)	13.3	(28.2)
.25	5.00	121.9	(400)	137.9	(200)	562	(552)	13.0	(27.5)
.50	5.50	121.9	(400)	137.9	(200)	589	(601)	12.7	(27.0)
.50	6.00	137.2	(450)	137.9	(200)	597	(615)	13.0	(27.6)
.50	6.50	137.2	(450)	137.9	(200)	594	(609)	13.3	(28.2)
.50	7.00	137.2	(450)	137.9	(200)	594	(609)	13.4	(28.4)
.50	7.50	137.2	(450)	137.9	(200)	594	(610)	13.4	(28.4)
.50	8.00	137.2	(450)	137.9	(200)	594	(610)	13.4	(28.4)
.50	8.50	137.2	(450)	137.9	(200)	594	(610)	13.4	(28.4)
.50	9.00	137.2	(450)	137.9	(200)	597	(615)	13.4	(28.4)
.50	9.50	137.2	(450)	172.3	(250)	605	(630)	16.5	(35.0)
.50	10.00	137.2	(450)	172.3	(250)	602	(624)	16.6	(35.2)
.50	10.50	137.2	(450)	206.8	(300)	600	(621)	19.4	(41.0)
.50	11.00	137.2	(450)	172.3	(250)	600	(620)	16.0	(34.0)
.50	11.50	137.2	(450)	206.8	(300)	598	(617)	19.4	(41.0)

Visual inspection of the test seal assembly when removed from the rig proved it to be in generally good condition. Bench testing of the seal assembly indicated deterioration had occurred during the course of testing similar to that shown by the static rig calibration.

Prior to testing, a pressure of 55.2 N/cm^2 (80.0 psi) was required to obtain a leakage rate of 0.0021 scms (4.4 scfm), whereas, in the post-test leakage check a pressure of only 20.7 N/cm^2 (30 psi) was needed before the same leakage rate was obtained. The leakage appeared to be equally divided among the seal face, piston ring, and the interface of the nosepiece and carrier. Profile traces across the carbon nosepiece shown in Figure 67 indicated no appreciable wear of the Rayleigh pads, but up to 31.75 microns (1.25 mils) of wear at the inner edge of the sealing dam. The appearance of the nosepiece can be seen in Figure 68.

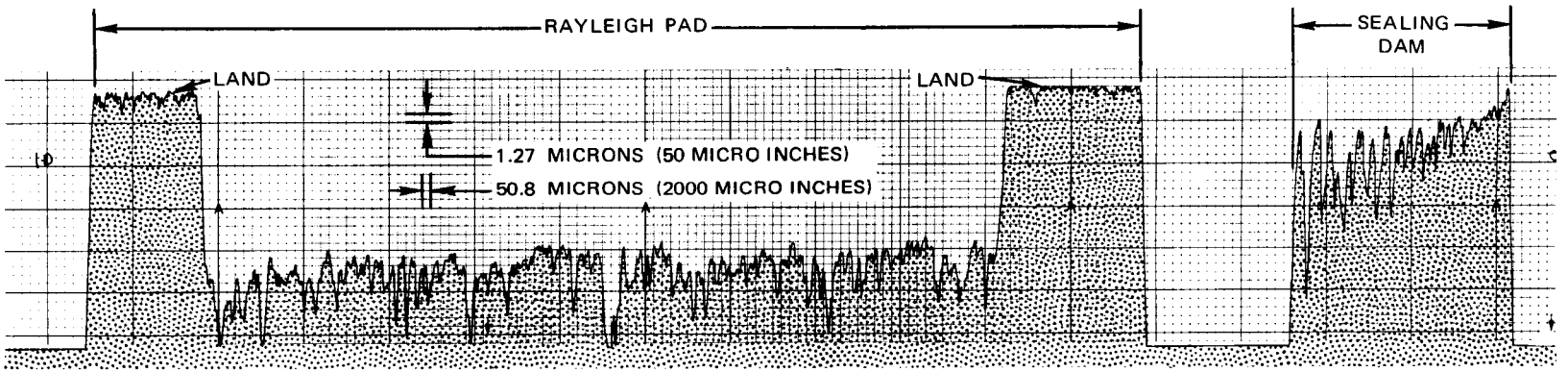

Figure 67 Representative Profile Trace Taken Radially Across the Face of the Carbon Nosepiece at Completion of Second Contaminated Air Test With a Dirt Windback. Total Time on Nosepiece 14.5 Hours

Figure 68 Seal Nosepiece After Completing Second Contaminated Air Test Using Dirt Windback. Total Time on Seal 14.5 Hours (XPN-36570)

The seal seat was removed from the hub assembly, Figure 69, and an optical flatness check showed it to be flat within 0.5 microns (0.02 mils). From profile traces made across the face of the seal seat, as shown in Figure 70, a circumferential wear groove approximately 4.45 microns (0.175 mils) deep was found to exist in the area corresponding to the inner edge of the nosepiece sealing dam.

Leakage results recorded during both contaminated air tests are shown in Figure 71. At the test point, 137 m/sec (450 ft/sec) and 206.8 N/cm^2 (300 psi), a 90 percent increase in seal air leakage resulted during the 10.5 hour test without the dirt windback, whereas, only a 28 percent seal air leakage increase resulted during the 11.5 hour test with the dirt windback employed.

Although wear was generated on the seal nosepieces, the satisfactory overall performance with the absence of erratic sealing of the gas-film seals in this phase of testing, has demonstrated that the Task I gas-film seal design is not abnormally sensitive and displayed tolerance to contaminate particles in the sealing air supply. Sealing performance was never erratic during evaluation.

The dirt windback was not effective in reducing or eliminating wear at the sealing dam by removing contaminate particles in the sealing air before reaching the seal face. The lower leakage rate increase during the testing with the dirt windback is felt to be attributable to the less severe conditions maintained during this evaluation rather than the presence of the windback.

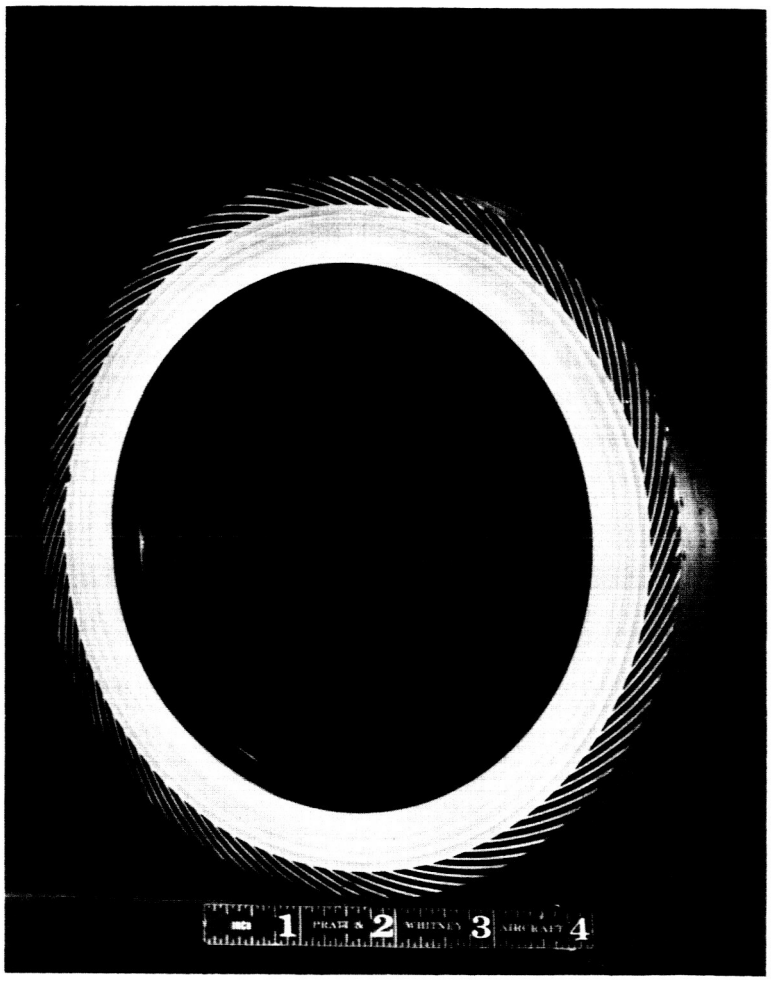

Figure 69 Seal Seat After Completing Contaminated Air Testing. Total Time on Seal Seat 25.5 Hours (XPN-36433)

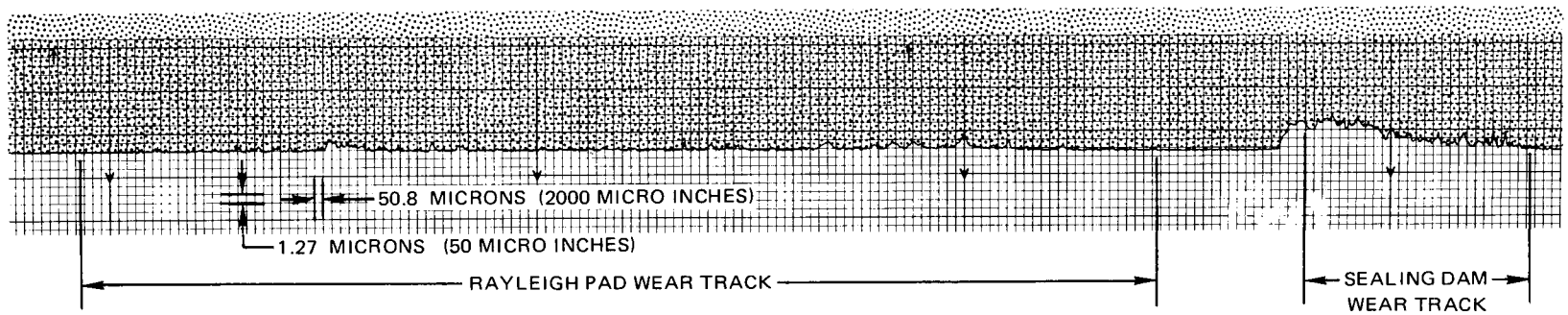

Figure 70 Representative Profile Trace Taken Radially Across the Face of the Seal Seat at Completion of Contaminated Air Testing Showing Nosepiece Wear Track. Total Time on Seal Seat 25.5 Hours

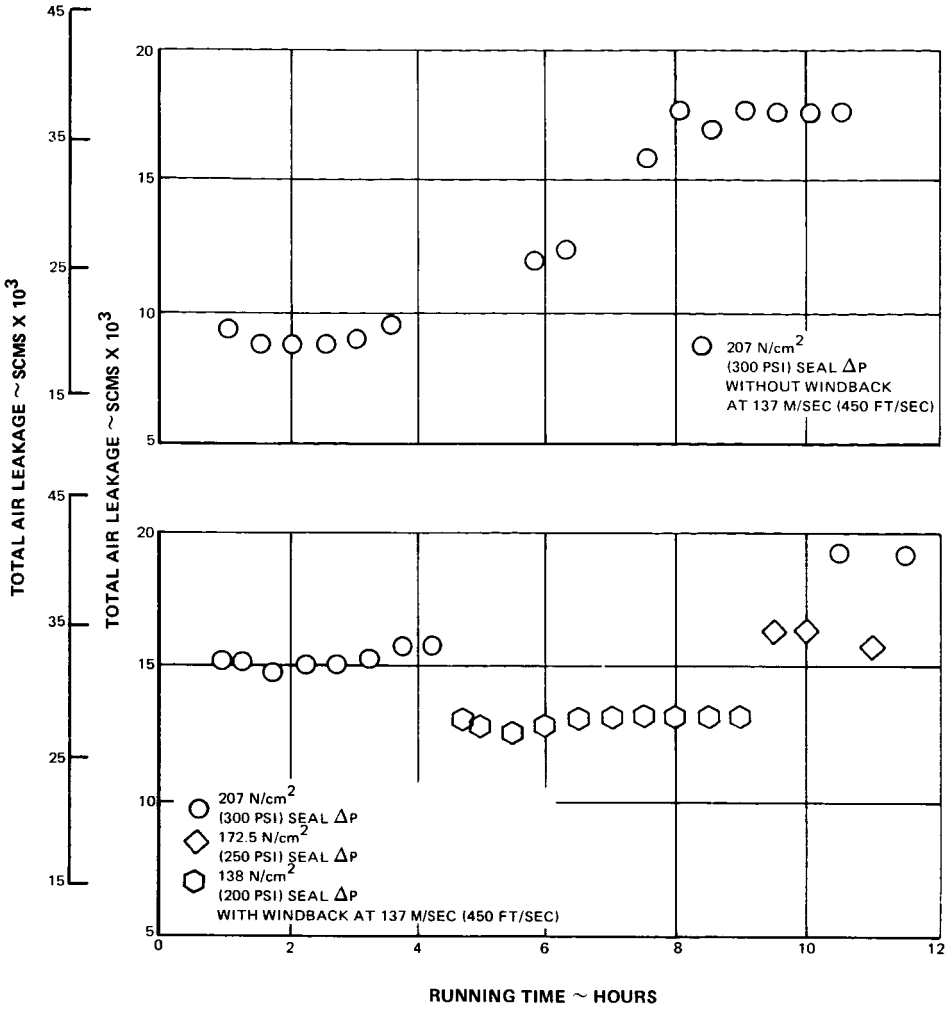

Figure 71 Comparison of Leakages Measured During Contaminated Air Testing With Windback (Lower Curve) and without Windback (Upper Curve)

E. ELEVATED TEMPERATURE ENDURANCE TESTS (TASK VIII)

The final task in this program was to evaluate the NASA seal design at temperatures from 700 to 922°K (800 to 1200°F) with differential pressures from 207 to 345 N/cm^2 (300 to 500 psi) and speeds from 122 to 183 m/sec (400 to 600 ft/sec). The test components were furnished by NASA. One nosepiece and one seal seat were used throughout 86.25 hours of testing accomplished in this portion of the program.

The test rig was assembled for elevated temperature endurance testing with a new gas-film seal, an oil windback, a new Ni-Span C seal carrier, and a carbon secondary seal piston ring (Figure 72). The total spring force for the seal assembly was established at 84.5 N (19.0 lb) and the assembled axial seal seat runout was measured at 7.5 microns (0.3 mils). The rotor assembly was balanced to within 3.6 gm-cm (0.05 oz-in).

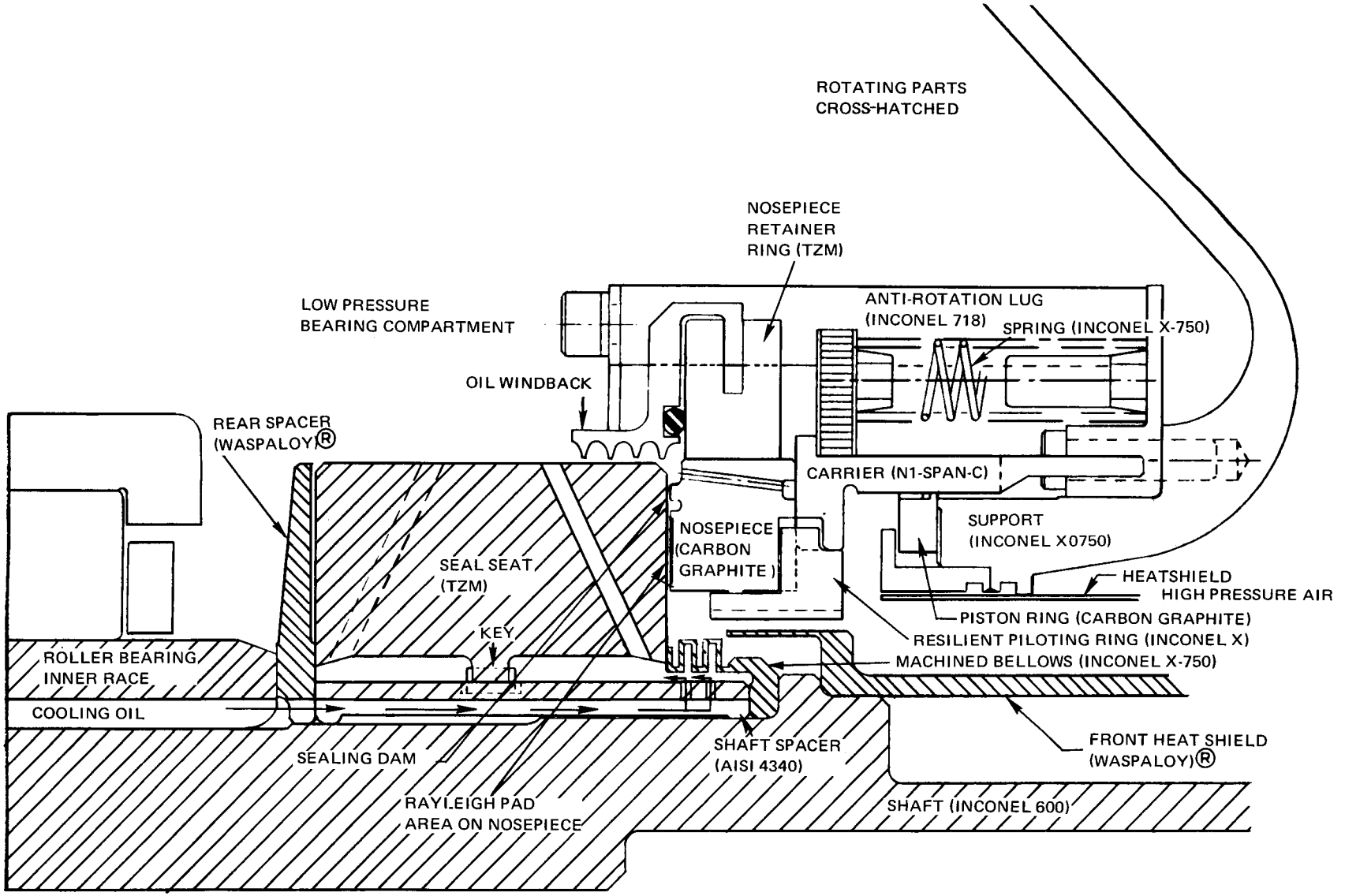

Figure 72 Initial Hub and Seal Assembly for Elevated Temperature Endurance Testing Showing Small Diameter Seal Seat and Oil Windback

The assembled rig was mounted in the test facility and a static leakage calibration was completed at incremental pressures up to 207 N/cm^2 (300 psi). The results of this calibration are shown in Figure 73.

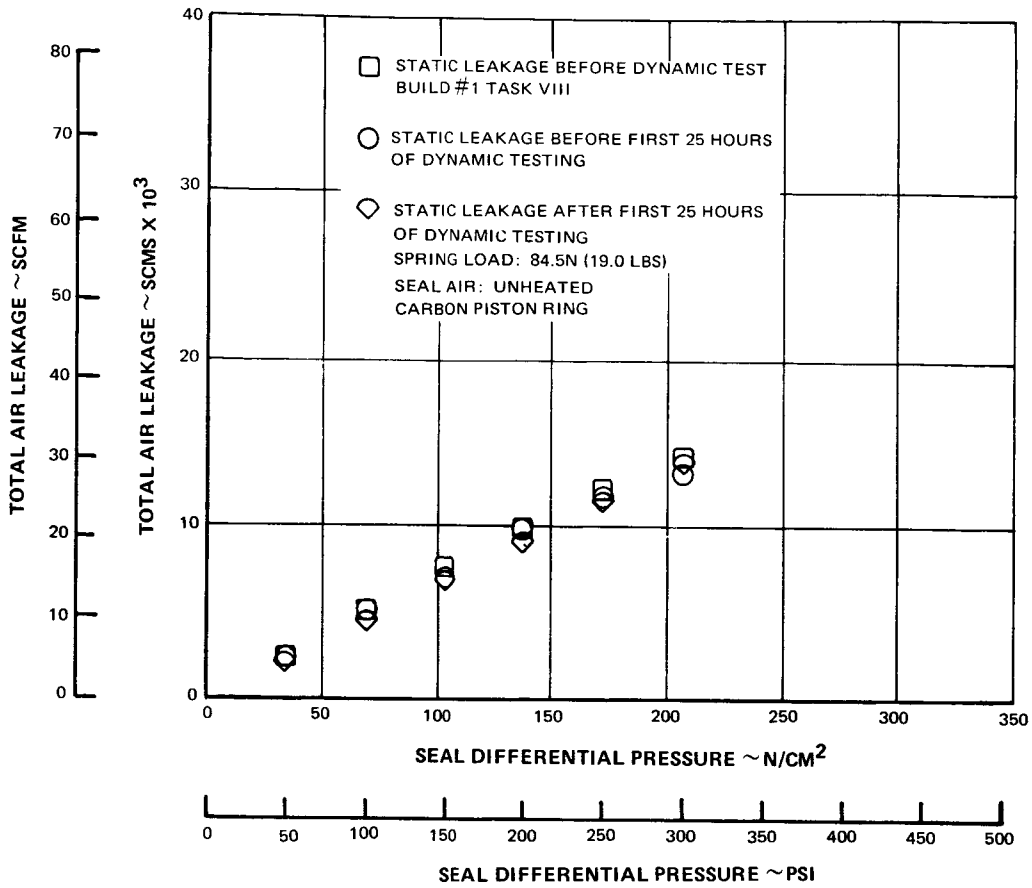

Figure 73 Static Seal Leakage Calibration for Elevated Temperature Endurance Test

Dynamic testing was initiated at 122m/sec (400 ft/sec) seal sliding speed, 207 N/cm^2 (300 psi) seal differential pressure, and 700°K (800°F) sealed gas temperature. Air leakage was measured at 13.69 x 10^{-3} scms (29.0 scfm). These conditions were maintained for 2.33 hours, at which time testing was terminated because of an overload condition on the rig drive engine and a simultaneous increase in the temperature of the support housing for the rig roller bearing. Investigation showed that a valve in the oil scavenge system had inadvertently been left open, allowing the scavenge pump to circulate oil without adequately pumping oil from the rig.

When the seal assembly was removed from the rig for inspection, it was observed that the Rayleigh pads had been worn from the seal face and that there was coke on the seal carrier. The chrome carbide flame coating on the seal seat was blistered and discolored in the area that had been rubbed by the seal. The rest of the test and rig hardware was in good condition. The condition of the nosepiece is shown in Figure 74 and of the seal seat in Figure 75.

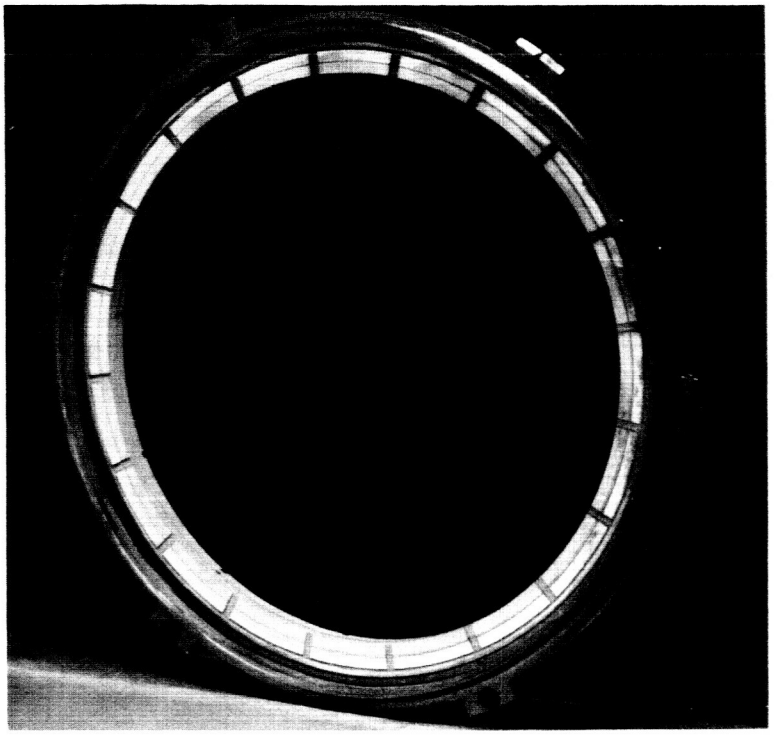

Figure 74 Result of Sump Flooding (Rig Malfunction) Carbon Nosepiece After 2.33 Hours of Elevated Temperature Endurance Testing Showing Rayleigh Pads Completely Worn (XPN-36609)

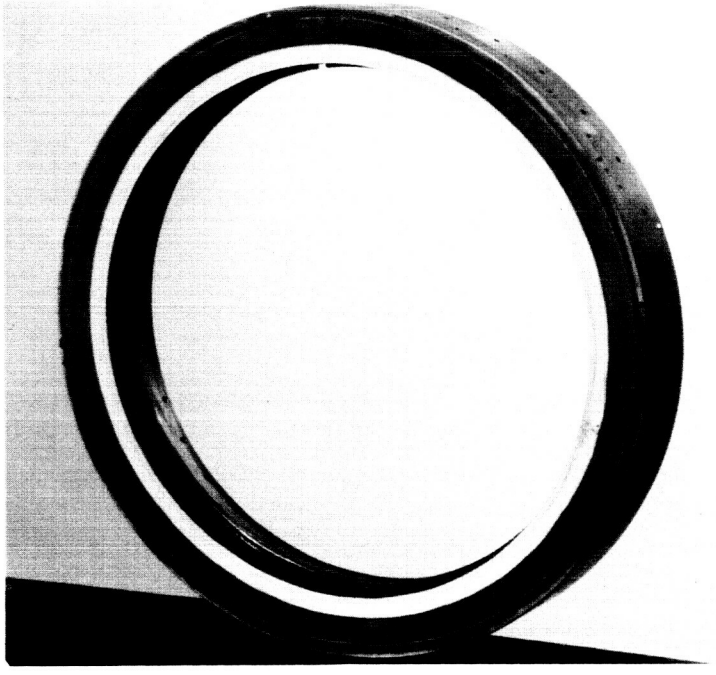

Figure 75 Result of Sump Flooding (Rig Malfunction) Seal Seat After 2.33 Hours of Elevated Temperature Endurance Testing Showing Over-Heated and Blistered Face (XPN-36610)

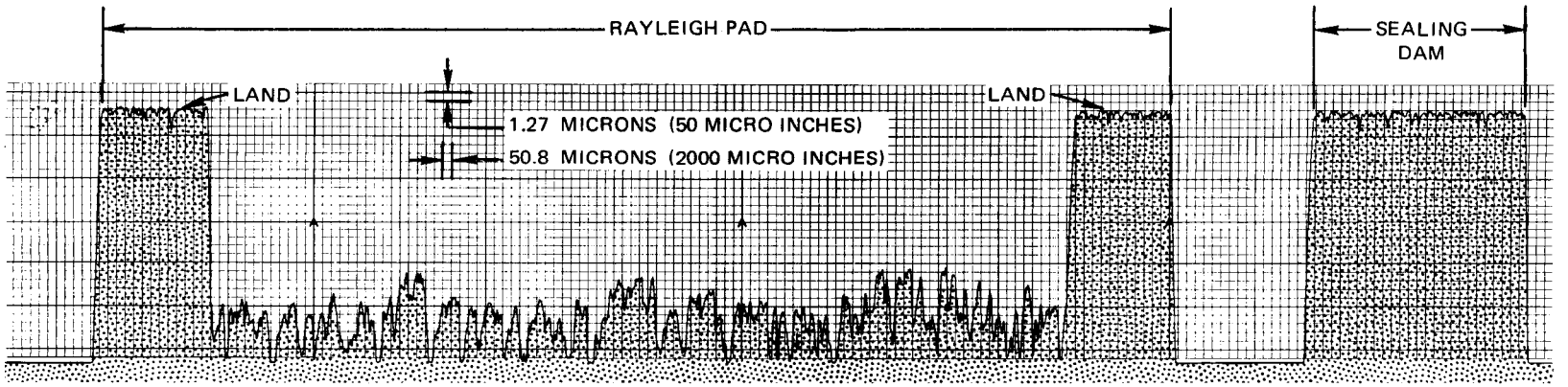

Figure 76 Representative Profile Trace Taken Radially Across the Face of the Carbon Nosepiece in New Condition Before Elevated Temperature Endurance Testing

The rig rotor assembly and seal assembly were rebuilt to the configuration used in Task IV, shown in Figure 31. A new nosepiece was used in the seal assembly without the oil windback. The carrier was cleaned and reinstalled in the assembly with the same carbon secondary seal piston ring. The spring force in the seal assembly was maintained at 84.5 N(19.0 lb). A seal seat of TZM material was lapped flat to within 0.5 microns (0.02 mils) and was installed in the rig. The rotor assembly was balanced to within 2.16 gm-cm (0.03 oz-in) and the assembled seal seat had a runout of 7.6 microns (0.3 mils). A profile trace of the new nosepiece is shown in Figure 76.

After reinstalling the rig in the test facility, a static leakage calibration was completed on the seal up to 207 N/cm^2 (300 psi). The results, also appearing in Figure 73, are in close approximation to those recorded in the previous static calibration.

Elevated temperature endurance testing was initiated on the second seal at 122 m/sec (400 ft/sec), 207 N/cm^2 (300 psi), and 700°K (800°F) sealed gas temperature. The program was interrupted after one hour because of high temperatures on the seal carrier, the seal support housing, and the rig roller bearing support housing. Inspection of the seal assembly revealed it to be in good condition. It had been anticipated that the elevated air temperature might substantially increase the temperature of the carrier and housings. An oil spray manifold containing three (3) spray nozzles was mounted in the rig but was left inoperative during this test to allow measurement of the temperature levels without supplemental oil cooling. Since this test confirmed that additional cooling was required to reduce the temperature levels of the carrier and housings, an oil supply line was installed to the spray manifold. Additional cooling oil was provided at a rate of 2.72 Kg/min (6.0 lbs/min).

Dynamic testing was resumed at the same operating levels as in the previous one hour test. Twenty-five (25) hours of testing were completed at three conditions, during which the total seal air leakage increased by approximately 11.7 percent (Refer to Figure 77). The temperature reductions resulting from the additional oil to cool the hardware are presented in Table XVII. As shown in Figure 73, the static seal leakage measured in the rig after test was essentially unchanged from the values recorded prior to dynamic testing.

TABLE XVII
ELEVATED TEMPERATURE ENDURANCE TEST
TEMPERATURES OF CRITICAL PARTS

	Temperature Without Oil Cooling °K	Temperature With Oil Cooling °K	Temperature Without Oil Cooling (°F)	Temperature With Oil Cooling (°F)
Air	702	711	(805)	(820)
Seal Support	500	477	(440)	(400)
Roller Bearing	453	450	(356)	(350)
Roller Bearing Housing	467	439	(382)	(330)
Carrier	550	544	(530)	(520)

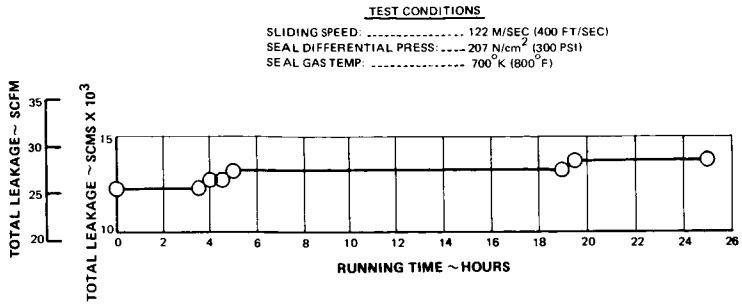

Figure 77 Leakage Measured During First Elevated Temperature Endurance Program

At the completion of the 25-hour test, visual inspection of the seal and seal seat revealed them to be in good condition. Static bench testing of the seal assembly indicated that the static air leakage had decreased from a pre-test rate of 0.0022 scms (4.3 scfm) at 17.23 N/cm^2 (25 psi) to a post-test rate of 0.0018 scms (3.9 scfm) at the same pressure differential. Profile traces across the carbon seal face, Figure 78, shows wear of approximately 1.22 microns (0.05 mils), after a total of 37.75 hours of testing.

For the planned second 25 hour elevated temperature endurance test, the rig was assembled with the same seal hardware used in the first 25 hour program, except that the carbon secondary seal piston ring was replaced with a ring made of Haynes 188 material. This substitution was intended to allow higher temperature seal evaluation. The total spring force was maintained at 84.7 N (19.0 lb) at the seal operating position.

A static leakage calibration on the seal prior to initiating the planned second 25 hour elevated temperature endurance was performed with the results shown in Figure 79.

The sealed air temperature was increased in the initial testing over the level in the previous 25 hours test to 810.8°K (1000°F). The seal sliding speed was increased to 129.5 m/sec (425 ft/sec) while the pressure differential was maintained at the same level at 207 N/cm^2 (300 psi). After four (4) hours of testing, a decrease in seal air leakage from 12.5 x 10^{-3} scms to 10.6 x 10^{-3} scms (26.5 scfm to 22.5 scfm) occurred with a corresponding increase in seal differential pressure from 207 N/cm^2 to 217 N/cm^2 (300 psi to 315 psi). These conditions were maintained for 4.5 additional hours for a total of 8.5 hours for this portion of the program. At that time, a shut down of the test was initiated; the speed was reduced to 91 m/sec (300 ft/sec) and the air heater was shut off to gradually cool down the rig. After 1.75 hours into the cool down period, with the sealed gas temperature at 569°K (565°F), pressure differential at 207 N/cm^2 (300 psi), and the air leakage at 22.2 x 10^{-3} scms (47 scfm), the seal suddenly opened resulting in a sharp increase in both seal leakage rate and breather pressure. Rig shut down was completed. Attempts to perform a static leakage calibration were unsuccessful indicating that the seal was unseated. Inspection of the seal assembly revealed it to be in good condition, however, a bench leak test revealed excessive leakage by the nosepiece and carrier interfaces. A detailed inspection of the seal assembly revealed a slight separation of the nosepiece and carrier due to coke buildup on the carrier interface. The O.D. of the carrier also had coke build-up, as did the I.D. of the Al_2O_3 surface outboard of the piston ring position. A profile trace of the carrier interface showed that the surface was flat within 2.27 microns (0.090 mils). The carrier was cleaned and the mating surface was lapped to remove all traces of coke.

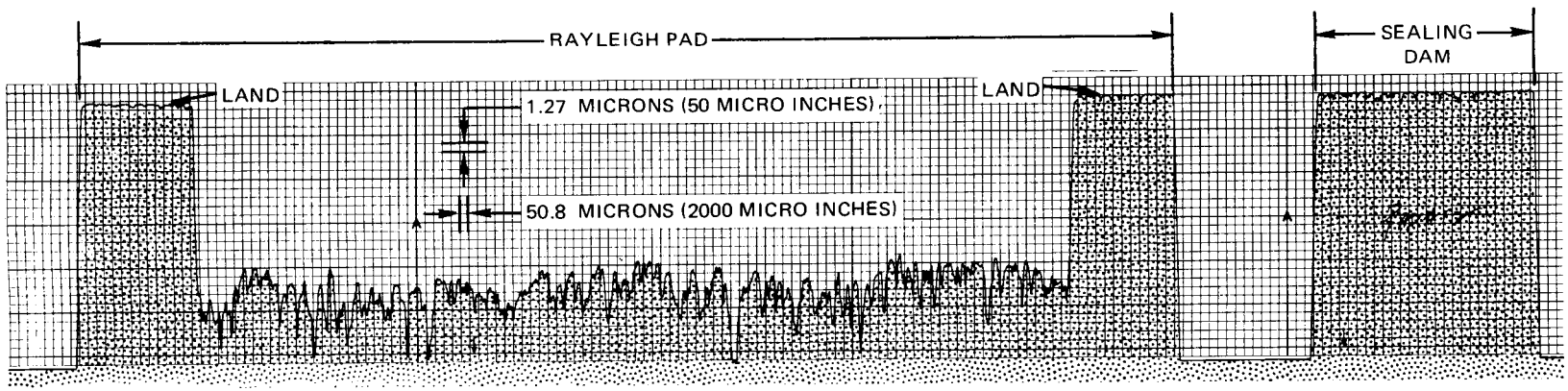

Figure 78 Representative Profile Trace Taken Radially Across the Face of the Carbon Nosepiece at Completion of First 25 Hours of Elevated Temperature Endurance Testing. Time on Nosepiece 37.75 Hour

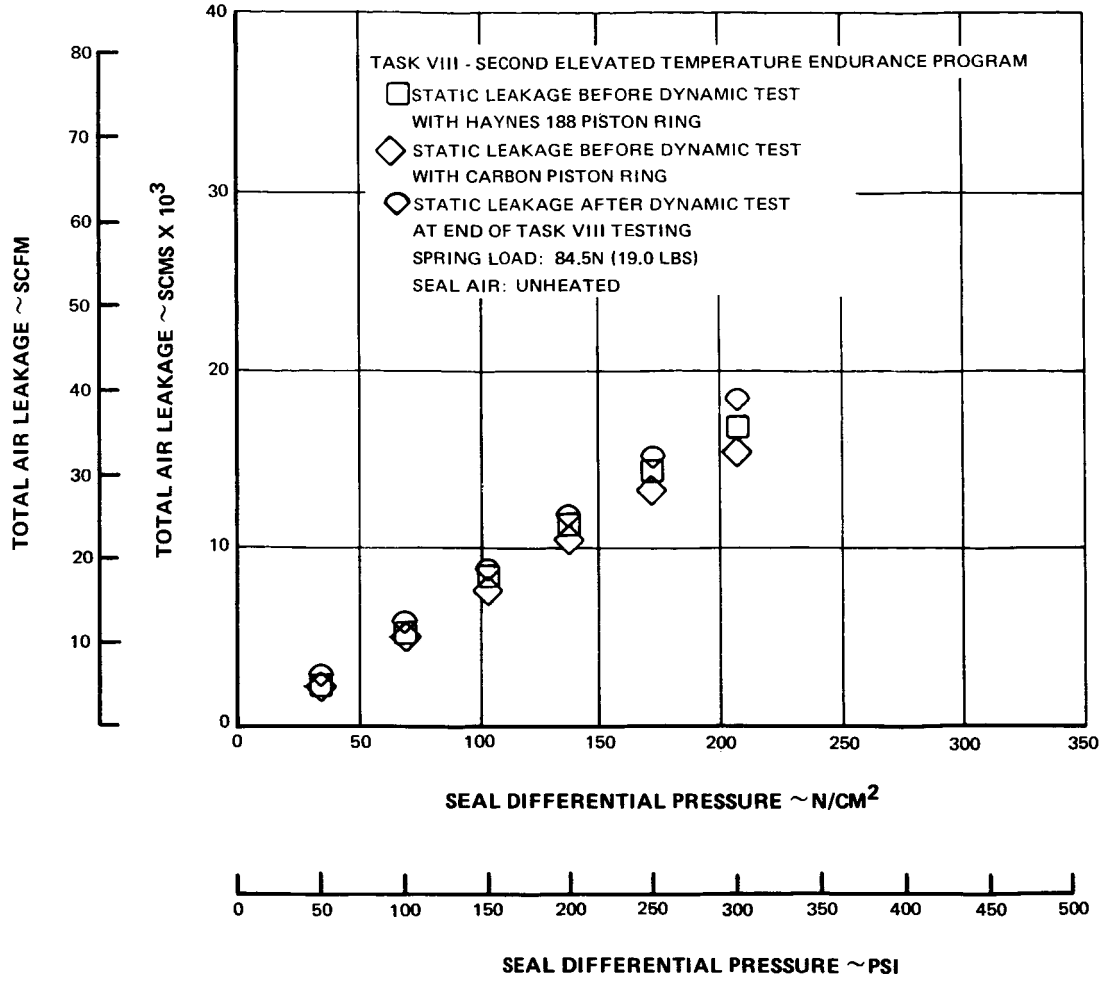

Figure 79 Static Seal Leakage During Second Elevated Temperature Endurance Test

The seal assembly was rebuilt with the same hardware as before and installed in the rig. Testing was resumed, starting at the conditions established for the previous 8.5 hours of test. Seven (7) hours of additional test were accumulated, of which 5.5 hours were at a sliding speed of 137.2 m/sec (450 ft/sec), seal differential pressures up to 241 N/cm^2 (350 psi), and sealed air temperatures in excess of 718°K (1000°F). A test shut down was initiated at this time following the same shutdown procedure used previously. After 1.5 hours into the cool down period, with the sealed gas temperature at 594°K (610°F), the seal differential pressure at 93.2 N/cm^2 (135 psi), and the air leakage at 7.1 x 10^{-3} scms (15 scfm), the seal suddenly opened as during the previous shutdown. After final rig shut down, an attempt to perform a static leak calibration was again unsuccessful, and the seal assembly was removed for inspection. Visual inspection showed the seal nosepiece to be in good condition, but coke was again present on the seal carrier. A profile trace of the carrier I.D. indicated that the bore deviated from a true circle as much as 63.6 microns (2.5 mils) at four (4) places approximately 90° apart. This out-of-roundness could have caused the piston ring to hang-up, as the temperature changed during rig cool down, thus causing the seal nosepiece to open or separate from the carrier.

The seal assembly was rebuilt with the same hardware except that the Ni-Span C out-of-round carrier was replaced with a TZM carrier, and the Haynes 188 piston ring was replaced with a carbon piston ring in an attempt to reduce friction. A static leak test was completed after the seal assembly was reinstalled in the rig and the results are shown in Figure 79.

Elevated temperature endurance testing was again resumed, and an additional 5.5 hours were completed at seal sliding speeds from 137.2 m/sec (450 ft/sec) to 152.4 m/sec (500 ft/sec), and at seal differential pressures from 241.5 N/cm^2 (350 psi) to 276 N/cm^2 (400 psi) while maintaining the sealed gas temperature at a minimum of 811°K (1000°F). The same cool down procedure was followed at rig shutdown that was used previously, however, no abnormal conditions were noted. The total test time for the second portion of the elevated temperature endurance testing was 21 hours at this seal inspection shutdown.

The seal assembly was removed from the rig for inspection, primarily to determine the condition of the carbon secondary piston ring seal. All seal hardware was in good condition, but coking on the carrier was as extensive as in the previous test, with some coke buildup evident on the carrier sealing surface. The seal hardware was cleaned and reinstalled in the rig for continued evaluation. In addition, an oil diverter baffle, Figure 80, was installed in the seal assembly, to direct oil exiting the seal seat to the carrier in an attempt to reduce the operating temperature level of the carrier and thus reduce or eliminate the coking on the carrier. It was found in subsequent testing, however, that the oil diverter baffle did not help in reducing the carrier temperature or the coke build-up on it.

Elevated temperature endurance testing was again undertaken at seal sliding speeds from 137.2 m/sec (450 ft/sec) to 152.4 m/sec (500 ft/sec) and at a seal differential pressure of 276 N/cm^2 (400 psi) while maintaining the seal gas temperature at a minimum of 811°K (1000°F). Four (4.0) hours of additional testing were successfully completed at these conditions which extended the total test time to 25.0 hours at a minimum seal gas temperature of 811°K (1000°F). At this point the heated sealing air temperature was allowed to gradually decrease while the seal sliding speed was increased to 152.4 m/sec (500 ft/sec) and the seal differential pressure was increased to 345 N/cm^2 (500 psi). The speed and pressure were maintained for one (1) hour, during which the sealed gas temperature was at 700°F (800°F) after 0.5 hour, and 622°K (660°F) after 1.0 hour. A shut down was initiated at this time and accomplished without any problems. The specific test combinations and seal leakage measurements for this second endurance program are presented in Figure 81. Table XVIII summarizes the leakage data at six (6) combinations of speed and pressure conditions. In addition, the predicted air leakage is shown. The calculated primary leakage from Task I is added to pre-test static leakage which was adjusted for temperature.

A post-test static leakage test of the seal still mounted in the rig, Figure 79, indicated an approximate 20 percent increase in total leakage at 207 N/cm^2 (300 psi) from the results obtained prior to initiating the second endurance program.

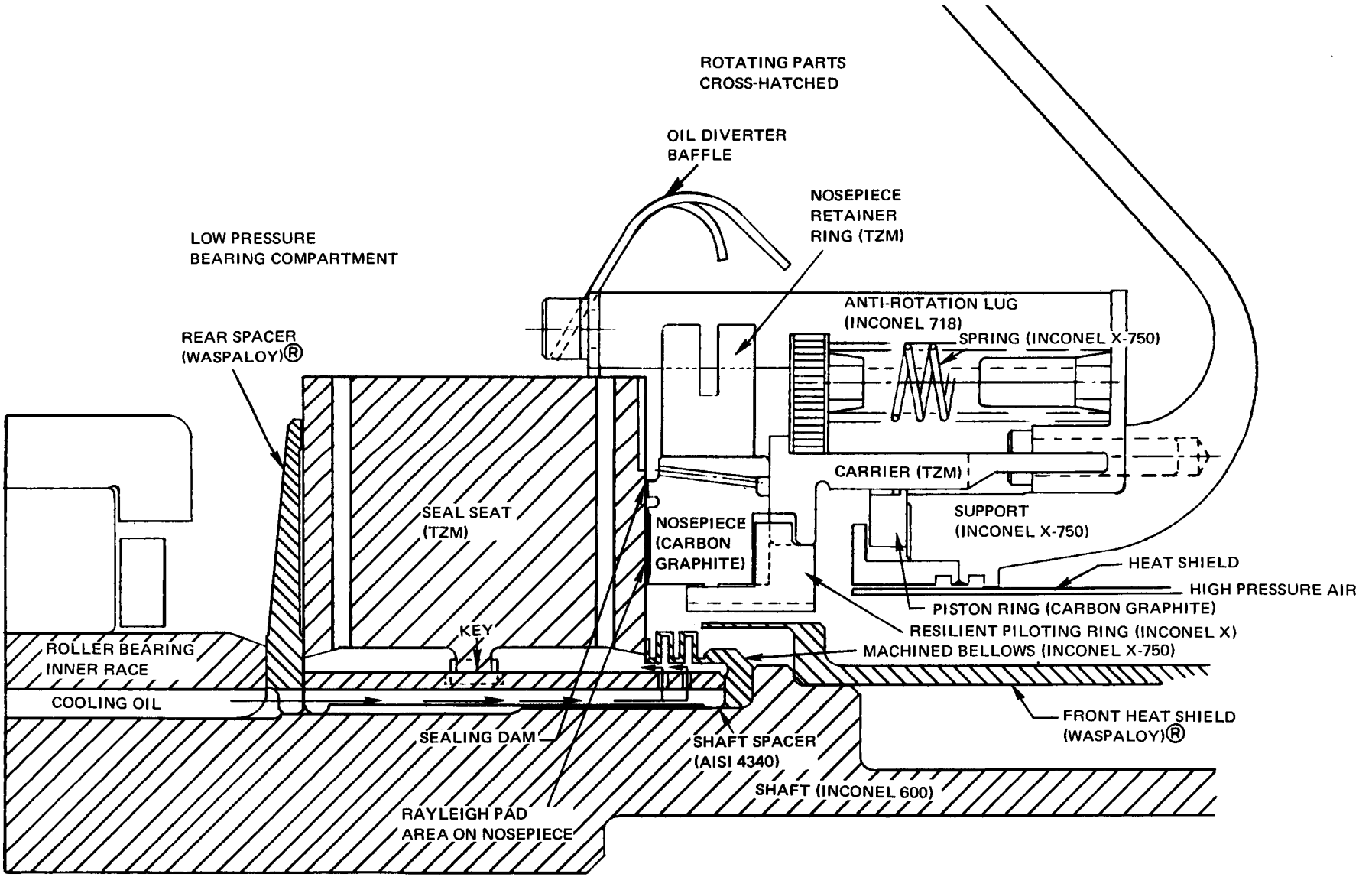

Figure 80 Hub and Seal Assembly Configuration Used During Elevated Temperature Testing Showing Addition of Oil Diverter Baffle

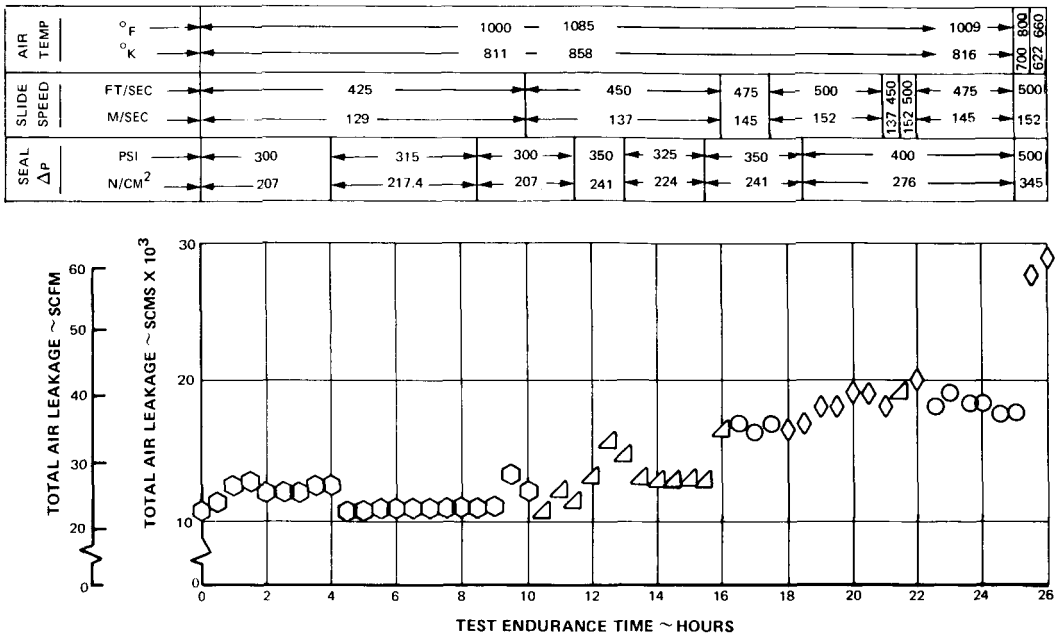

Figure 81 Leakage Measured During the Second Elevated Temperature Endurance Program. Spring Load 84.5N (19.0 lbs)

TABLE XVIII

ELEVATED TEMPERATURE ENDURANCE TEST AT 811°K (1000°F)

ΔP		SLIDING SPEED		Calculated Air Leakage Primary + Static = Total						Actual Total Air Leakage	
N/cm^2	(psi)	m/sec	(ft/sec)	scms x 10^3	(scfm)	scms x 10^3	(scfm)	scms x 10^3	(scfm)	scms x 10^3	(scfm)
207	(300)	129	(425)	3.78	(8.0)	9.96	(21.1)	13.74	(29.1)	12.0	(25.0)
217.4	(315)	129	(425)	4.24	(9.0)	10.62	(22.5)	14.87	(31.5)	10.86	(23.6)
224	(325)	137	(450)	4.72	(10.0)	11.04	(23.4)	15.76	(33.4)	12.74	(27.0)
241	(350)	145	(475)	5.90	(12.5)	10.90	(23.1)	16.80	(35.6)	16.52	(35.0)
276	(400)	152	(500)	7.55	(16.0)	12.60	(26.7)	20.15	(42.7)	18.88	(40.0)
276	(400)	145	(475)	7.32	(15.5)	12.60	(26.7)	19.91	(42.2)	17.94	(38.0)

Visual inspection indicated all parts to be in good condition except for the carbon nosepiece which was chipped in several places at the I.D. of the Rayleigh pads. The largest chip, approximately 5.54 mm (0.218 inch) long, apparently resulted during handling of the seal assembly. Coking of the carrier was as extensive as noted in previous inspections indicating the need for further cooling. The condition of the seal assembly is shown in Figures 82 and 83.

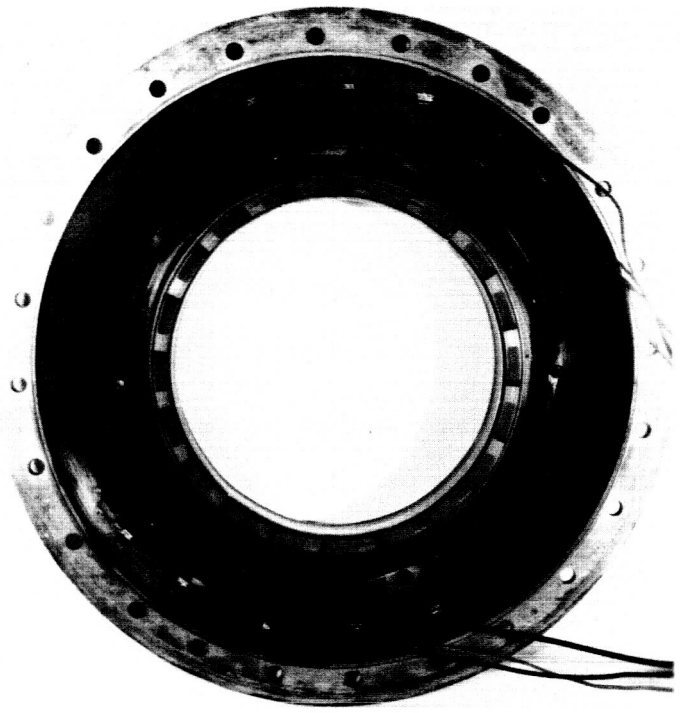

Figure 82 Seal Assembly After 79 Hours of Elevated Temperature Endurance Testing (X-38832)

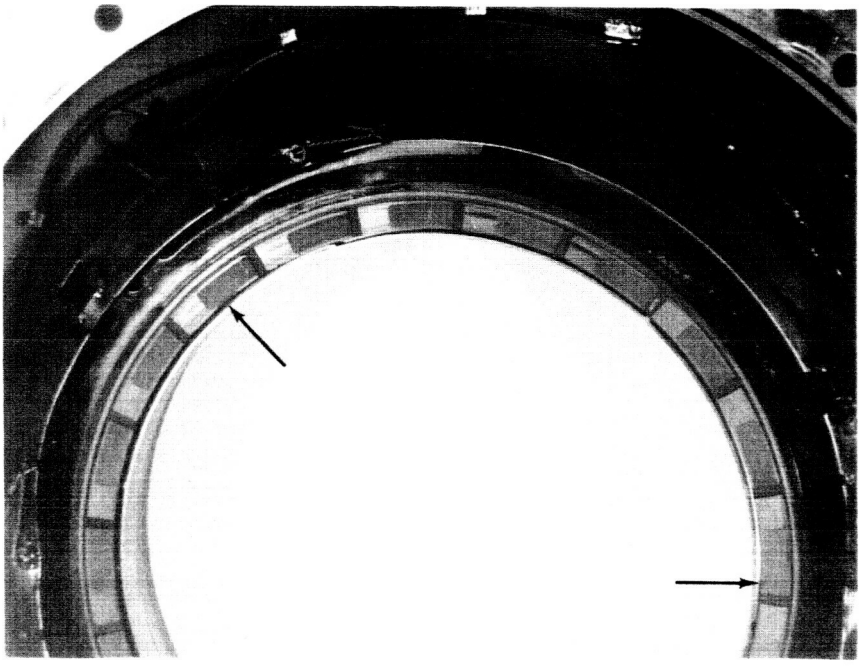

Figure 83 Carbon Nosepiece After 79 Hours of Elevated Temperature Endurance Testing (Large Chip at I.D. of Rayleigh Pad Due to Handling) (X-38833)

The seal assembly was reinstalled in the rig and 5.50 hours of additional endurance testing was completed at elevated temperatures. A maximum seal sliding speed of 183 m/sec (600 ft/sec) was obtained with a seal differential pressure of 310.5 N/cm^2 (450 psi) and a sealed gas temperature of 633°K (680°F). It was not possible to reach the sealed gas temperature of 700°K (800°F) at all of the higher combinations of speed and pressure because of the need to maintain a safe rig roller bearing temperature. The specific test combinations reached and the seal air leakage rates measured during this 5.5 hours of endurance testing are presented in Table XIX.

TABLE XIX

TEST CONDITIONS AND RESULTS FOR POST TASK VIII TEST

Time		Sliding Speed		Seal Press		Air Temp		Air Leakage	
Hrs	Total Hrs.	m/sec	(ft/sec)	N/cm^2	(psi)	°K	(°F)	scms x 10^3	(scfm)
.5	.5	122	(400)	207	(300)	542	(517)	16.0	(34.0)
.5	1.0	122	(400)	275	(400)	616	(650)	19.8	(42.0)
.5	1.5	137	(450)	275	(400)	683	(770)	20.5	(43.5)
.5	2.0	153	(500)	275	(400)	709	(816)	20.5	(43.5)
1.0	3.0	168	(550)	275	(400)	742	(876)	20.3	(43.0)
1.5	4.5	153	(500)	275	(400)	714	(825)	20.1	(42.5)
.5	5.0	168	(550)	275	(400)	666	(740)	21.7	(46.0)
.25	5.25	168	(550)	310	(450)	639	(690)	24.8	(52.5)
.25	5.50	183	(600)	310	(450)	633	(680)	27.1	(57.5)

Visual inspection of the test seal components proved them to be in good condition. The post-test condition of the carbon nosepiece is shown in Figure 84. This nosepiece had accrued a total test time of 86.25 hours, of which 37.75 hours were during the first endurance program and the remaining 48.50 hours during the second. Profile traces across the nosepiece face, Figure 85, indicated that wear to a depth of 5.08 microns (0.20 mils) across the Rayleigh pads was generated during the second endurance program. Extensive wear of the sealing dam is also shown in Figure 85 with the average wear being 10.16 microns (0.40 mils) and the maximum groove depth being 15.24 microns (0.60 mils).

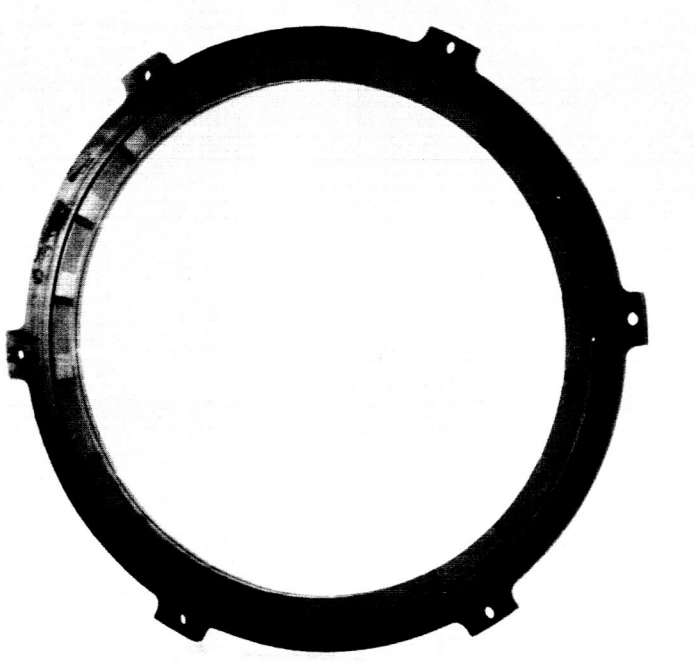

Figure 84 Carbon Nosepiece at Completion of Elevated Temperature Endurance Testing. Total Time on Nosepiece 86.25 Hours (XPN-36568)

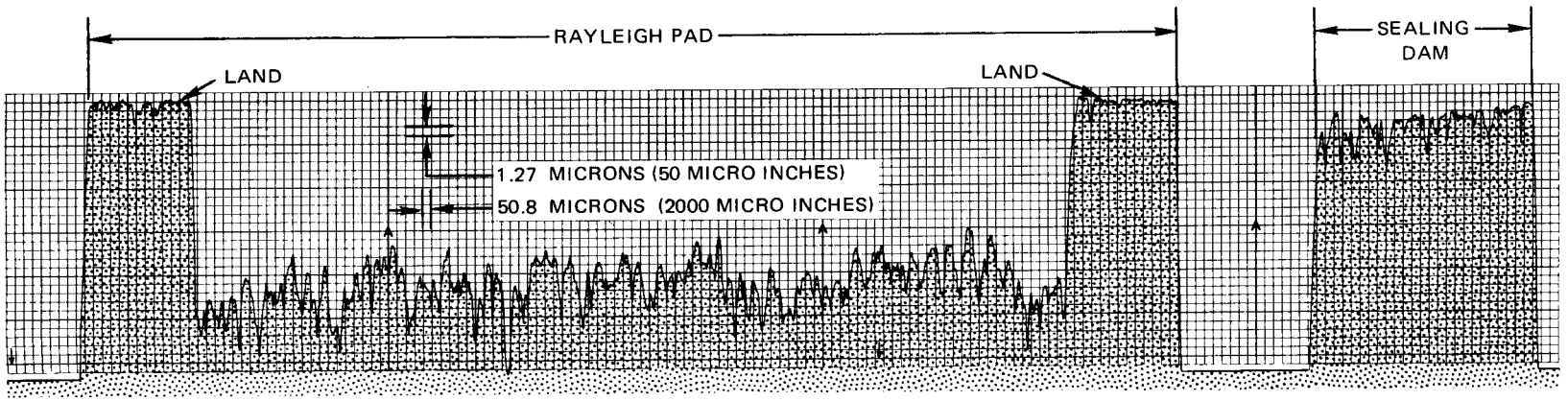

Figure 85 Representative Profile Trace Taken Radially Across the Face of the Carbon Nosepiece at Completion of Elevated Temperature Endurance Testing. Total Time on Nosepiece 86.25 Hours

For the entire testing completed on the nosepiece (86.25 hours), the total wear at the Rayleigh pads was 6.35 microns (0.25 mils) and the average wear across the sealing dam was 11.43 microns (0.45 mils).

The condition of the seal seat which was used throughout the elevated temperature endurance program is shown in Figure 86. A profile trace across the face of the seat, Figure 87, indicated it was still flat, but contained very shallow grooves within 0.6 microns (2.5 micro inches) in the areas corresponding to the nosepiece Rayleigh pads and sealing dam. Build-up of varnish on the seal seat face outboard of the sealing dam O.D. was also indicated on the profile trace.

Coking of the seal carrier was as extensive as noted at previous seal inspections during the elevated temperature endurance testing.

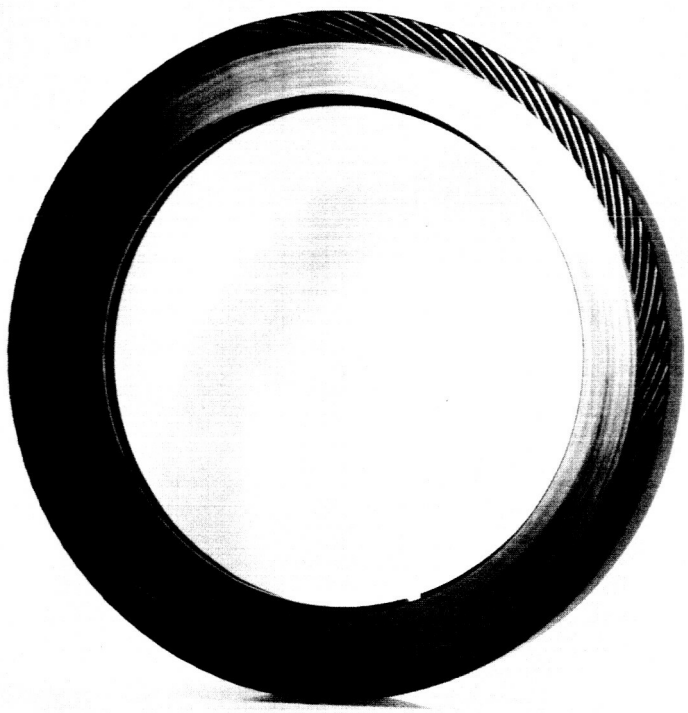

Figure 86 Seal Seat at Completion of Elevated Temperature Endurance Testing. Total Time on Seal Seat 86.25 Hours (XPN-36571)

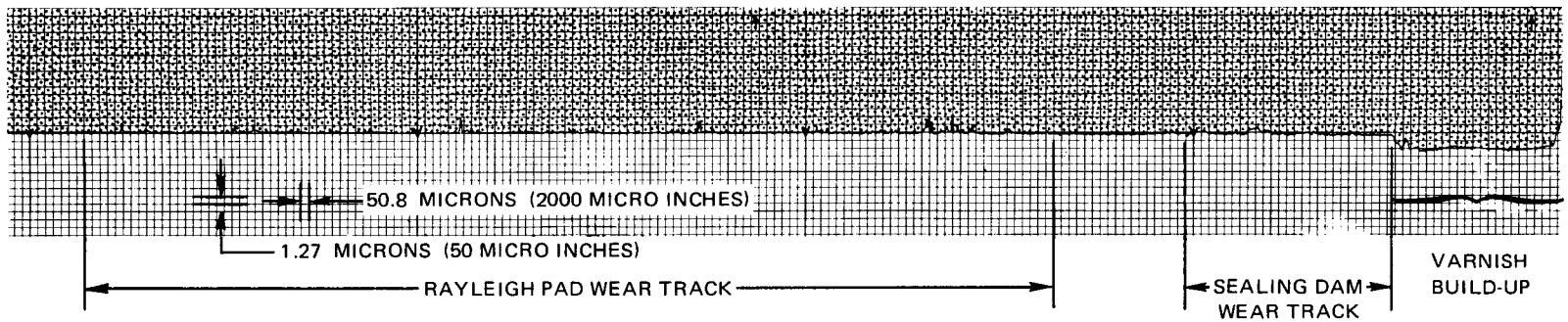

Figure 87 Representative Profile Trace Taken Radially Across the Face of the Seal Seat at Completion of Elevated Temperature Testing Showing Nosepiece Wear Track. Total Time on Seal Seat 86.25 Hours

APPENDICES

APPENDIX A

ASKA-A THREE DIMENSIONAL FINITE ELEMENT STRESS ANALYSIS COMPUTER PROGRAM

The acronym ASKA stands for "Automatic System for Kinematic Analysis". The name has been used to identify a sequence of computer programs as well as a simple computer language and a computational philosophy. ASKA is a general purpose problem solving computer program utilizing the finite element method. It was created at the University of Stuttgart under the direction of Professor J. H. Argyris. The program was purchased by Pratt & Whitney Aircraft and has been in general use throughout the company since 1970. A detailed description of the program may be found in References 4, 5 and 6 of this report.

APPENDIX B

TEST EQUIPMENT

A. TEST RIG

The test rig simulates the roller bearing sump at the turbine location in an advanced gas-turbine engine. The test seal provides the separation between the high-pressure hot gas (turbine side) and the low-pressure mixture of oil and air (sump side). The seals evaluated in the rig have had a maximum face diameter of approximately 17.78 cm (7 inches).

The seals evaluated in this Contract were tested in a full-scale test rig transferred from Contract NAS3-7609. The rig was mounted on a bed plate and driven by a Ford industrial engine through a five-speed truck transmission and a 12:1 ratio speed increaser. Facilities for heating the oil required for testing were located in the test cell, and the air was heated by an electrical heater. A schematic diagram of the test facility is shown in Figure 88 and a photograph is shown in Figure 89.

The test rig as used in Task III testing of the Contract was designed for evaluating mainshaft seals at sliding speeds of 152.4 m/sec (500 fps), pressure differentials across the seal of 206.8 N/cm^2 (300 psi) and sealed gas temperatures up to 922°K (1200°F). In Task II, the Contractor modified the design of the rig to allow operation to seal sliding speeds of 182.9 m/sec (600 ft/sec) and seal differential pressures of 345 N/cm^2 (500 psi). This configuration was used for testing in Task IV and Tasks VI through VIII.

A layout of the basic rig is shown in Figure 90. Pressurized and heated air entered the test compartment via the conical manifold attached to the inside of the pressure dome. The pressure dome was insulated to cut heat losses during testing. Air temperatures at the seal were continually monitored and adjusted by means of a bleed valve. Oil was brought to the thrust bearings by means of a calibrated jet and scoop arrangement. Oil was brought to the test seal from a jet via a scoop and passageways which allowed under-race cooling of the roller bearing. This oil was then centrifugally thrown out of the seal seat through radially drilled holes, thus providing cooling for the seal seat. The roller bearing was lubricated with mist and spray in the bearing compartment. The flight-weight parts used in the rig were:

- Duplex ball thrust bearing
- Inner and outer thrust bearing supports
- Thrust bearing support mount
- Roller bearing
- Roller bearing support mount
- Test seal seat
- Test seal assembly

B. PRESSURE CHECK FIXTURES

The seal pressure test fixture is shown in Figure 91. It consists of a pressure vessel which positioned the seal assembly against a simulated seat. The seal is pressurized through the bore and the air leakage into the low-pressure compartment is collected and measured. Additionally, removal of the fixture's cover allowed observation of the air leakage paths. This feature of the fixture is of great assistance in determining whether excessive leakage during some of the tests is coming past the primary seal or past the secondary-seal piston ring.

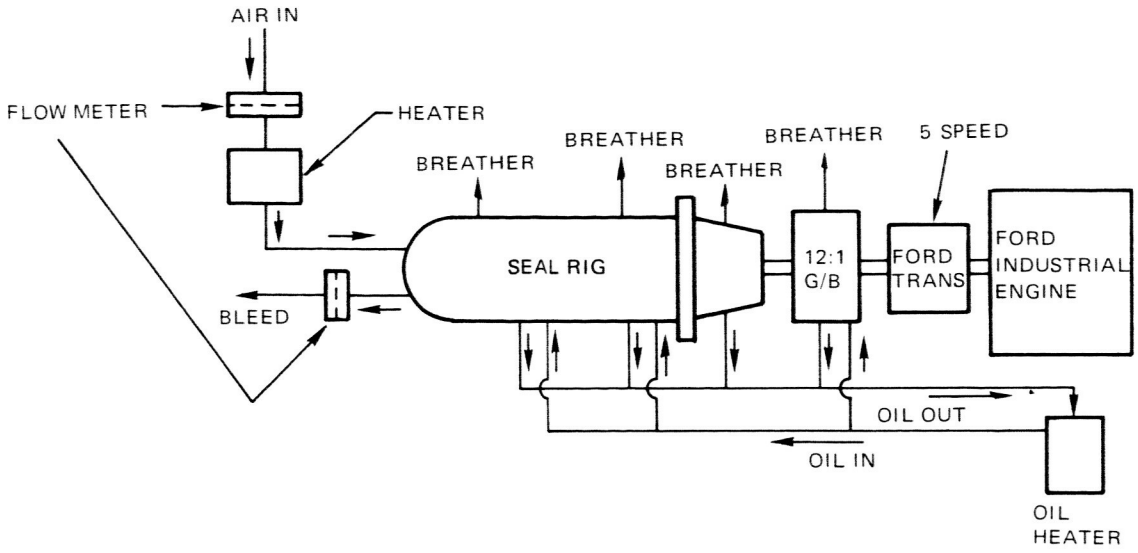

Figure 88 Schematic Diagram of Seal Test Facility

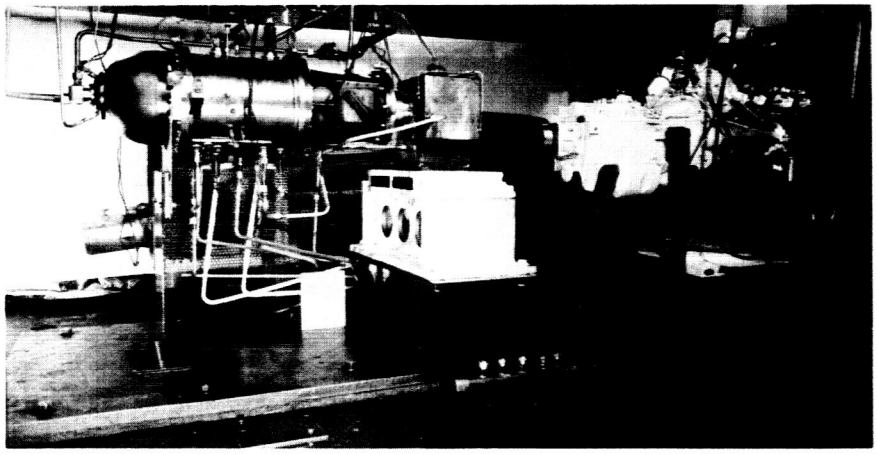

Figure 89 Overall View of the Test Stand Showing Mainshaft Seal Rig, Gearbox, and Drive Engine (CN-6928)

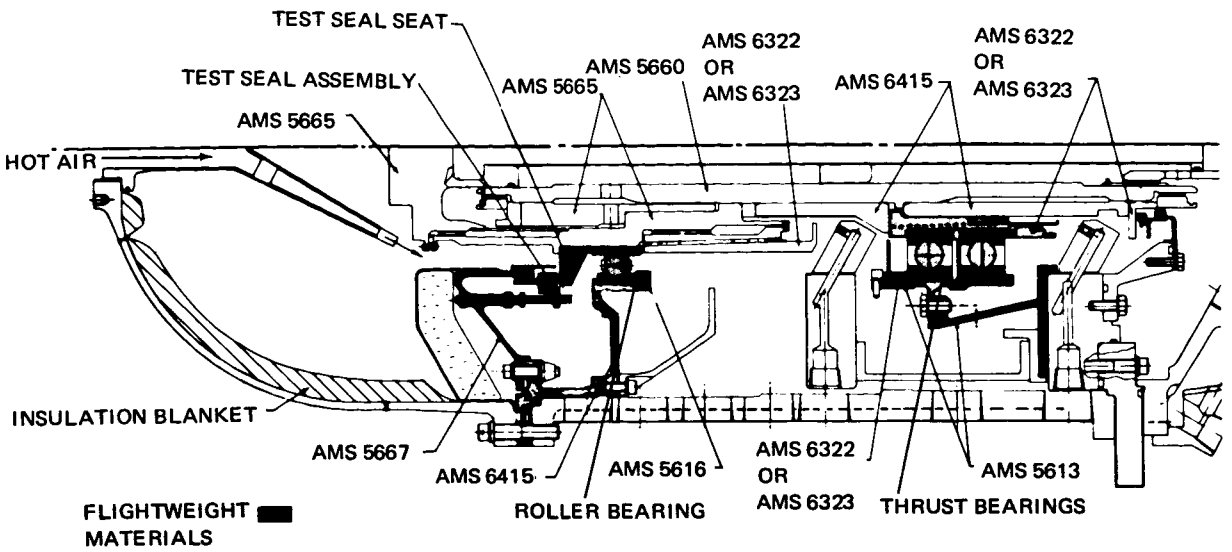

Figure 90 Rig Layout Showing Test Seal Location and Component Materials

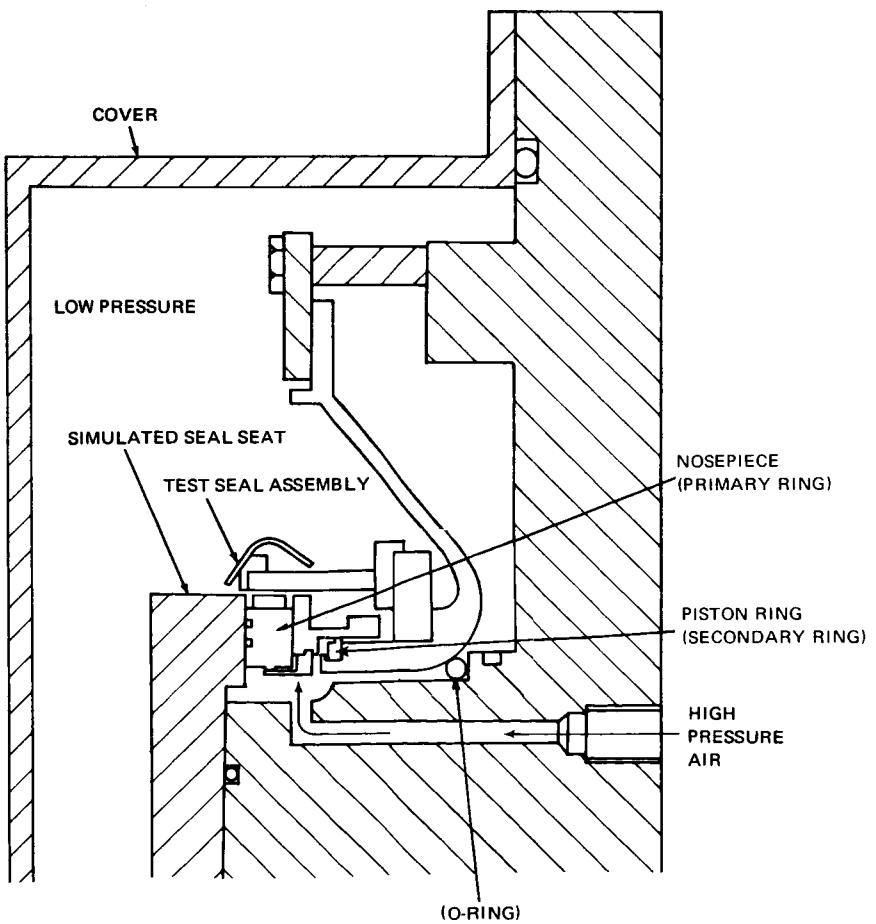

Figure 91 Schematic Diagram of Pressure Check Fixture for the Seal

C. TEST INSTRUMENTATION

During test evaluation the following parameters were monitored with the instrumentation indicated:

- Sealed gas leakage – Magnetic type air flowmeters with direct readout, installed in air supply line before heater
- Seal pressure differential – Pressure tap installed in rig dome with Heise pressure gage readout*
- Breather pressure – Pressure tap in rig compartment with U-tube mercury gage
- Rig speed – Tachometer generator signal from input of 12:1 ratio speed increaser, with digital counter readout
- Seal gas temperature – Chromel-alumel thermocouple at outlet of air manifold inside of pressure dome, with potential type readout
- Seal and rig bearing oil flow – Magnetic type oil flowmeters with direct readout, installed in oil supply lines
- Oil temperature – Chromel-alumel thermocouples installed in oil supply and discharge lines, with potential type readout
- Temperature of rig bearings – Chromel-alumel thermocouples tack-welded to housings, contacting bearing outer races, with potential type readout

* Compartment side of seal at atmospheric pressure.

APPENDIX C

LIST OF SYMBOLS

F_P	Rayleigh Pad Load Capacity ~ Newtons (Pounds)
F_D	Seal Dam Load Capacity ~ Newtons (Pounds)
F_B	Hydraulic Balance Force ~ Newtons (Pounds)
F_s	Spring Force ~ Newtons (Pounds)
k	Stress Concentration Factor ~ Dimensionless
d	Width of Minimum Section ~ Centimeters (Inches)
r	Fillet Radius - Seal Seat ~ Centimeters (Inches)
ΔP	Differential Pressure ~ N/cm^2 (psi)

REFERENCES

1. "Development of Mainshaft Seals for Advanced Air Breathing Propulsion Systems - Phase III"; PWA-4263, NASA CR-72987; V.P. Povinelli and A.H. McKibbin; Pratt & Whitney Aircraft, East Hartford, Connecticut; July 1971.

2. Semiannual Report No. 1, "Development of Compressor End Seals, Stator Inter-stage Seals, and Stator Pivot Seals in Advanced Air-Breathing Engines"; PWA-2752, NASA CR-54625; R. M. Hawkins et al; Pratt & Whitney Aircraft, East Hartford, Connecticut; January 1966.

3. "Compressible Flow Across Shaft Face Seals"; NASA TM X-52959; John Zuk, Lawrence P. Ludwig, and Robert L. Johnson; Lewis Research Center, Cleveland, Ohio.

4. "Review of the ASKA Programme" P. Meijers, O.N.R. International Symposium on Numerical and Computer Methods in Structural Mechanics, University of Illinois, September 1971.

5. "An Automatic System for Kinematic Analysis ASKA, Part I" Ernst Schrem, John R. Roy, A Paper presented on the IUTAM Colloquium High Speed Computing of Elastic Structures, University of Leige, Belgium Aug 23-28, 1970.

6. "Computer-Aided Structural Analysis The Machine-Independent System ASKA" Professor Dr. J. H. Argyris, Sivilingeniör O.E. Brönlund, Dr. - Ing. M. Sörensen. A Paper presented at the Nord Data-70 Conference, 26 - 28 August in Copenhagen.

DISTRIBUTION LIST

Addressee	Number of Copies
1. NASA Headquarters Washington, DC 20546	
Attention: N. F. Rekos (RLC)	1
A. J. Evans (RH)	1
J. Maltz (RWM)	1
2. NASA-Lewis Research Center 21000 Brookpark Road Cleveland, Ohio 44135	
Attention: A. Ginsburg, MS 5-3	1
E. E. Bisson, MS 5-3	1
R. L. Johnson, MS 23-2	1
L. P. Ludwig, MS 23-2	20
M. A. Swikert, MS 23-2	1
L. W. Schopen, MS 500-206	1
Report Control Office, MS 5-5	1
Library, MS 60-3	2
Technology Utilization Office, MS 3-19	1
Dr. B. Lubarsky, MS 3-3	1
C. H. Voit, MS 5-3	1
N. T Musial, MS 500-113	1
3. NASA-Scientific and Technical Information Facility P.O. Box 33 College Park, Maryland 20740	
Attention: NASA Representative	2
4. NASA-Langley Research Center Langley Station Hampton, Virginia 23365	
Attention: Mark R. Nichols	1
5. NASA-Manned Spacecraft Center Houston, Texas 77058	
Attention: C. D. Haines	1
6. United States Air Force Wright-Patterson Air Force Base AF Systems Command USAF Wright-Patterson AFB, Ohio 45433	
Attention: AFAPL (APDL), K. L. Berkey	1
AFAPL (AFTC), C. Simpson	1
APTP, I. J. Gershon	1
MANE, R. Headrick	1
MANE, P. House	1
TBC, C. Elrod	1
7. U. S. Naval Research Laboratory Washington, DC 20390	
Attention: Charles Murphy	1
8. Department of the Navy Bureau of Naval Weapons Washington, DC 20013	
Attention: A. D. Nehman, RAAE-3	1
C. C. Singletorry, RAPP-4	1
9. Department of the Navy Bureau of Ships Washington, DC 20525	
Attention: Harry King, Code 634A	1
10. Department of Navy Naval Air Systems Command AIR-330 Washington, DC 20360	1
11. U.S. Navy Marine Engineering Laboratory Friction and Wear Division Annapolis, Maryland 21490	
Attention: R. B. Snapp	1
12. Department of the Army U. S. Army Aviation Materiel Labs. Fort Eustis, Virginia 23604	
Attention: John W. White, Chief, Propulsion Division	1
13. AMMRC Watertown, Massachusetts 02172	
Attention: Dr. R. Singler	1
14. U. S. Army Ordnance Rock Island Arsenal Laboratory Rock Island, Illinois 61201	
Attention: R. LeMar	1
15. Aerospace Corporation Building A-2 P.O. Box 95085 Los Angeles, California 90045	
Attention: James Todd	1
16. AVCOM AMSAVEGTT Mart Building 405 South 12th Street St. Louis, Missouri 63166	
Attention: E. England	1
17. Aerojet-General Corporation 5100 West 164 Street Cleveland, Ohio 44142	
Attention: W. L. Snapp	1
18. AiResearch Manufacturing Corporation 402 S. 36th Street Phoenix, Arizona 85034	
Attention: F. Blake Wallace	1
19. Avco Corporation Lycoming Division 550 South Main Street Stratford, Connecticut 06497	
Attention: R. Cuny	1
P. Lynwander	1

DISTRIBUTION LIST (Cont'd)

Addressee	Number of Copies
20. Battelle Memorial Institute 505 King Avenue Columbus, Ohio 43201 Attention: Dr. S. S. Bupra	1
21. Bendix Corporation Fisher Building Detroit, Michigan 48202 Attention: R. H. Isaacs	1
22. B. F. Goodrich Company Aerospace & Defense Products Division Troy, Ohio 45373 Attention: L. S. Blalkowski	1
23. Boeing Aircraft Company P.O. Box 3399 Seattle, Washington 98124 Attention: W. S. Lambert, 2-1100	1
24. The Boeing Company Vertol Division P. O. Box 16859 Philadelphia, Pennsylvania 19142 Attention: A. J. Lemanski, MS P-32-09	1
25. Borg-Warner Corporation Roy C. Ingersoll Research Center Wolf and Algonquin Roads Des Plaines, Illinois 60018	1
26. Chicago Rawhide Manufacturing Company 1311 Elston Avenue Chicago, Illinois 60622 Attention: R. Blair	1
27. Clevit Corporation Cleveland Graphite Bronze Division 17000 St. Clair Avenue Cleveland, Ohio 44110 Attention: J. Ross	1
28. Continental Aviation & Engineering 12700 Kercheval Detroit, Michigan 48215 Attention: A. J. Follman	1
29. Cooper Bessemer Mt. Vernon, Ohio 43050 Attention: K. Smith	1
30. Crane Packing Company 6400 W. Oakton Street Morton Grove, Illinois 60053 Attention: Harry Tankus	1
31. Defense Ceramics Information Center Battelle Memorial Institute Columbus Labs, Room 11-9021 505 King Avenue Columbus, Ohio 43201	1

Addressee	Number of Copies
32. Dresser Industries Dresser Clark Division P.O. Box 560 Olean, New York 14780 Attention: J. W. Kirkpatrick E. Tanzberger	1 1
33. Durametallic Corporation Kalamazoo, Michigan 49001 Attention: H. Hummer	1
34. Fairchild Hiller Corporation Republic Aviation Division Farmingdale, L.I., New York 11735 Attention: C. Collis	1
35. Franklin Institute Laboratories 20th and Parkway Philadelphia, Pennsylvania 19103 Attention: W. Shapiro	2
36. Garrett Corporation AiResearch Manufacturing Division 9851-9951 Sepulveda Boulevard Los Angeles, California 90009 Attention: A. Silver	1
37. General Dynamics Corporation 1025 Connecticut Avenue, N.W. Washington, DC 20036 Attention: G. J. Vila	1
38. General Electric Company Advanced Engine & Technology Department Cincinnati, Ohio 45215 Attention: L. B. Venable N. Pope W. McCarty I. E. Sumey	1 1 1 1
39. General Motors Corporation Allison Division Plant # 3, Department 7339 Indianapolis, Indiana 46206 Attention: E. M. Deckman	1
40. Gould Information Center 540 E-150th Street Cleveland, Ohio 44108 Attention: L. A. Noble	1
41. IIT Research Foundation 10 West 35 Street Chicago, Illinois 60616 Attention: Dr. Strohmeir M. A. Schwartz	1 1

DISTRIBUTION LIST (Cont'd)

	Addressee	Number of Copies
42.	Koppers Company, Inc. Metal Products Division Piston Ring and Seal Department P. O. Box 626 Baltimore, Maryland 21203	
	Attention: F. C. Kuchler	1
	E. Taschenburg	1
	J. Heck	1
43.	Lockheed Aircraft Company 118 West First Street Dayton, Ohio 45402	
	Attention: R. R. Witte	1
44.	Los Alamos Scientific Laboratory University of California Los Alamos, New Mexico	
	Attention: M. C. Smith	1
45.	Martin Marietta Corporation 1700 Needmoor Road Dayton, Ohio 45414	
	Attention: Z. G. Horvath	1
46.	McDonnell Douglas Corporation 333 West First Street Dayton, Ohio 45402	
	Attention: R. G. Donmoyer	1
47.	Mechanical Technology, Inc. 968 Albany-Shaker Road Latham, New York 12110	
	Attention: Donald F. Wilcock	1
48.	Midwest Research Institute 425 Volker Boulevard Kansas City, Missouri 64110	
	Attention: V. Hopkins	1
49.	NASA Scientific Technical Information Facility Acquisitions Branch P. O. Box 33 College Park, Maryland 20740	10
50.	North American Rockwell Corp. 5100 West 164 Street Cleveland, Ohio 44125	
	Attention: George Bremer	1
51.	North American Rockwell Corp. Rocketdyne Division 6633 Canoga Avenue Canoga Park, California 91304	
	Attention: R. E. Burcham	1
52.	Northrop Corporation 379 West First Street Dayton, Ohio 45402	
	Attention: Dr. W. A. Martin	1
53.	Pesco Products Division Borg-Warner Corporation 24700 N. Miles Bedford, Ohio 44146	
	Attention: W. J. Cieslik	1
54.	Poco Graphite, Incorporated P. O. Box 1524 Garland, Texas 75040	
	Attention: Dr. R. F. Wehrmann	1
55.	Pure Carbon Company, Inc. 441 Hall Avenue St. Mary's, Pennsylvania 15857	
	Attention: Dr. R. R. Paxton	1
	J. Sherlock	1
56.	Rexnord-Seal Division 1311 Elston Avenue Chicago, Illinois 60622	
	Attention: John Harrop	1
57.	Sealol, Incorporated P. O. Box 2158 Providence, Rhode Island 02905	
	Attention: Justus Stevens	1
	E. Moran	1
58.	Sikorsky Aircraft North Main Street Stratford, Connecticut 06497	
	Attention: L. Burroughs	1
59.	SKF Industries, Incorporated 1100 First Avenue King of Prussia, Pennsylvania 19406	
	Attention: L. B. Sibley	1
60.	Southwest Research Institute P. O. Drawer 28510 San Antonio, Texas 78228	
	Attention: P. M. Ku	1
61.	Space Craft, Incorporated 5670 Markdale Drive Dayton, Ohio 45459	
	Attention: J. W. Sharp	1
62.	St. Marys Carbon Company 1939 State Road St. Marys, Pennsylvania 15857	
	Attention: J. E. Lanzel	1
63.	Stackpole Carbon Company St. Marys, Pennsylvania 15857	
	Attention: Dr. E. I. Shobert	1
64.	Stanford Research Institute 333 Ravenwood Avenue Menlo Park, California 94025	
	Attention: R. C. Fey	1

DISTRIBUTION LIST (Cont'd)

Addressee	Number of Copies
65. Stein Seal Company 20th Street and Indiana Ave. Philadelphia, Pennsylvania 19132 Attention: Dr. P. C. Stein	1
E. Goldring	1
66. Ultra Carbon Corporation 1300 N. Madison Avenue Bay City, Michigan 48706 Attention: Del Hughes	1
67. Union Carbide Carbon Products Division P. O. Box 6116 Cleveland, Ohio 44101 Attention: P. Petrunich	1
68. United Aircraft Corporation Pratt & Whitney Aircraft Division Engineering Building EB2B-2 East Hartford, Connecticut 06108 Attention: R. Shevchenko	3
69. Wickes Engineered Materials 1621 Holland Saginaw, Michigan Attention: Paul Dahlenberg	1
70. The University of Tennessee Department of Mechanical and Aerospace Engineering Knoxville, Tennessee 37916 Attention: Professor W. K. Stair	1
Dr. C. Fisher	1
71. Westinghouse Electric Corp. 5100 W. 164 Street Cleveland, Ohio 44142 Attention: Lynn Powers	1
72. Williams Research Corporation 2280 W. Maple Road P. O. Box 95 Walled Lake, Michigan 48088 Attention: K. J. Bremner	1